Modelling the Effects of Element Doping and Temperature Cycling on the Fracture Toughness of β-NiAl / α-Al_2O_3 Interfaces in Gas Turbine Engines

By

Tyler Samson

Thesis submitted to the Department of Mechanical Engineering
in partial fulfillment of the requirements for the degree of
Master of Applied Science

University of Ottawa
Ottawa, Ontario, Canada
January 10th, 2013

"Give me six hours to chop down a tree

and I will spend the first four sharpening the axe."

-Abraham Lincoln

Abstract

This document describes work performed related to the determination of how elemental additions affect the interfacial fracture toughness of thermal barrier coatings at the bond coat/thermally grown oxide interface in gas turbines. These turbines are exposed to cyclical thermal loading, therefore a simulation was designed to model this interface in a temperature cycle between 200 K and 1000 K that included oxide growth between 2 μm and 27 μm. The fracture toughness of this interface was then determined to elucidate the function of elemental additions. It was shown that minimal concentrations of atomic species, such as hafnium and yttrium cause notable increases in the toughness of the bond coat/thermally grown oxide interface, while other species, such as sulphur, can dramatically reduce the toughness. Furthermore, it was shown that, contrary to some empirical results, the addition of platinum has a negligible effect on the fracture toughness of this interface.

Acknowledgements

Sometimes things just work out the way you hoped they would, however randomly they come to pass. I hadn't exactly planned on starting graduate studies when I did, but I always knew I eventually would. By sheer happenstance, I was offered my opportunity by Dr. Kuiying Chen who needed another team member to assist with his research at the National Research Council. He then approached Dr. Bertrand Jodoin, who graciously accepted to supervise my progress and also integrated me into his team at the University of Ottawa. I would therefore like to extend my thanks to both of them for their expertise, unwavering support and enthusiasm throughout my time conducting this research. Their encouragement to take the freedom to explore my research topics as I deemed appropriate provided for an incredibly rewarding experience.

My time at uOttawa and NRC wouldn't have been as great as it was without the following people: Dr. Mohammed Yandouzi, Susan Rennie, James MacDermid, Dr. Natalie Baddour, Dr. Ming Liang, Dr. Wieslaw Beres, Andrew Bugg, Melanie Lambert. Your generosity with your time, help and patience was invaluable and greatly appreciated. Thanks!

Thanks to my lab mates: Jamil Assaad, Antoine Bacciochini, Mathieu Bolduc, Rubén Fernández, Leon Guo, Daniel MacDonald, Jean-Louis Pelletier, Jean-Michel Roy and Patrick Trahan. Hours spent working together, troubleshooting, experimenting, debating sense and nonsense alike, trying

to solve the world's problems and learning lessons in time management have provided me with countless lasting memories. I couldn't have been luckier to work with such great teammates.

I'd also like to note that this experience wouldn't have gotten off the ground without Mike Greco, Dr. Patrick Oosthuizen and Dr. Brian Surgenor. Thank you for your support in pursuing this opportunity!

Lastly, and most importantly, I want to extend my sincerest heart-felt thanks to my parents, Juanita Romard and Alfred Samson, my family and my friends. You've all always encouraged me in my pursuits and strengthened my desire to explore the world we live in. Words can't express how much your support has always meant to me. Thank you!

Contents

List of Figures

List of Tables

Nomenclature and List of Symbols

APS: air plasma spray

BC: bond coat

CVD: chemical vapour deposition

EB-PVD: electron beam physical vapour deposition

GDMS: glow discharge mass spectrometry

HVOF: high velocity oxyfuel

PS: plasma spray

RE: reactive elements

SEM: scanning electron microscopy

TBC: thermal barrier coating

TGO: thermally grown oxide

VPA: vapour phase aluminising

YSZ: yttria-stabilised zirconia

E_c: coating (thermally grown oxide) elastic modulus [GPa]

E_s: substrate (bond coat) elastic modulus [GPa]

$F(\alpha_D)$: elastic mismatch function

K_{IC}: mode I uniaxial fracture toughness [MPa $m^{1/2}$]

λ: buckle profile wavelength [μm]

μ: shear modulus [μm]

R: buckle profile radius [μm]

σ_b: interfacial bond strength [MPa]

σ_c: critical interfacial stress [MPa]

σ_r^i: residual stress perpendicular to buckled interface [MPa]

σ_{ys}: bond coat yield strength [MPa]

t: coating (thermally grown oxide) thickness [μm]

$w_o(y)$: wave profile function

w_{ad}: work of adhesion [J/m^2]

Chapter 1

Introduction

Gas turbine engine designs for aircraft propulsion and industrial power generation continue to improve upon previous generations by incorporating advances in materials science and engineering. Improvements in both aerospace and industrial platforms are driven by the need to improve engine reliability, efficiency and performance while decreasing costs. As designs improve, the demand for increasingly higher service temperatures grows in order to improve efficiency. This increase in service temperature is ultimately limited by the properties of the materials used to fabricate the turbine.

To maximize fuel efficiency and power delivery, aerospace gas turbine engines must often operate at temperatures well above $1200^{\circ}\mathrm{C}$, which can be greater than the melting point of metals used in some engine components. Therefore, thermal barrier coatings, combined with internal cooling systems, are used to reduce the temperature of hot section metal components, protecting them from thermal damage. The design of these thermal barrier coatings (TBC) is of critical importance as

the overall reliability of the engine can be attributed, in part, to the reliability of these coatings [1].

Thermal barrier coatings consist of material layers bonded to the superalloy of the turbine blades. These layers traditionally consist of a thermally resistant ceramic top coat, commonly yttria-stabilized zirconia (YSZ), bonded to the nickel-based superalloy turbine component through the use of an intermetallic bond coat (BC). A schematic of a TBC deposited on a turbine blade is seen in Figure 1.1, from Evans *et al.* [2].

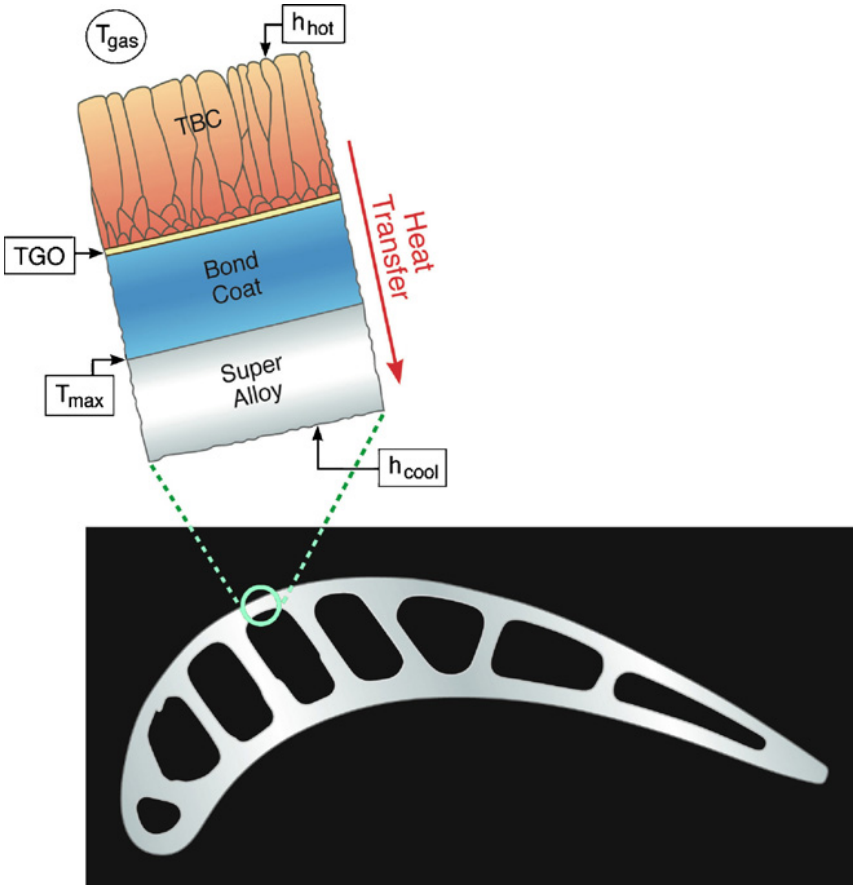

Figure 1.1: Overview of a thermal barrier coating system on a blade [2].

As hot combustion gases pass through the turbine, heat is transferred to the engine components. In order to protect these components from thermal damage, the TBC is deposited such that the substrate is shielded from the combustion gases. Furthermore, these components are fabricated with internal cooling channels which allow the part to be cooled from within. This internal cooling scheme, combined with the protection offered by the TBC, ensures the part remains below the critical melting temperature. As noted previously, the TBC system is deposited in layers. The innermost coating layer is the metallic bond coat deposited onto the substrate, followed by a thermally grown oxide (TGO). Finally, the outermost layer is a ceramic top coat which is, as previously mentioned, typically composed of an yttria-stabilized zirconia (YSZ)[1]. The bond coat layer serves as an intermediate layer between the superalloy substrate and the ceramic top coat to accommodate the mismatch in the coefficients of thermal expansion. It also provides an aluminium reservoir to support oxidation and the formation of the TGO layer. The second layer, the TGO, provides protection against further oxidation and minimizes direct interaction of the combustion gas with the bond coat. This is accomplished by the formation of a dense layer of oxide that prevents gases that diffuse through the permeable top coat from interacting with the substrate and bond coat. Limiting this interaction precludes the formation of rapidly forming oxides. Lastly, the top coat provides enhanced thermal resistance and reduces heat transfer to the underlying layers and substrate. To complement the schematic in Figure 1.1, Figure 1.2 provides a SEM image of a TBC system.

[1]It should be noted, that while the term TBC is often used to represent the entire coating system, it is sometimes used to designate only the ceramic top coat specifically, as seen in Figure 1.1. From this point forward in this document, 'TBC' will be used to refer to the entire coating system, consisting of the ceramic top coat, bond coat, and thermally grown oxide.

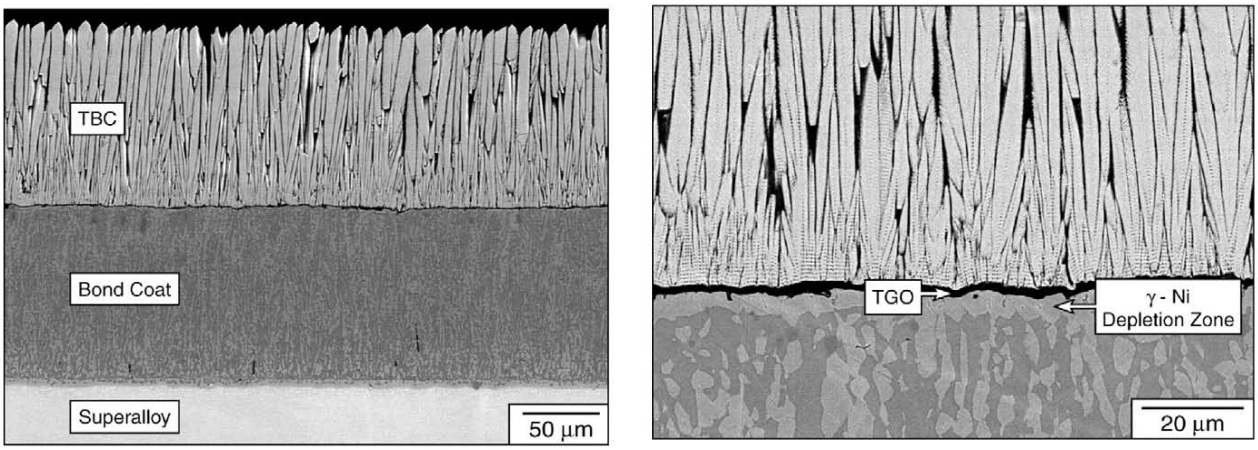

a) b)

Figure 1.2: A scanning electron miscroscope (SEM) image of: a) a typical TBC system and b) a close-up of the thermally grown oxide layer [2].

These coatings must protect against substantial temperature differences between the superalloy substrate and the exposed surface of the TBC system [3]. Figure 1.3 provides an example of the temperature gradient that can exist in a typical hot section turbine component coated with a TBC.

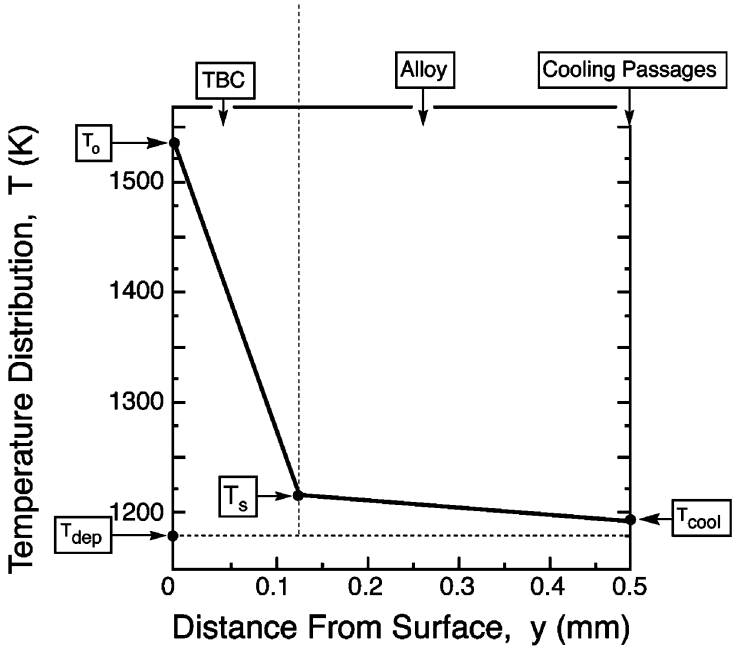

Figure 1.3: A thermal gradient profile schematic showing the effectiveness of a TBC system with internal cooling channels [4].

Some of the first commercial bond coats were MCrAlY(where "M" denotes the elements that are in addition to chromium, aluminium and yttrium) alloy coatings developed in the 1960's [5]. These alloys were first iron-based (FeCrAlY), followed by cobalt-based (CoCrAlY) and then nickel / cobalt-based (NiCoCrAlY). Fe-based coatings were first used on iron-based superalloys, followed by the development of Co-based superalloys. NiCoCrAlY BC were then developed for use on Ni-based superalloys as their commercial deployment became more common [6]. These coatings were initially deposited using either vacuum deposition or electron beam physical vapour deposition (EB-PVD). Eventually, these coatings would also be applied using air plasma spray (APS) and high-velocity oxy-fuel (HVOF) spray for economic reasons. Regardless of the deposition method, these coatings were observed to have a binary microstructure composed of β and γ phases. While the β-phase provides the Al reservoir required for aluminium oxide formation, the TGO, the γ-matrix provides enhanced ductility, which increases its thermal fatigue strength [5]. As the coating oxidizes, it forms a protective layer of oxide, preferably α-Al_2O_3, that is regularly replenished by aluminium in the β-phase until the Al is depleted to a point where it is no longer available for oxide formation. While initial compositions were effective, MCrAlY bond coats have since benefited from the addition of reactive elements (RE). Although the roles of these elements remain elusive, it has been established that yttrium (Y), hafnium (Hf) and zirconium (Zr) play a role in either enhancing adhesion or preventing spallation [5].

Another class of bond coat that has been developed is the diffusion aluminide coating based on β-NiAl. The Al application process is carried out at high temperature (between 800°C to 1100°C), and then the component is diffusion heat treated to produce a homogeneous layer of β-NiAl. Further to the initial development of diffusion aluminides, platinum was identified as an atomic addi-

tion that provided a noted improvement to the performance of these coatings, and could be readily included in the diffusion process. The inclusion of platinum led to the development of platinum aluminide coatings, β-NiPtAl.

Although β-aluminides are reliable bond coats that have proved effective, they also suffer from long term Al depletion due to oxidation and interdiffusion, which causes degradation. This degradation is caused by diffusion between the superalloy substrate and the bond coat. This interdiffusion causes an increase in Al consumption as two phases are formed, namely a γ' and a β phase [7]. A newer class of bond coats containing Ni, Pt and Al is being investigated that forms a γ-γ' phase structure. This phase structure is very similar to the structure present in the underlying superalloy substrate, thus the coating undergoes less interdiffusion and displays better mechanical properties than β-aluminides [8].

The top coat layer is generally composed of zirconia, stabilized with yttria in solid solution, to form its cubic/tetragonal structure. This tends to be the preferred top coat material as it has low thermal conductivity (about 2.5-3 W/m K) and minimal sensitivity to temperature changes [2]. It also exhibits a linear thermal expansion coefficient and elastic modulus that is well matched to some nickel-based superalloys [9].

The key measure of a TBC system's success is its performance under cyclical thermal loads, most notably its total lifecycle. The overall performance and dependability of the TBC system depend, in part, on the methods that are used for deposition and the chemical composition of the coating layers. Two of the key mechanisms controlling the long-term durability of these systems are the growth and stability of the TGO and the behaviour of the BC/TGO interface. This interfacial

zone has been identified, in particular, as a region of interest [10] as the adherence between the TGO and BC is a key component in assuring TBC durability. Various mechanisms contribute to the failure of these coatings but it has been stipulated that the genesis of most failures lies in this zone [10, 11]. One of the phenomena that occurs in this interfacial zone is the continuous oxidation of the bond coat layer, which generates and further builds the TGO layer. The formation of this oxide depends, fundamentally, on the composition of the bond coat and the exposure temperature and time. Furthermore, it is generally accepted that the adherence at this interface can be affected greatly by the segregation of impurities. In particular, the segregation of sulphur atoms is known to reduce the adherence of the TGO layer [10, 12]. The relationship between these two layers is of critical importance as this is the transition zone between the metallic properties of the substrate and the ceramic properties of the TBC system.

The oxidation performance, and ultimate behaviour, of coated systems has been identified as being particularly varied depending on the elemental composition of the bond coat [12]. Other studies have provided hypotheses into how these elemental additions affect the behaviour of these coatings [10, 13, 14]. These studies focus on the effect that segregated impurities have on the adherence of the BC/TGO interface. It has been stipulated that the presence of Pt may limit the segregation of impurities [10], or may limit the co-segregation of binary impurities, such as Cr and S, which in turn limits deleterious effects on adhesion. Other studies [11, 12] focus on the morphological aspects of the growth of the TGO layer. These stipulate that voids or "pegs" may form at the interface, the result of which is in dispute and will be discussed in the following chapter.

Investigations into the performance of TBC systems are extensive and on-going. The difficulty

in establishing a full description of the behaviour of these systems is, arguably, four-fold. Firstly, these coatings undergo either cyclical thermal loading or isothermal loading. These two dissimilar loading criteria share the common trait in that they both experience phenomena such as atomic diffusion. However, highly cyclical applications may not be as susceptible to other phenomena, such as creep, as isothermal applications may be, and vice versa. These dissimilarities complicate analysis and modelling, as they require separate parameters to adequately define the true behaviour of these systems. Secondly, these coatings are made up of coating layers of various thicknesses that, quite often, vary over time. These variations can impose modulating residual stress fields, which alter the global behaviour of these systems. Furthermore, these coated layers are also on the scale at which microscopic details are critical. Adequately robust analysis and modelling are required to properly describe a complete TBC system. Finally, the inclusion, or exclusion, of atomic species can have marked influences on the manifestation of various phenomena, such as cracking, and the performance of these systems. This can further complicate a holistic description of coatings designed to protect under high temperature conditions.

As previously indicated, the effect of temperature is of critical importance for oxide formation, BC/TGO integrity and the behaviour of the constituent materials. A system in either a stable isothermal condition, or in a cyclical condition scenario, will have a marked difference in the behaviour of the TBC system. Changes in temperature can affect the mechanical properties of the constituent materials. More importantly, temperature can also increase diffusivity. This in turn affects the oxidation characteristics of the coating. Firstly, the temperature is a major contributor in the phase of the oxide that forms. While there exist many forms of aluminium oxide, the main polymorphs of alumina that may typically form in gas turbines are γ, θ and α-phases, and trans-

form from one phase to the next in the same order [15]. α-alumina is the most stable and occurs at higher temperatures. The transformation from one to the next occurs as temperature increases and is irreversible. Generally, γ-alumina will transform into θ-alumina around $700 - 800^{\circ}\mathrm{C}$ and then to the α phase at approximately $1050^{\circ}\mathrm{C}$. Changes in exposure temperature of as little as $50^{\circ}\mathrm{C}$ can have a substantial impact on the growth and stability of the aluminium oxide [8]. Therefore, temperature can have an effect on the thickness of the coating as a result of influencing oxide growth, while also affecting the properties of the constituent materials.

1.1 Motivation and Research Objectives

As indicated, there are many considerations that must be taken into account when considering TBC systems. It is well known that the presence of atomic species in the composition of the bond coat, and even the substrate, can have an effect on the performance of the BC/TGO interface. However, the mechanisms driving this phenomenon are not well understood. In order to design better TBCs to support the need to increase the operating temperatures of gas turbine engines, the function of these elements must be determined.

The main objective of this work is to elucidate the contribution that some elemental additions present in TBC systems, such as platinum (Pt), sulphur (S), yttrium (Yt) and hafnium (Hf), have on the interfacial fracture toughness of the BC / TGO interface. More specifically, the effect these elements have on the fracture toughness at the interfacial zone between the BC and TGO is to be determined as a function of oxide thickness and exposure temperature. Although it is preferable to also study the contributions of these elements under cyclic conditions, representative of in-service

aerospace turbines, this investigation concentrates on increasingly higher temperature isothermal conditions. This provided a pseudo-cyclical scenario appropriate for analysis.

This investigation is a component of a larger research study focused on generating a more complete understanding of elemental effects related to the application of thermal barrier coatings in order to optimise material compositions for high performance systems. As a companion study, this research builds upon an atomistic modelling investigation that considered interfacial effects of adhesion of doping elements at the BC/TGO interface. As the genesis for a continuum level model of these systems, the current research considered the following:

1. The simulation had to be carried out as a temperature cycle, therefore the thermo-elastic properties, such as yield strength and elastic moduli, of the constituent materials had to be expressed as functions of exposure temperature.

2. Since the coatings fail through spallation, a reasonable course of action was to centre the investigation on fracture mechanics. Therefore, the stress states of the BC/TGO interface needed to be determined. Analytical results for the following had to be established:

    - These coatings undergo thermal cycling; therefore residual stresses at the interface had to be defined.

    - To balance the stress to simulate an intact interface, the effect of bond strength had to be taken into account.

    - The balance of these stress states had to be determined to establish a critical stress criteria.

3. Once the stress states were described and expressions for the thermo elastic properties were found, a simulation was developed that would determine the fracture toughness of a uniaxially-loaded interface.

1.2 Thesis Outline

The details of this research have been divided into six chapters.

Chapter 1 provides general background into the subject of thermal barrier coatings and the impact of elemental additions. It also provides details related to the objectives of this research.

Chapter 2 is a review of the pertinent literature related to this research undertaking. This review provides detailed information about thermal barrier coating manufacturing, compositions and failure and also highlights experimental investigations that were reviewed in preparation for this research. Details concerning analysis techniques, including finite element modelling and material related to atomic modelling, including quantum mechanics, are also included.

Chapter 3 provides an overview of how the model that was built as part of this research was designed. This investigation serves as an initial foray into attempting to bridge atomic modelling with fracture mechanics. Therefore, this chapter serves to describe the approach and methodology used to generate a reliable simulation that combined these two length scales. This includes considerations for the development of mathematical equations used to describe thermo-elastic properties, stresses in thin films as well the bond strength of the bond coat / thermally grown oxide interface, as well as terms describing its fracture.

Chapter 4 presents the results from modelling single element doping simulations as well as co-doping simulations.

Chapter 5 provides a discussion of the results that were the outcome of this investigation. The first model that was simulated was a clean interface that had no element doping. These findings were used as a baseline against which subsequent simulations were compared in order to ascertain what effect the elemental additions were having on the interfacial fracture toughness of the system.

Finally the conclusion, Chapter 6, serves to summarize the findings of this investigation. The closing remarks will also provide suggestions and recommendations for future work that may build upon this study.

Chapter 2

Literature Review

This chapter will serve to familiarize the reader with the topics of thermal barrier coatings, bond coat compositions, oxidation behaviour, BC/TGO interfacial properties as well as atomistic modelling and simulation.

2.1 Thermal Barrier Coatings

As previously indicated, thermal barrier coatings in aerospace and industrial turbine applications consist of material layers bonded to the superalloy substrates of the turbine blades. These layers traditionally consist of a thermally resistant ceramic top coat, commonly yttria-stabilized zirconia (YSZ), bonded to a nickel-based superalloy substrate (turbine material) through the use of an intermetallic bond coat (BC) [5, 8, 16]. The YSZ is most commonly deposited using electron beam physical vapour deposition (EB-PVD), though other methods such as chemical vapour deposition

(CVD) and plasma spray (PS) are also relatively common [9]. YSZ top coats deposited by the EB-PVD process are typically 100 – 200 μm thick. Similarly, BC layers can be deposited using a variety of technologies, including cold spray, high velocity oxyfuel (HVOF) and EB-PVD, but are most often applied using plasma spray or CVD [17, 18]. In the fabricated, or "as-deposited" state, the YSZ and the BC layers are the only constituents of the TBC. During fabrication or, rarely, as the turbine is operated and thermally cycled, this TBC develops a layer of thermally grown oxide (TGO) [9]. This TGO is a very thin layer, typically an order of magnitude smaller ($<$10 μm), of oxide that forms at the interface between the YSZ and the BC. Experimental testing has shown that the failure of the TBC system is often associated with the failure of the oxide scale along the TGO/BC interface [10]. Therefore, this TGO layer is of utmost importance and the design of the TBC must take the growth of this oxide scale into account.

Currently, zirconia, stabilized in its cubic/tetragonal structure with yttria in solid solution, is the preferred top coat material. Since it has low thermal conductivity (about 2.5-3 W/mK), minimal sensitivity to temperature changes [2], as well as a linear thermal expansion coefficient and elastic modulus that is well matched to some nickel-based superalloys [9], it is an ideal top coat. Developments in top coat materials are on-going, and new materials, such as dysprosia stabilized zirconia [19], are currently being studied but YSZ remains as the standard. The EB-PVD deposition process results in a columnar grain structure, which allows the YSZ layer to adapt and expand to address thermal expansion mismatches. Although the columnar grain structure provides excellent thermal properties, it does result in a layer that is permeable to oxygen. This permeability promotes oxidation of the layers underneath the top coat during thermal cycling. There are many different oxides that may form as a result of the oxidation of the intermetallic bond coat. The composition

of these oxides is dependent on the available elements present in the bond coat. Alpha-alumina (α-Al_2O_3) has been identified as being the preferred oxide as it exhibits low oxygen diffusivity and superior adherence [20]. It is also known to provide adequate protection with minimal thickness and has a uniform morphology [2]. The characteristic of forming a uniform morphology creates an oxide layer that is highly adherent [20], as a nonuniform morphology can lead to discontinuities lowering the coatings ability to adhere to either the bond coat or the top coat. Therefore, the TBC system should be designed to be partial to α-Al_2O_3 formation instead of other oxides, such as $NiAl_2O_4$, for example.

In order to preferentially form alumina, a nickel-based high-aluminium concentration bond coat must be applied to serve as an Al reservoir to support oxide formation. Two typically used bond coats are NiCoCrAlY, known as a "MCrAlY" or Pt-modified diffusion aluminides. MCrAlY bond coats are usually two-phase layers consisting of a β-NiAl with either a γ-matrix Ni or γ'-Ni_3Al [20].

There is a wide range of considerations that must be taken into account when designing TBC systems. Oxidation performance and reactive element effects, including such phenomena as platinum and sulphur effects, are issues that have a substantial impact on the overall performance and lifetime of these coatings systems. Many scientists and engineers have investigated the performance of these systems and have developed a vast amount of knowledge. Unfortunately, a complete understanding of the overall behaviour of these coatings remains elusive.

2.2 Bond Coat Compositions

There are several commonly used commercial bond coat families used for aerospace and industrial applications, and these are; MCrAlY, β-NiAl and γ-γ'. Since the modelling requirements of this investigation focus primarily on nickel-aluminides, the review will focus primarily on the elements that are present, the size of the deposited layer, and the conventional material properties related to this specific bond coat composition.

TBC coatings can often include many additions and modifications to their compositions to improve the performance of the various aspects of a thermal barrier coating. Elemental additions are often included in order to enhance the bond coat's ability to preferentially form an α-Al_2O_3 oxide layer, increase the toughness of the coating and/or to improve the adhesion characteristics of the system. Aside from elemental additions in the bond coat, it should also be noted that elemental reduction is also performed to enhance properties, or limit the negative impact some elements can have on the system. One such reduction is the minimization of sulphur in substrate materials. For example, in an effort to reduce the effect sulphur can have on the TGO/BC interface, superalloys can often have a sulphur content below 1 ppma (parts per million, atomic) [17] to limit S diffusion.

The β-NiAl and MCrAlY systems have often been used in investigations into the performance of TBC systems [7,8,10,14,18,19,21,28]. This is partly due to the obvious presence of aluminium, which enhances the preferential formation of α-Al_2O_3, but is also indicative of the ability of the coatings to include platinum in substitution. These two systems also appear to have been the most commonly applied compositions used in the turbine industry. As a result, there are still substantial

areas of investigation related to γ-γ' bond coats, as they seem to be a less commonly applied material in the field. This by no means implies that research into MCrAlY or β-NiAl is out-dated, as there are still many questions that remain unanswered.

2.2.1 Bond Coats – MCrAlY

The first use of commercial MCrAlY bond coats were formulations patented by Pratt & Whitney in the 1960's [5]. As previously noted, the first was an iron-based FeCrAlY, followed by a CoCrAlY and finally a NiCoCrAlY [5]. These coatings were initially deposited using vacuum induction or EB-PVD and were used primarily as airfoil coatings to reduce oxidation and hot-corrosion of turbine components. Deposition eventually progressed to plasma spraying processes, HVOF and more recently as combined electroplating – powder entrapment processes developed by Praxair Surface technologies [5]. As the methods of deposition evolved, so did the use of the MCrAlY coatings, eventually being used as abradable coatings and TBC bond coats [5].

The composition of these coatings, combined with their application as overlay coatings, provides increased flexibility when compared to diffusion coatings. As MCrAlY coatings have four or more elements, the composition can be tailored to the anticipated application of the coated component. One particular element of note is the addition of chromium, which, similarly to corrosion resistant steels, provides corrosion and oxidation resistance. The presence of chromium means that less aluminium is required to maintain a protective oxide as the chromium itself provides some inherent protection.

These coatings generally consist of a binary microstructure including β-NiAl and γ-matrix.

While the β-phase provides the Al reservoir required for aluminium oxide formation, the γ-matrix provides enhanced ductility. As the coating oxidizes, it forms a protective layer of oxide, preferably α-Al_2O_3, that is regularly replenished by the β-phase. Oxide protrusions called "pegs" typically also form. The function of these pegs is disputed. Some argue that they are one of the phenomena that provide an enhanced adhesion in MCrAlY coatings [11]. It has been observed that while cracks may be in the vicinity of these pegs, it does not seem that the cracks can propagate from, or are able to propagate through, these protrusions, thus enhancing adhesion [11]. However, others argue that they encourage spallation since these pegs generate areas of higher stress, thus encouraging delamination [12]. Similar to the other bond coat families, MCrAlY bond coats have also benefited from the addition of reactive elements. Yttrium (Y), hafnium (Hf) and zirconium (Zr) as well as silicon (Si), rhenium (Re), tantalum (Ta) and platinum (Pt) have been observed to provide some beneficial effects to these coatings, but their addition, like other elemental additions, must be carefully controlled.

2.2.2 Bond Coats – γ-γ'

The development of γ-γ' bond coats is a result of identifying Al depletion that occurs in β-aluminide coatings. The γ-γ' phase structure is very similar to the structure present in the underlying superalloy substrate, thus the coating undergoes less interdiffusion and displays better mechanical properties than β-aluminides [8]. Haynes *et al.* published cyclical testing results for these coatings, indicating a life of up to 1600 cycles at 1100°C and 600 cycles at 1150°C [24]. This also indicates a strong dependence on exposure temperature. Unfortunately, since this approach is more recent, the overall oxidation behaviour of these coatings over wide ranges of temperatures

and conditions is uncertain.

The process to manufacture this class of bond coat starts with electroplating Pt, similar to β-aluminides. Following electroplating, the specimens are then annealed to form the γ-γ' structure through interdiffusion with the substrate. The reported advantages of this form of coating are reduced coating thickness, reduced manufacturing costs, improved phase stability, reduced coating rumpling and maintaining good oxidation resistance while reducing Al depletion [24]. The primary concern with these coatings lies in their oxidation performance over longer time frames at high temperature.

2.2.3 Bond Coats – β-NiAl

As previously noted, β-NiAl bond coats are part of a bond coat family known as diffusion aluminide bond coats and typically range between 50 – 100 μm in thickness [5]. These coatings are often produced using a pack cementation process, or more advanced processes, such as vapour phase aluminising (VPA) or chemical vapour deposition (CVD), beginning with a Ni-based substrate. VPA and CVD are used when internal features require coating. Since pack cementation deposition is a 'line of sight' process, parts of a component that may be internal, or otherwise obscured, must be coated using a vapour phase process. These diffusion aluminide coatings have shown to have excellent protective properties during thermal cycling. An example of this behaviour can be seen when analysing mass gained as a result of thermal cycling in Figure 2.1.

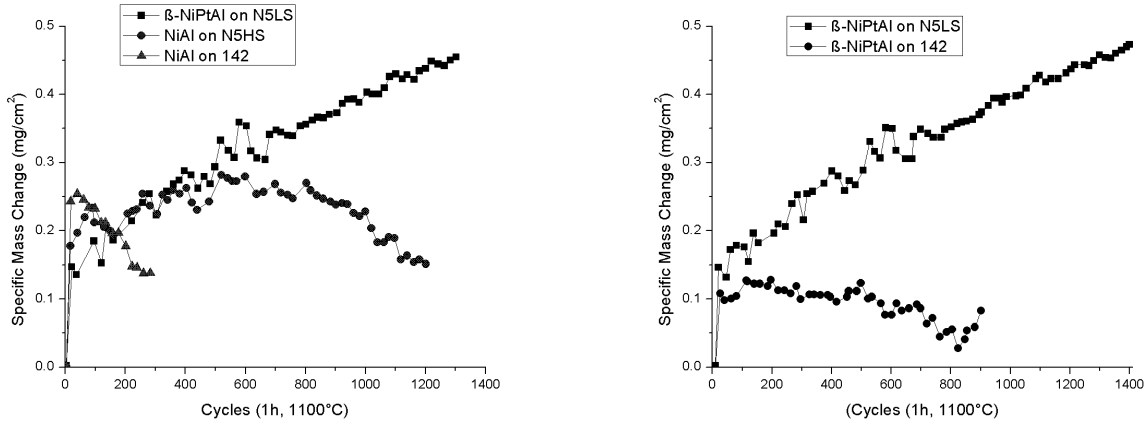

a) b)

Figure 2.1: Bond coat oxidation as a result of thermal cycling up to 1100°C for a) NiAl and NiPtAl bond coats and b) NiPtAl and γ-γ' bond coats on various superalloy substrates [13].

This figure shows the various oxidation behaviours that can occur as a result of material composition. The compositions of the substrates noted in Figure 2.1a) and b) can be seen in the table that follows.

Table 2.1: Trace element compositions for various superalloy substrates [13].

Alloy	S	Hf	Zr	Y
N5LS	1.4	679	100	3.6
N5HS	5	582	57	4.6
N5Y	3.7	427	55	106
R142	11	5180	66	N/A

(*ppma = parts per million, atomic)

These compositions obviously have varying effects on the oxidation characteristics of the bond coats. For example, when simply comparing high sulphur and low sulphur substrates in Figure 2.1, denoted by “HS” and “LS” respectively in Table 2.1, low sulphur samples generally have a more consistent oxide growth that remains adhered throughout the thermal cycling. By contrast, the high sulphur samples have unpredictable oxide growth and often show premature spallation compared

to their low sulphur counterparts. Specifically, when comparing the mass change of the R142 alloy to the N5LS alloy in Figure 2.1b), both coated with β-NiPtAl, it is evident that the substrate has had some significant impact on scale growth and adhesion. Empirical results have shown that the higher sulphur content could be the primary reason for this phenomenon, though to the author's knowledge, no conclusive analytical results have yet been reported. This shows how interdiffusion between the bondcoat and substrate can affect the oxide growth. Since the behaviour of the oxide layer can be a determining factor for the overall lifecycle of the coating system, it is critical to have predictable and reliable oxide growth and adherence.

Another phenomenon can also be noted from Figure 2.1. The addition of platinum can also have an effect on the oxidation of these bond coats. Therefore, it can be stated that these coatings can be imparted with different properties as a result of reactive element additions, such as hafnium, yttrium and sulphur, as well as platinum addition to the composition. In particular, one noted effect is that platinum has been observed to enhance aluminium diffusion during diffusion aluminising and improves the oxidation properties of the resulting coating [5]. However, the mechanisms that determine these behaviours remain undefined.

2.2.4 Bond Coats – β-NiPtAl

The process of incorporating platinum in the coating comprises of grit blasting the substrate and then electroplating with a layer (5 to 10 μm) of platinum. This can be achieved by either:

- First electroplating a thin layer of Pt on a Ni substrate, followed by a heat treatment. Then a layer of Al is deposited and then heat-treated again to encourage diffusion.

- First creating a layer of Al on a Ni substrate, then heat treating, followed by electroplating a thin layer of Pt and then heat treating to encourage further diffusion; the opposite deposition order as that identified in the first point.

Once the electroplating is complete, the diffusion aluminide process begins. This can result in somewhat different morphologies, as seen in Figure 2.2, below.

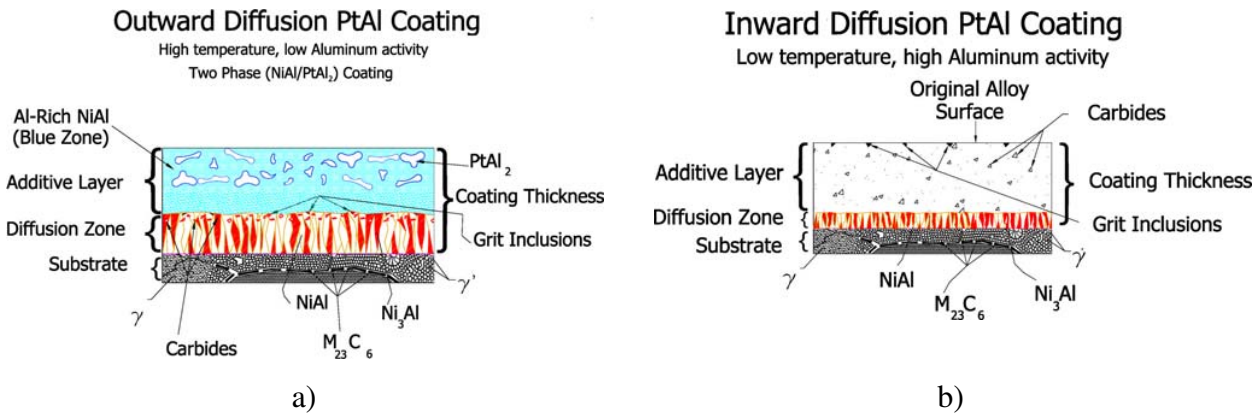

Figure 2.2: Microstructure schematics showing outward and inward diffusion coatings, created from low activity and high activity processes [5].

These two morphologies are dependent on the temperature at which the aluminising process proceeds, as well as the Al concentration. It is important to note that in the inward diffusion process, carbides and other inclusions can be trapped near the alloy's surface. These inclusions often result in reduced performance, as they will typically lower the corrosion and oxidation resistance of the coating. Another deleterious effect can arise from the presence of a substantial $PtAl_2$ phase. Although this phase can provide an obvious platinum reservoir, an abundance of this compound can also result in the embrittlement of the coating [5]. Therefore, since the platinum aluminide coating will react readily with the substrate, the deposition of the NiPtAl bond coat must be tailored to the specific superalloy composition being used. If the deposition isn't adequately controlled, the

process could give rise to a sizeable fraction of a $PtAl_2$ phase, which may embrittle the interface, as well as a secondary reaction zone, which would both impede the performance of the coating [5].

2.3 Oxidation Behaviour

Oxidation performance is a key characteristic in the overall behaviour of the thermal barrier coating. Coating spallation is often a result of the oxidation behaviour at the underlying TGO and BC interface. TGO formation typically occurs at three stages. First, during initial fabrication, the recently deposited Al coating is oxidized in a heat treatment chamber. The second stage of TGO formation occurs when the YSZ TBC layer is deposited. Finally, as an engine is first cycled to service temperature, the oxygen penetrates the YSZ top coat and begins to interact with the surface of the metallic bond coat. This interaction begins the third oxidation process. As indicated previously, the high concentration of aluminium in the BC provides a reservoir that, provided with adequate temperature control, promotes the preferential formation of an α-Al_2O_3 oxide layer. There are many factors involved in the growth of this oxide, though the mechanisms are not well understood. Many studies [1, 2, 8, 10, 13, 17, 24] have been conducted into the behaviour of the TGO layer, though specific and concise mechanisms to properly describe the overall behaviour are yet to be developed [1, 2, 4, 6, 9, 14, 15]. Many of these experiments studied the effects of substrate and bond coat compositions on TGO behaviour during cyclic and isothermal oxidation.

One difficulty that does exist in developing a complete theory for oxidation behaviour and elemental addition effects is the fact that experimental studies have included a very wide range of substrates, bond coats and processing methods. Each of these variables can lead to significant

changes in experimental results. For instance, Haynes *et al.* [13] investigated the cyclic oxidation behaviour of three different bond coatings applied to four separate substrates, each with various elemental compositions. The testing was also composed of three separate temperature exposures during hour long sample cycling. The results of these tests showed that the elemental composition of the substrates and bond coats alone had tremendous impacts to the performance of the oxide/bond coat interface, regardless of the exposure conditions. Further to the composition of the substrates, the composition and development of the bond coat also has an effect on the resulting oxide layer.

Kim *et al.* [25] provide an interesting point of view related to the study of TBC systems, exploring the variety of testing conditions. They aptly observe that many of the conclusions in this area of materials research have been made on similar coatings, but under varying exposure conditions. The study describes how vastly different results are gathered from exposing samples to different cycling temperatures. In their study, they observed that a Pt-Aluminide coating failed after 1570 1100°C cycles when the "cool" phase of the cycle was held for one hour at 35°C. Conversely, when the same sample composition was exposed to a "cool" phase of one hour at 210°C, the sample failed after 2403 cycles, a 53% lifecycle increase. This indicates that differences in exposure conditions during cycling can have a large impact on results. Therefore, this additional variable must be taken into account when considering the studies undertaken by different investigators.

Additionally, Haynes [12] noted that the surface characteristics of the substrate influence the oxide growth as well as void formation. It was indicated that roughened surfaces cause a stable α-alumina scale to form more rapidly than smoother surfaces. Concordantly, this can cause differences in transformation rates for other alumina phases which can result in enhanced void formation

on smooth surfaces related to the reduction in local stress and volume. Another suggestion was that interfacial voids might form due to the influence of sulphur impurities at or near the surface of the as-deposited bond coat that exceed a critical concentration.

As previously indicated, sulphur has been identified as an element of concern when dealing with thermal barrier coating systems. Many investigators [12–14, 17, 26] have explored the influence of sulphur, and industrial production has also focused on minimizing the sulphur content of substrate materials. Many potential mechanisms by which sulphur may act have been presented, though no conclusive interaction has been agreed upon. Gaudette *et al.* [26] found that a Ni-20at.%Cr foil sandwiched between two sapphire plates and then heat treated showed failure at the interface where sulphur had segregated. This implied that the trace elements of sulphur led to the local embrittlement, or loss of ductility, at the interface. A loss of ductility at the interface could also be cause for a reduction in fracture toughness. From Molins *et al.* [14], it is identified that sulphur can increase interfacial porosity at the TGO/alloy interface, weaken interfacial bonding or lower the fracture toughness of the interface. They found that oxidizing a NiPtAl coating bonded to a Ni-base superalloy substrate, that contained a γ-matrix with γ' precipitates, resulted in the detection of sulphur along with chromium particles that had precipitated to the boundaries of the γ' platelets. This demonstrates a co-segregation between chromium and sulphur. Zhao and Xiao [10] also identified a clear correlation between the presence of chromium and the presence of sulphur along the TGO/BC interface. It should be noted that these findings are not in agreement with findings from Haynes [18]. A co-segregation phenomenon between chromium and sulphur was not apparent from glow discharge mass spectrometry (GDMS) from testing conducted in 2001. These disparate results may have been caused by reduced resolution in the case of GDMS since the shape of any

re-deposited material and the geometry of the sputter crater can influence the data collected using this method. Since sulphur is known to segregate to surfaces and interfaces it is speculated [17] that the reduced scale adherence is likely due to the increased formation of voids at the TGO/BC interface or bond weakening at the interface. The negative influence of sulphur, Figure 2.3, can be inferred for raw alloy samples that are not yet coated.

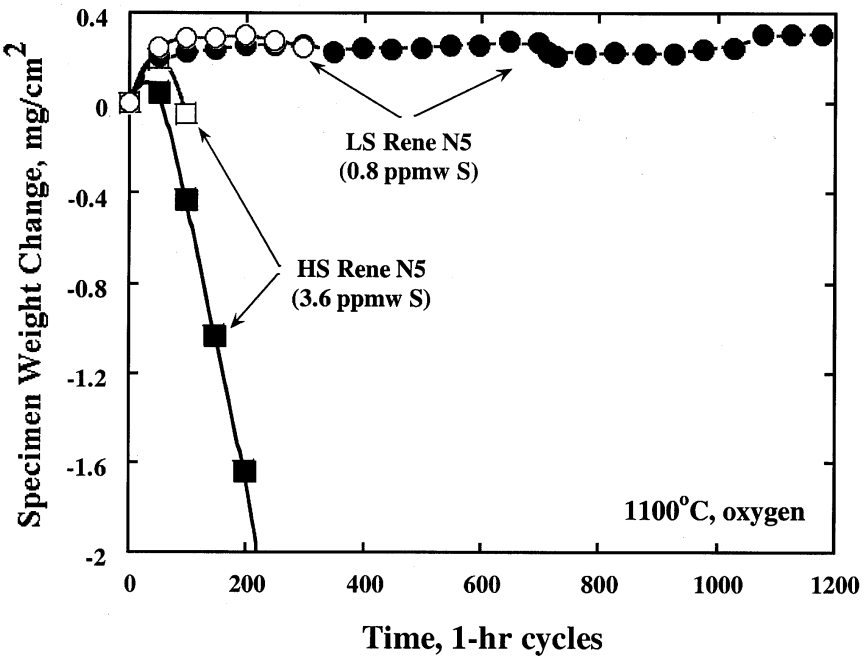

Figure 2.3: Plot indicating mass change as a function of 1-hour cycles for uncoated raw alloy samples [17].

This would tend to indicate that, while other elemental concentrations remain unchanged, sulphur concentration clearly has a substantial effect on the oxidation and subsequent spallation of the sample, even without any effect attributed to the presence of a bond coat.

All these experimental findings would indicate that the elemental composition of these coating systems, especially when considering the bond coat material since it's atoms readily diffuse, play a substantial role in the oxidation performance of these coatings. Since failure is generally

accepted to begin at the TGO/BC interface [10, 14, 26], it can then be concluded that the elemental compositions play a key role in the lifetime of the coating.

2.4 BC / TGO Interface

Since the failure of TBC systems generally tends to begin at the interfacial zone of the bond coat and thermally grown oxide, it is of value to consider this region with more depth. One must consider the morphology of this interface, the presence of voids or other perturbations as well as material handling and processing in order to accurately describe the physical characteristics of this zone.

2.4.1 Interfacial Morphology and the Interdiffusion Zone

The morphology of the interface between the bond coat and TGO layers is one major factor affecting the adherence of TGO and, by extension, the entire TBC system. This morphology is heavily dependent on sample preparations related to experimental investigations as well as commercial manufacturing methods. An aspect related to the interfacial morphology is the development of an interdiffusion zone that forms beneath the bond coat. This zone can play a serious role in the performance of the TBC. As indicated by Taylor *et al.* [21], the composition of this zone can vary depending on the substrate alloy and may be comprised of discrete particles with elements from the superalloy. These elements can be expected to diffuse and act like reactive elements through the lifecycle of the component, thus affecting the development of the TGO scale. Therefore, this layer can have a marked effect on the growth and formation of the oxide layer and its morphology.

2.4.2 Interfacial Void Formation

The formation of voids in the interfacial zone between the bond coat and the thermally grown oxide is one of the most critical phenomena in TBC systems. It has also been observed that large internal voids can also form within the Al_2O_3 scale [27]. The primary concern with interfacial voids is the likely reduction in adhesion properties between the two layers. As interfacial voids grow larger, they cause a reduction in the contact surface between the BC and TGO, which can often be the cause of spallation during later cycles. Pint proposed a model [27] related to the formation of internal and interfacial voids that takes the surface energies of the system into account. The preface to developing the model was the fact that the interface between the metallic bond coat and the oxide scale was often characterized by small perturbation voids. The voids, which are between 20 to 200 nm in diameter, are presented as being the root from which larger interfacial and internal voids grow. Based on the presence of these small voids, it was proposed that adding reactive elements may not necessarily inhibit the formation of interfacial voids, but may instead slow the formation of perturbation voids. Pint's model was presented as a two-dimensional simplification based on liquid wetting as follows:

$$\sigma = \gamma_m cos\phi + \gamma_{ox} cos\phi - \gamma_{int} \tag{2.1}$$

The stress required for void growth is σ while γ_m, γ_{ox}, γ_{int} are the surface energies of the metal, oxide and interface, respectively and:

$$\phi = cos^{-1}\left(\frac{\gamma_{int}}{\gamma_m + \gamma_{ox}}\right) \tag{2.2}$$

Based on this formulation, the presence of sulphur at the metal surface could cause a reduction in the γ_m term thus making void growth more likely. Segregation of the sulphur ions to the interface would also likely cause a reduction in γ_{int}, which would have a similar impact. Although this model may also indicate that reactive element segregation to the metal/oxide interface would cause a reduction in γ_{int}, this does not seem to be the case. This would indeed cause a reduction in void growth, yet some observations have shown that RE additions do not improve performance beyond what is observed for desulphurised samples. If RE additions did reduce γ_{int}, then they would also be expected to have additional benefits, though this has not been observed.

Pint indicates [27] that reactive element additions may instead hamper the segregation of sulphur from the bulk material to the metal/oxide interface. The mechanisms by which the RE elements provide this benefit are not understood, but it is argued that the mechanism is purely an interface phenomenon and does not rely on any sulphur gettering in the bulk material. Furthermore, it is indicated that the presence of Y_2O_3 at the interface is at least as sufficient as alloying with yttrium or desulphurisation in improving scale adherence performance. This would tend to indicate that the presence of RE ions at the interface is enough to limit the segregation of sulphur, thus inhibiting void growth. This argument implies that there is no sulphide forming activity driven by the RE additions in the bulk material. Therefore the mechanism by which the RE doping provides a benefit to the system would seem to be interface-specific and may not depend on compound forming characteristics.

Consequent to interfacial voids, it is possible that internal voids form in the oxide as a result of oxide growth. As interfacial voids grow, it is possible that they become incorporated into the grow-

ing oxide and become fully enveloped. Should the growing oxide undercut an interfacial void, it can become an internal void, at which point it would have little impact on the scale adhesion properties at the metal-oxide interface. However, if internal voids were to coalesce, it can be concluded that the large voids would ultimately cause a reduction in local internal integrity. Unfortunately, the specific impact this may have on the interfacial characteristics of the system remains to be investigated [22].

Based on Pint's observations, it may be suggested that interfacial adherence relies on void growth rather than nucleation. Since it would seem that perturbation voids are commonly present regardless of RE-doping techniques or treatment processes, it would be reasonable to expect that inhibiting the growth of these voids is of primary concern rather than attempting to inhibit their nucleation. These observations also seem to indicate that RE-additions have little effect on the presence of bulk S in the bond coat, but do clearly have an effect on the segregation of deleterious elements and void growth at the interface of the oxide and bond coat layers.

2.4.3 Experimental Sample Preparation and Surface Treatment

When preparing samples for oxidation testing, many different configurations have been used. Cylindrical, plate, and disk shape specimens are often used in both isothermal and cyclical oxidation testing processes. One interesting consideration to note is whether plate and disk samples undergo appropriate envelopment of both Pt-electroplating, for Pt-added samples, and bond coat aluminising. It has been noted in one case [22] that cylindrical samples have indeed been identified as having been enveloped by all layers of the TBC system, but this same characteristic has not been

explicitly defined in other specimen shapes. This note is simply based on the fact that if samples that are not completely enveloped undergo oxidation testing, it is possible that the mass growth associated with the formation of oxides does not necessarily correspond to the growth of oxides at the bond coat/top coat interface. This could occur in specimens, particularly plates and disks, where uncoated substrate surfaces oxidize concurrently with interfacial zones, thus leading to an aberration in data related to mass gain resulting from cyclical or isothermal exposure.

2.4.4 Commercial Processing and Surface Contamination

Based upon previous observations indicating the effect atomic elements can have on the oxidation of these coatings, it is clear that the properties of the BC/TGO interface can be affected by the presence of surface contaminants. One such contaminant is sulphur. As previously indicated, the presence of sulphur can have substantial detrimental effects on the performance of TBC systems. One potential reason for this reduction in performance is the increase in void formation. Haynes [12] indicated that surface concentrations of sulphur can exceed 20 ppmw (parts per million, weight), which is more than 40 times the bulk material concentration. This surface contamination can be caused by many factors in commercial processing including, but not limited to; specimen handling and cleaning, processing equipment such as CVD or EB-PVD systems, Pt electroplating, or local impurities. If local impurities are considered, surface treatment such as grit blasting can remove excess sulphur. Grit blasting also causes the surface roughness to increase, which has previously been indicated to affect α-alumina growth [18]. The combination of these two factors was shown to decrease void formation.

Another result of specimen preparation using grit-blasting is the evidence of reduced presence of non-α-phase Al_2O_3 scales. Haynes *et al.* [18] proposed a ratio between $\theta - Al_2O_3$ and α-Al_2O_3 oxide phase volumes, Figure 2.4c). These results indicated a large tendency towards having the presence of greater than 90%, on average, of α-phase alumina for samples that were grit blasted. This may indicate that grit blasting also has an effect on decreasing the nucleation of θ-phase alumina, or promoting the α-phase. This same study also concluded that biaxial residual stresses had been reduced after grit-blasting, as seen in Figure 2.4a). These results indicate that the compressive stresses in grit-blasted samples were likely of a lower magnitude than surfaces that hadn't been grit-blasted due to surface perturbations causing higher out-of-plane tensile stresses.

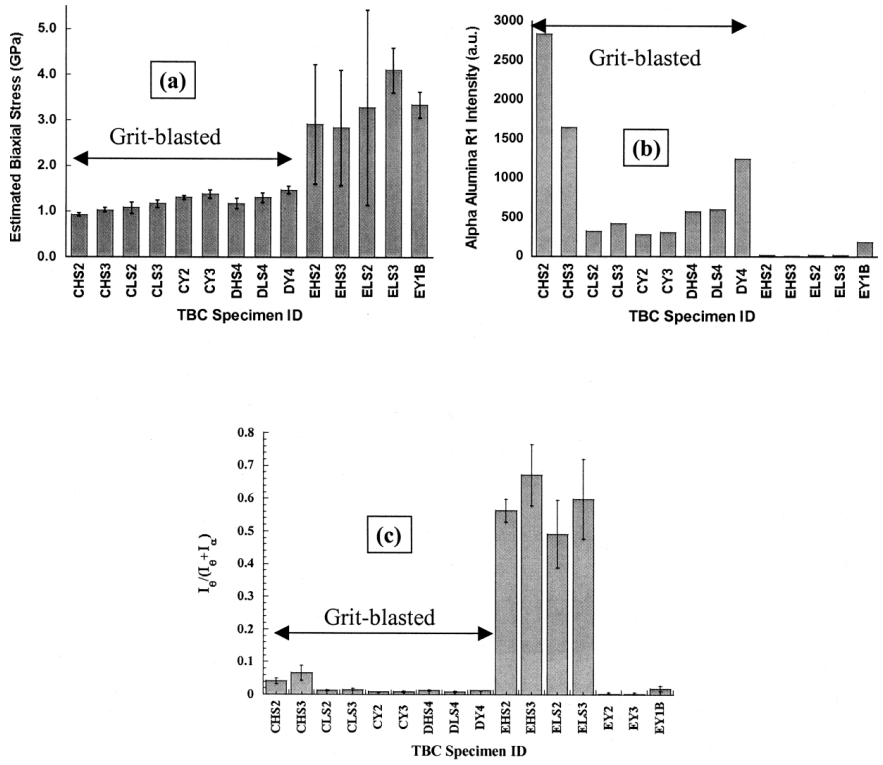

Figure 2.4: Photo-Stimulated Luminescence Spectroscopy (PSLS) measurements of various substrate compositions and surface reparations coated with EB-PVD TBC systems. a) Residual stress measurements; b) α-Al_2O_3 signal intensity; c) ratio of α to θ intensities with grit blast surface preparation [18].

A drawback to this process is that it is also likely that roughening the surface may result in a reduction in interfacial adherence. Thus, for commercial applications, reducing the concentrations of surface contaminants through surface roughening may also ultimately cause a reduction in component lifetime. Therefore, as stipulated by Haynes [12], treatments that remove impurities without increasing surface roughness should be of higher priority.

The importance of having "clean" or contaminant-free interfaces is highlighted in discussions presented by Evans *et al.* [28], where it is indicated that strong and stable interfaces are achieved by:

- ensuring contaminants are excluded during the bonding process, and/or
- introducing alloying elements, such as Cr or Ti, to capture contaminants and segregants and form precipitates

These points support the claims made previously and are demonstrated by Lipkin *et al.* [29] with an example of a clean interface. As this interface is systematically infused with contaminants, it was observed that weakening of the interface occurs more often than not. This is further exacerbated if moisture is introduced, especially at free edges, as this moisture can lead to stress corrosion. The idea that interfaces are inherently strong is further supported by findings that show that when an interface is clean, the energy release rates that are achieved in the metal exceed the critical energy release rate of the oxide [30].

2.5 Mechanical Properties

The basis for the development of many of the testing methods used by contemporary investigators is based on the field of fracture mechanics. As the principle conditions upon which these coatings are evaluated mechanically tend to focus on the incidence of fracture, leading to eventual spallation, this section focuses on these same considerations. These methods have been determined to be most effective when implementing a modelling approach. Therefore, this section will provide salient points on fracture and how it is modelled.

There now exist a variety of testing methods and specimens that can be used to provide reliable measurements of interface toughness. These range from compound tensile tests to sandwich specimens that are tested for delamination [31]. Each method provides results over various phase angles, which are the orientations of the applied loads relative to the sample. Therefore it is important to investigate multiple methods. This allows an investigator to achieve more complete results across a range of mode mixities.

Another critical property that is considered when studying high temperature materials is creep. Finite element analyses have now been conducted on TBC coatings that include creep and consider time-dependent effects within the TBC for both MCrAlY and Pt-aluminide bond coats, though MCrAlY-related results are more prevalent. Pan *et al.* [32] have succeeded in studying the stress relaxation of the interdiffusion zone from chemically and mechanically extracted β-rich bond coats. Their results indicate that this interdiffusion zone will creep readily at high temperatures.

The theoretical evaluation and prediction of the performance of thermal barrier coatings spans

a variety of disciplines. Two of the more common methods include finite element modelling and fracture mechanics. These methods attempt, with some significant success, to analyse and determine the mechanics of failure related primarily to the spallation of the oxide component of these ceramic-metal coating systems.

2.5.1 Theoretical Evaluation – Finite Element Modelling

One method used to theoretically evaluate the performance of TBC systems is finite element (FE) simulations. These simulations must be designed with exacting detail in order to properly characterize coating systems. This includes many variables, most important of which are oxide growth and surface morphology. Oxide growth is highly dependent on the composition of the bond coat, while the surface morphology is dependent on the deposition method. Some FE models of note by Busso *et al.* [23, 33] have analysed PS and EB-PVD systems. These systems have incorporated the growth characteristics of the oxide layer related to the cyclical and isothermal simulations as well as the anticipated surface morphologies. It is also valuable to note that these simulations include creep properties of the substrate and sintering of the YSZ top coat. These two phenomena lend a great deal of influence to the overall performance of these systems. Creep can potentially lead to stress relaxation, which may be amplified within specific regions of the bond coat/TGO interface. Secondly, sintering of the YSZ will result in a top coat whose elastic modulus increases during service, resulting in a higher elastic stiffness [33].

The incorporation of an oxide growth simulation is of particular interest, as it seems to be a novel application in existing FE models. Including this behaviour is notable due to the increase in

internal stress that this growth causes. The growth model presented by Busso *et al.* [33], presented schematically in Figure 2.5, relies on the understanding that the oxide layer's rate of growth is determined by two mechanisms:

- the inward diffusion of oxygen, primarily along grain boundaries at the TGO/BC interface
- the outward diffusion of Al cations along the boundaries of existing alumina particles reacting with oxygen anions at the TGO/ceramic interface

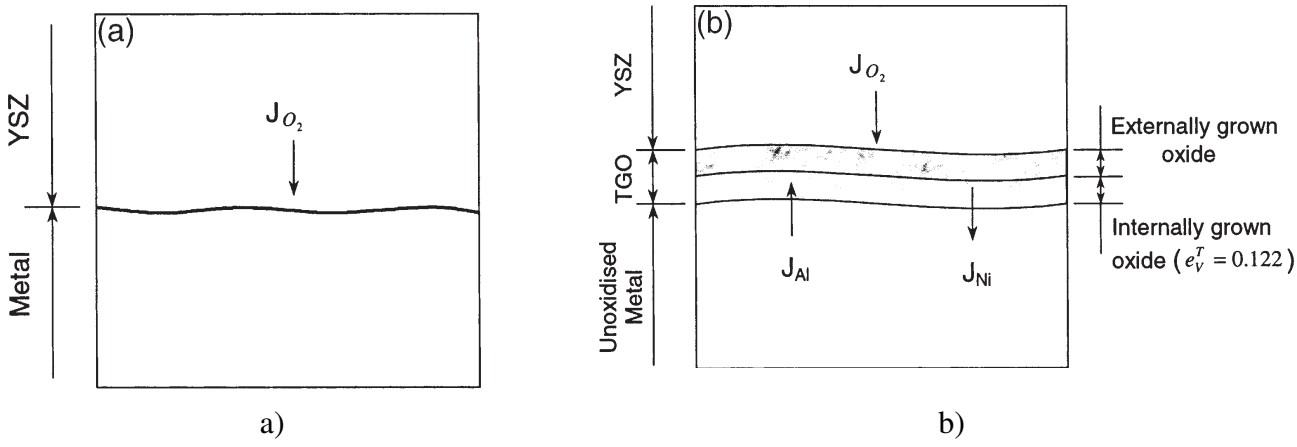

Figure 2.5: Schematic depicting the inward and outward growth of oxide during the oxidation process where a) is unoxidized and b) is the oxidized result [33].

This leads to the growth of oxide on two fronts. It is also possible for Al cations to react with oxygen anions at internal TGO interfaces, causing lateral oxide growth, but in the present model this is ignored for simplicity. Knowing this, the model was then developed based on the chemical reactions present at the interface. These reactions, from Busso *et al.* [23, 33], are:

- $\frac{2}{3}NiAl + \frac{1}{2}O_2 \longrightarrow \frac{1}{3}Al_2O_3 + \frac{2}{3}Ni$, for Plasma-Spray on NiCoCrAlY
- $NiAl + \frac{1}{2}O_2 \longrightarrow \frac{1}{3}Al_2O_3 + \frac{1}{3}Ni_3Al$, for EB-PVD on CVD Ni(Pt)Al

Incorporating effects of creep, sintering and oxide growth provides for a FE model that encompasses a wide array of the phenomena experienced by a TBC. This allows researchers to more accurately predict the behaviour of these coating systems.

2.5.2 Theoretical Evaluation – Analytical Approach

Analytical models have also been proposed regarding the failure of TBC systems. These models often focus on the local properties of the systems with relation to their failure characteristics. Consideration for stress states, geometry and the energy state of the material at local crack sites are taken into account to analyse the failure and delamination of samples.

Two different failure morphologies are often presented to explain delamination in these layered materials: edge delamination and buckle delamination, as seen in Figure 2.6.

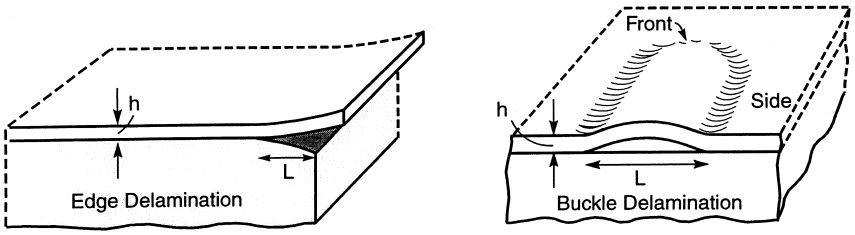

Figure 2.6: The two most common forms of delamination are represented schematically by this edge and buckle-type delamination [34].

Hutchinson *et al.* [34] present a model for buckle driven delamination. During cyclical loading, the layer of thermally grown Al_2O_3 will undergo various stress states, though most often it will be in compression once the system cools. In this state, the most commonly observed failure results from buckling delamination and spalling that arises from cracking at the BC/TGO interface. When

a thermal expansion misfit exists between the substrate and the film, it is presented that the equi-biaxial compressive stress state, σ_o, is:

$$\sigma_o = \frac{E\Delta\alpha\Delta T}{(1-\nu)} \tag{2.3}$$

where E is the Young's Modulus, $\Delta\alpha$ is the coefficient of thermal expansion misfit, ΔT is the drop in temperature from stress-free state and ν is Poisson's Ratio. From this, the energy per unit area that is available in the film once it is released but still constrained to in-plane plane strain, G_o, is:

$$G_o = \frac{(1-\nu^2)h\sigma_o^2)}{2E} \tag{2.4}$$

where h is the film thickness.

Hutchinson *et al.* [34] also provide a buckling index:

$$\Pi = (1-\nu^2)(\sigma_o/E)(L/h)^2 \tag{2.5}$$

where L is the width of separation for plane strain or the diameter of separation for axisymmetric applications.

This index provides the condition from which buckling can be determined. In order for buckling to occur, Π must exceed the critical index value, Π_c. This value stands as follows, from the same

publication [34]:

$$\Pi_c = 3.29 \text{ (plane strain buckle)}$$

$$\Pi_c = 4.89 \text{ (circular buckle, ie: axisymmetric)}$$

Substituting these values into Equation 2.5 above for the buckling index yields results for the buckling condition expressed as the ratio of the width/diameter of the distortion at the site of initiation to the thickness of the film, as follows:

$$L_b/h = 1.81\sqrt{(\bar{E}/\sigma_o)} \quad \text{(plane strain)} \tag{2.6}$$

$$L_b/h = 2.21\sqrt{(\bar{E}/\sigma_o)} \quad \text{(circular buckle)} \tag{2.7}$$

where:

$$\bar{E} = E/(1-\nu^2): \quad \text{plane strain modulus} \tag{2.8}$$

These ratios indicate the critical size ("smallest") of interface separations where buckling will cause delamination in the absence of imperfections. Based on work from Hutchinson *et al.* [35], this ratio will typically be ~ 20, where the width/diameter of the buckling is roughly 20 times larger than the film thickness for typical levels of compression and moduli.

It is stipulated [35] that a thin elastic film that is under compression and bonded to a substrate will undergo buckling-driven delamination at the interface in the event that there is an initially

debonded region within the interface when under sufficient compressive stress. This buckling-driven delamination can manifest in a number of morphologies. These morphologies depend on the activity of the crack growth front. Initially a crack may manifest as a circular blister, but this same crack may then evolve into a "worm" or "telephone cord" type blister, as seen in Figure 2.7. Though they may visually appear different, these morphologies still manifest based on the activity of buckling-driven delamination. The images in Figure 2.7 demonstrate how the change in morphology progressed as a result of generating an equi-biaxial compressive stress state by lowering the temperature of the sample [35]. This change in morphology can be accounted for by considering the relative proportions of mode I (tensile) and mode II (in-plane shear) failure modes. This requires an examination of the mixed-mode toughness of the interface.

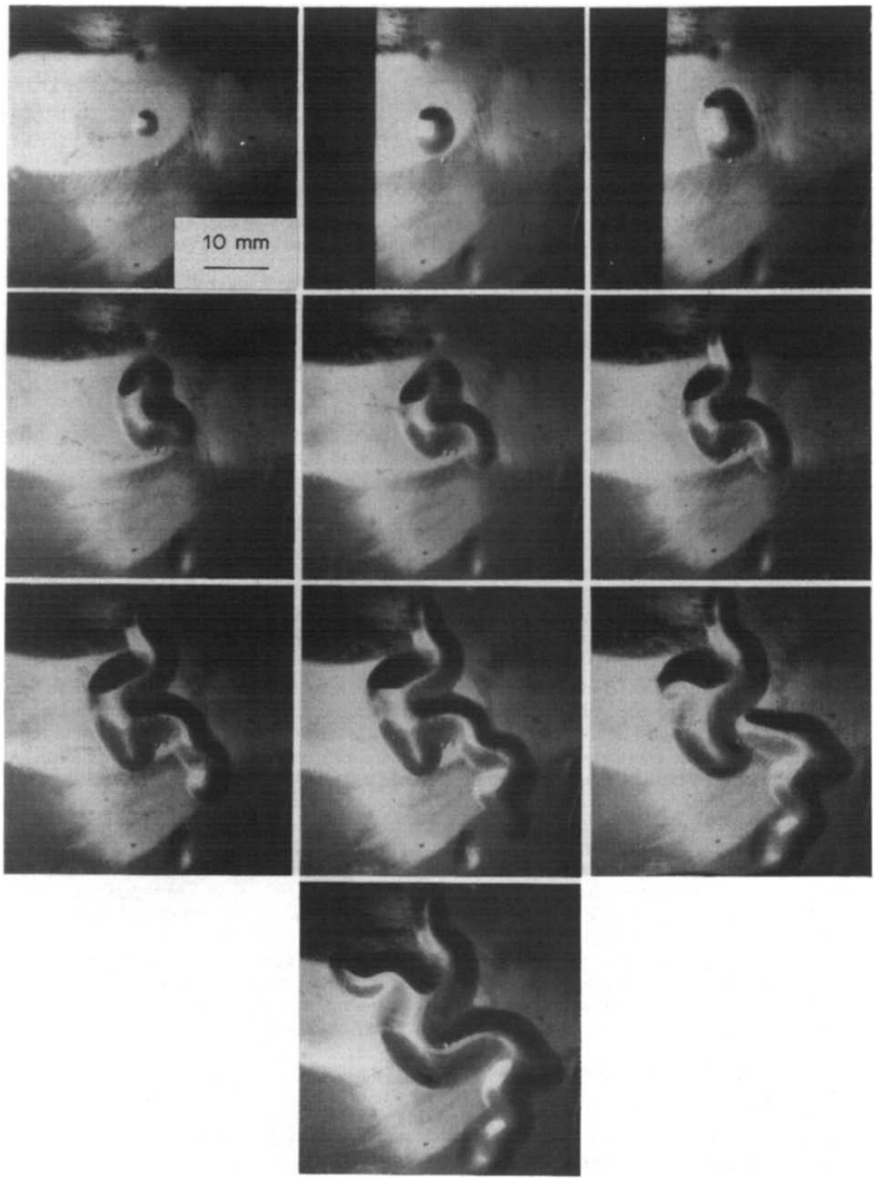

Figure 2.7: Evolution of a buckle-driven delamination circular blister to a "worm" blister [35].

Based on work from Hutchinson and Suo [36], conditions related to the energy release rate, G, and failure mode mixities, ψ, can be considered based on their determinations for plane strain and circular (blister) buckle delaminations. At this point, it would be valuable to consider the Dundurs parameters, α and β, which govern the crack fields at the plane strain interface:

$$\alpha = \frac{\mu_1(1-\nu_2) - \mu_2(1-\nu_1)}{\mu_1(1-\nu_2) + \mu 2(1-\nu_1)} \tag{2.9}$$

$$\beta = \frac{\mu_1(1-2\nu_2) - \mu_2(1-2\nu_1)}{2\{(1-\nu_2) + \mu_2(1-\nu_1)\}} \tag{2.10}$$

Also, from the relation indicated above for the plane strain modulus, $\bar{E}$, the following expression for α can be developed:

$$\alpha = \frac{(\bar{E}_1 - \bar{E}_2)}{(\bar{E}_1 + \bar{E}_2)} \tag{2.11}$$

This expression indicates that this parameter measures the plane tensile modulus mismatch across the interface. For example, if the top layer is stiffer than the substrate, α approaches +1, while if the opposite is true where the top layer is more compliant, α approaches -1. The second Dundurs parameter, β, in the form above indicates a measure the in-plane bulk modulus mismatch for plane strain conditions. From Evans *et al.* [31], when β is a non-zero value, the crack tip stress and displacement fields oscillate, which causes the crack to interpenetrate. This would obviously cause some difficulty in characterizing fracture at the interface. The envelope within which these two parameters must lie can be seen in Figure 2.8.

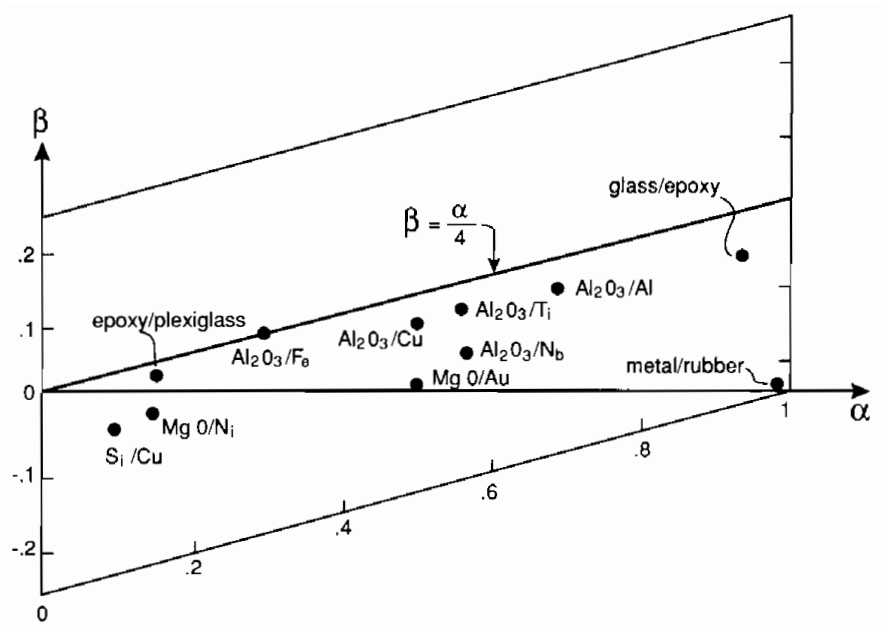

Figure 2.8: Envelope of Dundurs parameters for plane strain for a selection of materials [36].

Experimental results from Suo and Hutchinson [37] and Suga *et al.* [38] have demonstrated, however, that β is small for many bimaterial systems. Therefore, in order to suitably characterize interface fracture, it has been proposed that β equals zero.

The mode mixities, or the relative amount of mode I to mode II behaviour at the track tip can then be approached whilst $\beta = 0$, along with the stress field tractions at the tip.

$$(\sigma_{2,2}, \sigma_{1,2}) = (K_I, K_{II})(2\pi r)^{(-1/2)} \tag{2.12}$$

$$\psi = tan^{-1}(K_I/K_{II}) \tag{2.13}$$

Where K_I and K_{II} are the mode I and II stress intensity factors, respectively. Hutchinson and Suo [36] indicate that the interface toughness, Γ, of a given material is not a unique value, instead it is a function of the mode mixities, based on work by Hutchinson *et al.* [35].

2.6 Atomistic Modelling and Simulation

One factor affecting understanding of the behaviour of TBC systems is the effects of atomic phenomena that lead to microscopic and macroscopic observations. Given the increasing performance of computers, more compelling results can be achieved using atomistic modelling. Using modern computational methods, it is possible to model larger atomic clusters with more complex interactions that more closely reproduce observed and anticipated results. Many considerations must be made in order to develop an effective model. Taking these considerations into account and providing appropriate parametric data can allow researchers to develop atomistic models of TBC systems. Specifically, models of the metal/oxide interface can be effectively simulated.

The approach to developing an atomistic model must first begin with the selection of an appropriate structural model to represent the real system [9]. There exist two primary platform classes:

cluster and slab representations. A schematic example of these can be seen in Figure 2.9.

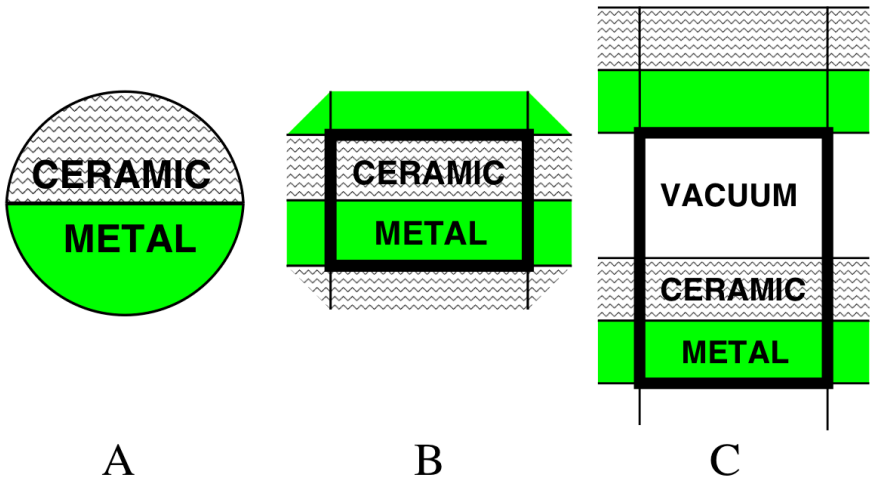

Figure 2.9: Schematic of metal/ceramic interface structural models. a) Cluster model surrounded by vacuum, b) Dense unit cell corresponding to a sandwich or superlattice structure and c) Slab model with vacuum between periodically replicated images [9].

Cluster models consist of focusing on a small representative region of a real metal/ceramic interface. This region often comprises 5-30 atoms and typically considers only local physics and ignores long-range effects that may occur. Another potential issue arising from the use of these small regional representations is the mismatch of interfacial geometry. Due to lattice mismatch of the metal and ceramic, it is unlikely that one metal atom will be able to occupy a site immediately neighbouring another metal atom. If the cluster is not large enough, this mismatch will occur, effectively impeding the model [9].

Slab models consist of a unit cell representing a metal/ceramic interface with periodic boundary conditions, seen in Figure 2.9b) and c). These representations are restricted to coherent interfaces, thus periodicity parallel to the interface exists. There are two general types of slab models; one where there is a vacuum around the unit cell and one where vacuum is excluded. When the vacuum is excluded, “dense” unit cells are representative of superlattice or sandwich structures. This style

requires substantial symmetry leading to identical interfaces, which locks the interface, effectively restricting transverse relaxation. Dense slab models also require the metal and ceramic layers to be sufficiently thick in order to avoid interaction between interfaces. The more general form of slab representations includes a vacuum and physically corresponds to an infinite array of thin metal/ceramic films separated by a vacuum layer. Similar to the dense form, the vacuum layer in this instance must be sufficiently thick to ensure adjacent film representations do not interact. One shortfall of the vacuum slab model approach is the potential to have a geometry that does not extend far enough parallel to the interface. This leads to the introduction of artificial strains as the interface is forced to be coherent. To correct this shortfall, it is possible to increase the size of the unit cell, but this will invariably increase the computational demand of the simulation.

Another consideration for atomistic modelling is the orientation of the two species' crystals at the interface. In this case, symmetry and free energy considerations are both useful. From free energy, weakly interacting interfacial pairs will bond on low-energy surfaces while strongly interacting pairs will likely bond on high-energy surfaces. This is a result of high-energy surfaces having more atoms available for bonding. From Christensen *et al.* [9], the most stable interfaces that will form between a metal and ceramic atom pair is the configuration with the smallest interface tension, γ^{MC} (free energy), which is from the Dupré relation:

$$\gamma^{MC} = \gamma^{M} + \gamma^{C} - W - \Sigma_i \mu_i \Delta N_i \tag{2.14}$$

where γ^{MC},γ^{C} are the surface tensions of the metal and ceramic, respectively, while W is the work of separation, μ_i is the chemical potential and ΔN_i is the change of abundance of species 'i'

at the interface region upon forming the interface.

The next consideration for how the interfaces will align requires a determination of the orientation and translation of the interfacial surfaces. Based on the lattice of each species, there will likely be many potential orientations, though certain directions are more likely to align to form a stable interface. Therefore, an appropriate size and shape of the unit cell must be determined that minimizes strain for both species. The most basic method of determining the match between the unit cells is to assign a mismatch factor, and choosing the configuration that minimizes mismatch using Equation 2.15 where A and B are the area of the unit cells while Ω is the overlap area, A+B.

$$\mu = 1 - \frac{2|\Omega|}{|A| + |B|} \tag{2.15}$$

The finesse of atomistic modelling appears once these considerations have been made. Due to the complexity of the systems and the phenomena that may occur at the interface, most simulations require some amount of *ab initio* development. These will often include quantum mechanical and quantum chemical effects, some of which include full wave function methods. The inclusion of these effects obviously demands notable computational resources, typically requiring parallel processing units.

Due to the increasing requirement for processing capabilities for *ab initio* techniques, a method known as density functional theory (DFT) has been developed. This method optimizes the compromise between the accuracy and efficiency of required calculations. The main tenet of DFT is to show that the total quantum mechanical energy present in the system is only a function of total elec-

tron density. This function is three-dimensional and takes into account the electronic waveform, which itself is a $3N$-dimensional function of the total number of electrons *(N)*. This is expressed in relation to the total energy:

$$\begin{aligned} E[\Psi] &= <\Psi \left| \hat{T}^{elec} + \hat{U} \right| \Psi > + T^{ion} \\ &= T_s^{elec}[\rho] + U_{classical}[\rho] + U_{xc}[\rho] + T^{ion} \\ &= E[\rho] \end{aligned} \tag{2.16}$$

where ρ is the electron density, Ψ is the electronic wavefunction, T^{ion} is the ionic kinetic energy, $U_{classical}$ is classical mean field Coulomb energy for ionic cores and charge distribution while T_s^{elec} is the kinetic energy of the noninteracting electrons.

In the previous equation, only U_{xc} has a functional form that is not explicitly known. This term serves to describe the lowering of electron-electron repulsion by correlated electronic motion, electronic change and kinetic energy due to electron-electron interactions. In order to use this formulation, an approximation must be made. Many approximations exist, though the local density approximation (LDA) and the generalized gradient approximation (GGA) are the two most commonly used approximations to date. The choice of which approximation to use depends wholly on the investigator developing the model, though potential shortcomings, such as failure to describe strongly correlated oxides [9], must be taken into account prior to implementation.

Another aspect of slab atomistic modelling consists of examining the potential correlation between the electronic structures and the interfacial adhesion. This is accomplished by calculating

the electronic density of states (DOS) and the electron localization function (ELF). The ELF is calculated, as shown below, and can be used to visualize calculated results, seen in Figure 2.10 and Figure 2.11, from Ozfidan *et al.* [39]. ELF values approach zero (0) when electrons are highly delocalized, one (1) when they are highly localized and 0.5 for a region with a valence charge distribution similar to a homogenous electron gas.

$$ELF = \frac{1}{1 + \left(\frac{D(\vec{r})}{D_h(\vec{r})}\right)^2} \tag{2.17}$$

where:

$$D(\vec{r}) = \frac{1}{2}\nabla_{\vec{r}}\nabla_{\vec{r}}{}'\rho(\vec{r},\vec{r}')|_{\vec{r}=\vec{r}'} - \frac{1}{8}\frac{|\nabla n(\vec{r})|}{n(\vec{r})} \tag{2.18}$$

$$D_h(\vec{r}) = \frac{3}{10}(3\pi^2)^{\frac{2}{3}} n(\vec{r})^{\frac{5}{2}} \tag{2.19}$$

In these equations ρ is the first order reduced density matrix, $D(\vec{r})$ is the von Weizsäcker kinetic energy functional of a ground state kinetic energy density for a non-interacting system at density $n(\vec{r})$ and $D_h(\vec{r})$ is the kinetic energy density of a uniform electron gas with a spin density equal to the local value of $n(\vec{r})$.

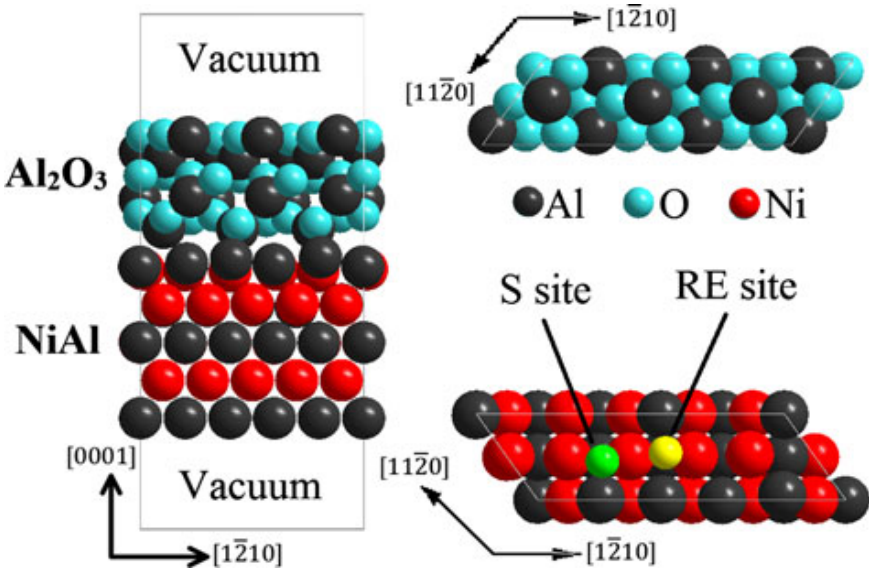

Figure 2.10: Atomistic model of a bond coat/TGO interface with sulphur and reactive element dopants included in bond coat [39].

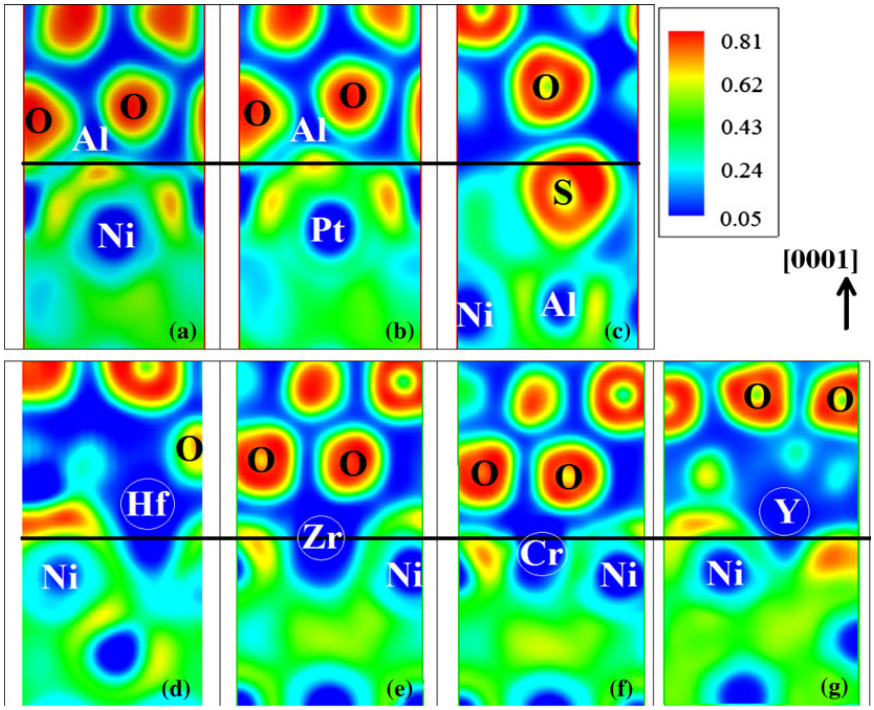

Figure 2.11: ELF of single element doped interfaces compared to a clean bond coat/TGO interface. Doping elements are as follows: a) clean interface, b) platinum, c) sulphur segregated, d) hafnium, e) zirconium , f) chromium, g) yttrium [39].

Chapter 3

Model Development

It is evident that TBC systems have numerous variables that affect their behaviour. In order to build a simulation that adequately describes the interfacial fracture toughness of the BC/TGO, it is critical to identify specific parameters. Firstly, since the focus is to design a model for cyclical turbine operations, it is obvious that the model must incorporate representative thermal characteristics. This includes the consideration for material properties that change as a function of temperature. Then, the stress states of the coating must be ascertained. This must include the residual stress incurred through thermal cycling, the strength of the bond between the BC and TGO layers, as well as the critical stress of the system. Lastly, these variables must be combined in order to simulate the coating to determine the fracture toughness of the interface. The determination of these variables will be explained in greater details in the sections that follow. Furthermore, it is important to note that in order to explore only the contributions of the bond coat and the thermally grown oxide to the relationship, the ceramic top coat was not included in the model that was developed for this

investigation since it would have seemingly little direct impact on the fracture behaviour of the BC/TGO interface.

In order to develop a model, the components of the coating to be investigated were first decided upon. β-NiAl was chosen as the bond coat material based on its prevalence as one of the most commonly applied types of bond coat. Similarly, due to its desirability, $\alpha - Al_2O_3$ was selected as the thermally grown oxide. Since the investigation was focused on the behaviour of the interface between the BC and the TGO, the top coat material and substrate material is not specified. Therefore, it should be noted that effects such as oxygen diffusion from the top coat as well as aluminium diffusion related to the substrate are not modelled in this study. It should also be noted that, in this study, the subscript 's' refers to the bond coat, which in this case is in fact the substrate, while the subscript 'c' refers to the TGO layer, the coating.

3.1 Thermo-Elastic Properties

Since these coatings undergo cyclical thermal loading, it is evident that the material properties of the system constituents will vary as the temperature increases. The properties that are of value in this model are the yield strength of the bond coat, the elastic modulus of the bond coat and the elastic modulus of the thermally grown oxide. As previously discussed, considerations for creep can become important at higher temperatures. However, since this model focuses on determining the fracture toughness of the interface, it was decided that creep would be excluded from the simulation since it would serve to relax stresses at the interface, thus reducing likelihood of failure through spallation. Instead, a model that excludes creep would provide values that are representative of a

worst-case scenario for the coating system, provided that external loads are ignored and only bond strength and residual stress are considered.

In order to determine the aforementioned thermo-elastic properties incurred during the cycle temperature, data from previous investigations were analysed to build representative relationships.

3.2 Bond Coat Yield Strength

It was decided that the bond coat would be modelled as a β-NiAl since it is a commonly applied commercial bond coat. It was also modelled without any platinum addition, in order to serve as a baseline material. Without any elemental additions, the contribution of specific doping elements later would provide clearer evidence of any effect these additional inclusions might provide. The composition range of β-NiAl can be seen in the phase diagram presented below in Figure 3.1.

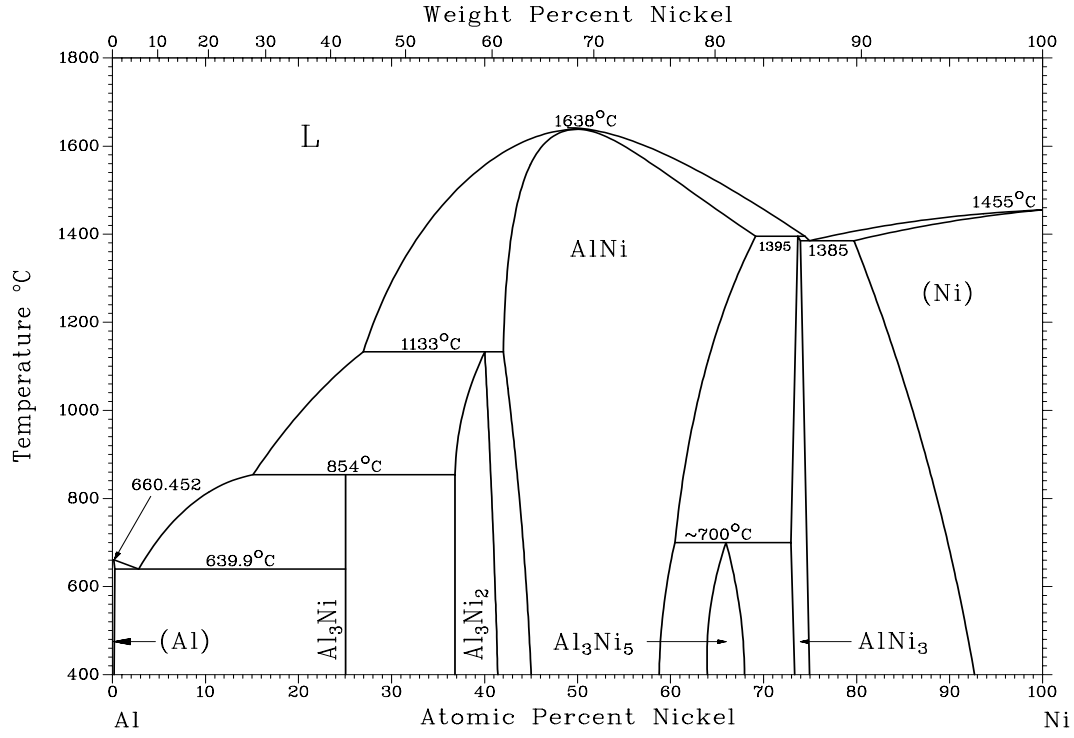

Figure 3.1: NiAl phase diagram. The β-NiAl phase lies between 43 at.% Ni and 69 at.% Ni.

The bond coat properties were determined from experimental results published by Noebe *et al.* [40], seen in Figure 3.2. This investigation focused on fully describing NiAl's physical and mechanical properties. This included a noted focus on the yield and flow characteristics of the alloy, as these two are particularly sensitive to factors such as temperature, composition and strain rate. The results published in this investigation were the basis for the properties imparted into the model for yield strength.

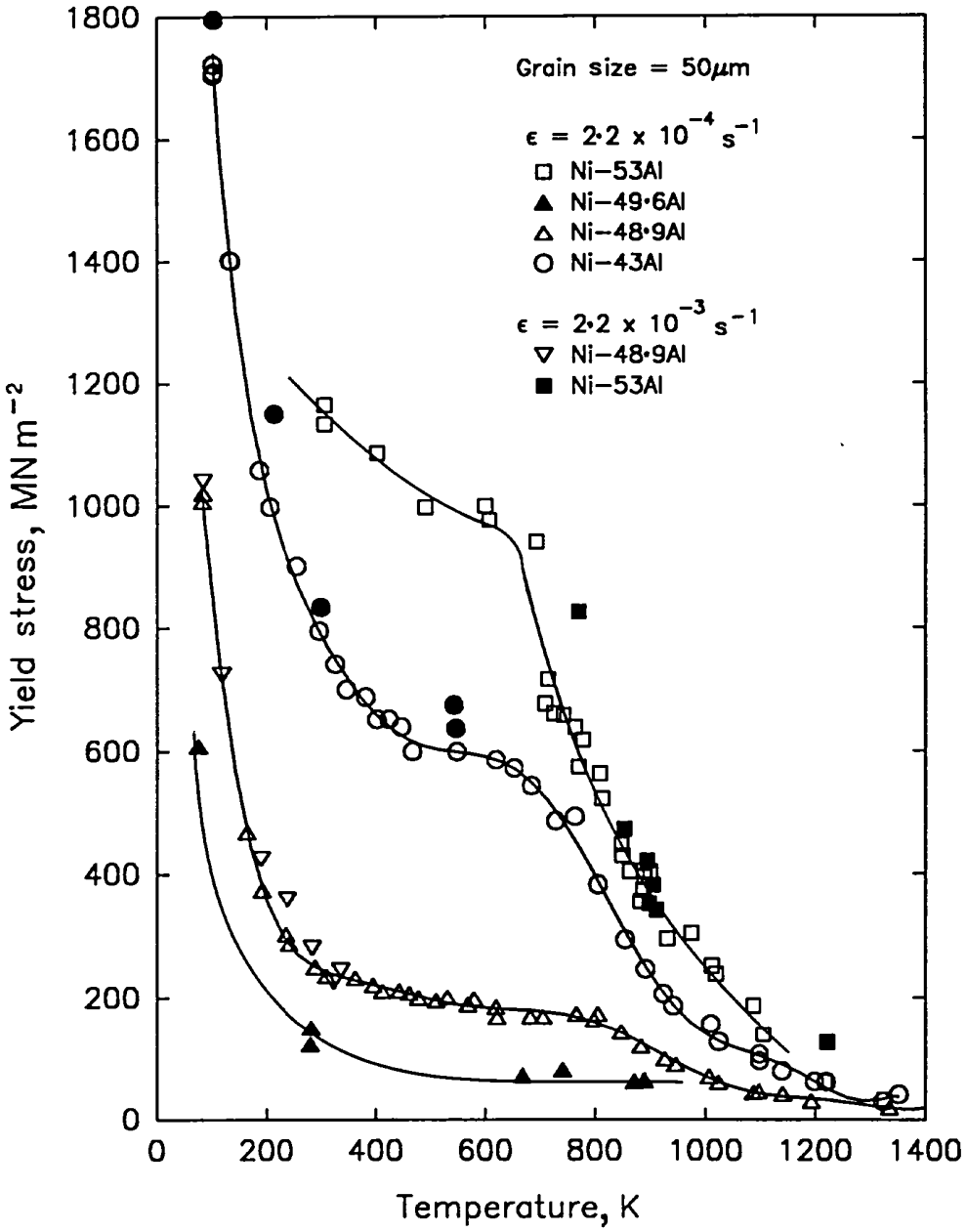

Figure 3.2: Yield stress as a function of temperature for polycrystalline NiAl [40].

From this data, the Ni-43Al compound was chosen as it provided the most resilient yield properties and coincided with the minimum Al% composition for the alloy. The data for this specific compound was then extracted and input into Origin®, a data analysis program. The data was then

analysed using a 5th order regression algorithm to determine the mathematical relationship of the data, seen in Figure 3.3.

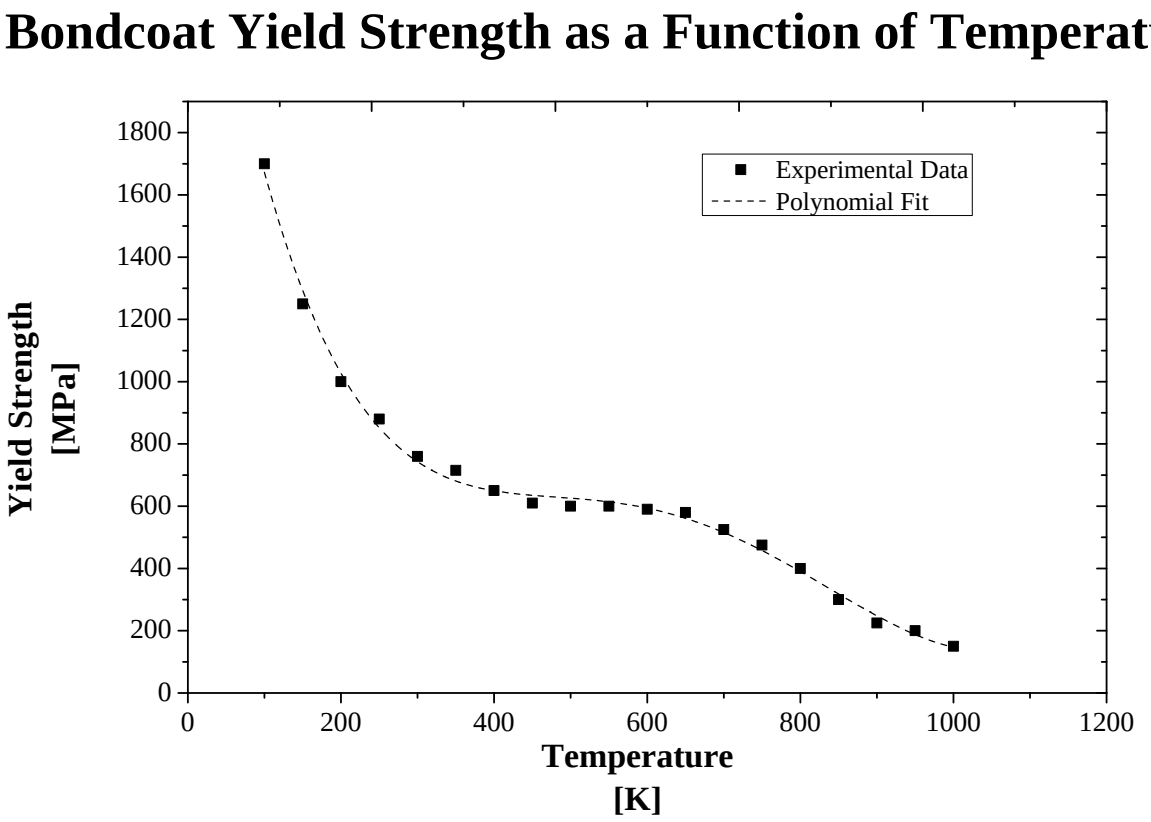

Figure 3.3: Regression analysis of the Ni-43Al B2 compound yield strength.

The regression provided the following equation for the relationship between the yield strength and the exposure temperature up to 1000 K:

$$\sigma_{ys} = -9.89 \times 10^{-5} T^5 + 4.25 \times 10^{-8} T^4 - 6.80 \times 10^{-5} T^3 + 0.0050 T^2 - 17.36 T + 2979.96 \times 10^6 \quad (3.1)$$

Error analysis indicated that the regression provided a good fit with a total average error of 4.61% for temperature data between 100 K and 1000 K. The overall error ranged between 0.021% to 13.74%, with the largest aberration noted between 600 K and 800 K.

3.2.1 BC and TGO Elastic Moduli

In order to properly describe the BC properties, it was also required to determine the relationship between the temperature and the elastic modulus. This was also performed by analysing data published from experimental results. The data for the elastic moduli was drawn from Busso *et al.* [23], who conducted a mechanistic study of microcracking in isotropic metal/ceramic systems. The results of this analysis are provided in Figure 3.4.

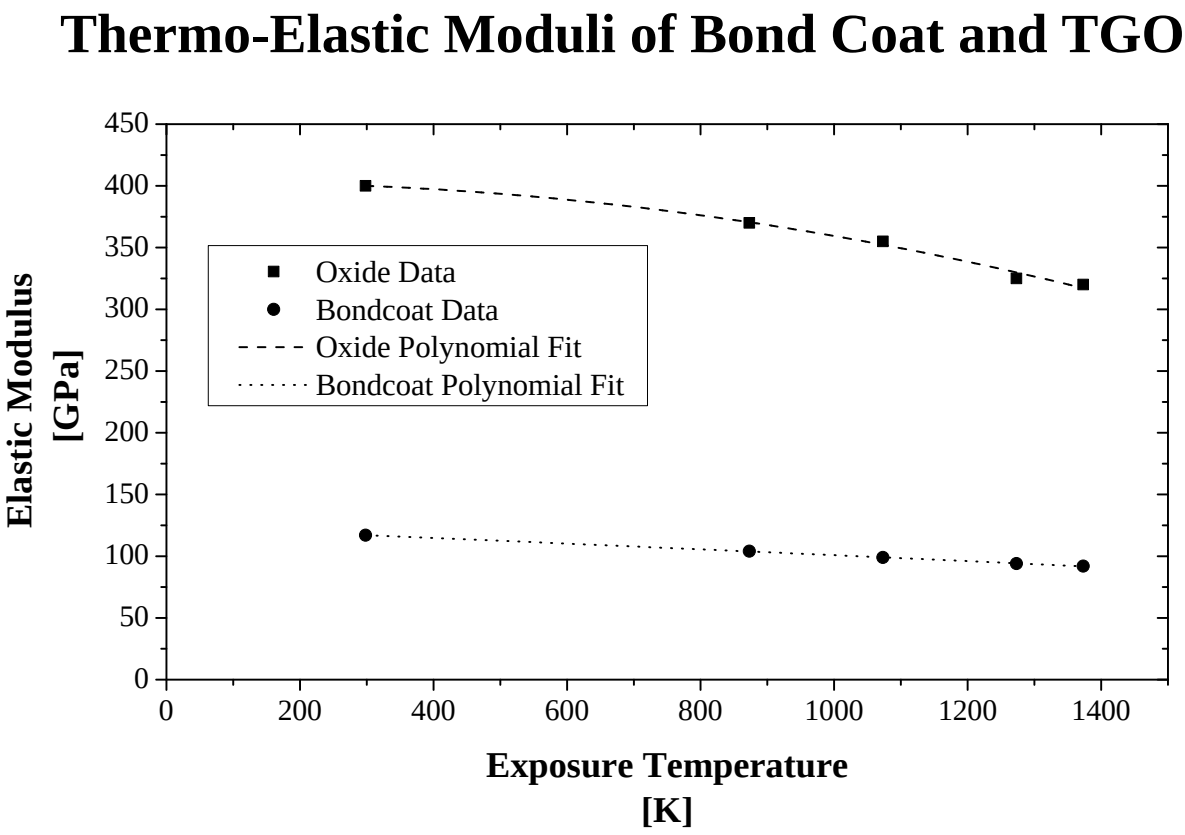

Figure 3.4: Regression analysis of elastic moduli for β-NiAl bond coat and α-alumina, with their corresponding polynomial regression fitting curves.

The fitting algorithm provided the two following equations for describing the elastic moduli as a function of temperature:

- Bond Coat Elastic Modulus, E_s [GPa]:

$$E_s = -0.01 \times 10^{-4} T^2 - 0.022T + 122.79 \tag{3.2}$$

- Thermally Grown Oxide Elastic Modulus, E_c [GPa]:

$$E_c = -0.05 \times 10^{-4} T^2 + 0.0052T + 402.23 \tag{3.3}$$

These regressions were performed using Excel® as it was determined that the error in the resulting equations was low enough to provide reliable results. The average error for the BC data was 0.40% (ranging from 0.11% to 0.68%) while the average error for the TGO data was 2.68% (ranging from 1.31% to 4.05%) due to a noticeable gap at approximately 1300 K.

The equations determined from the regression analysis for both the BC yield strength and the elastic moduli were then used to assist in the determination of the bond strength, critical stress and ultimately the fracture toughness.

3.3 Determination of Stress States

As TBC systems are thermally cycled, they develop stresses. These stresses will often resolve to a compressive state, causing an undulating profile. A schematic of an idealized undulating profile is provided in Figure 3.5.

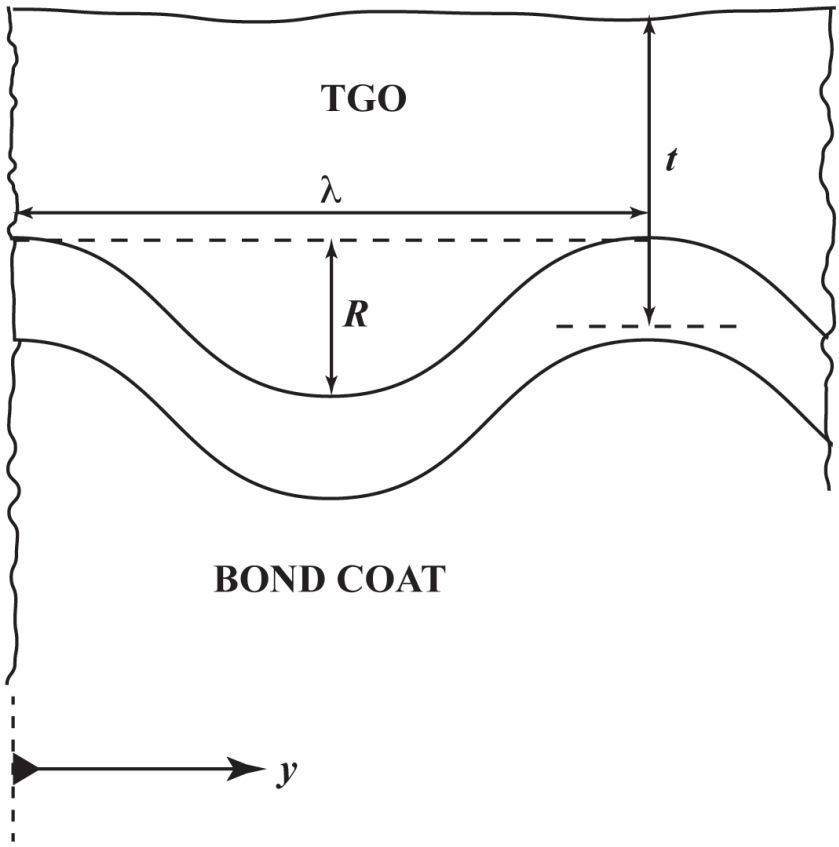

Figure 3.5: Undulating profile schematic of a compressed stress state incurred due to thermal cycling.

This schematic was derived from the von Karman equation [34] for an imperfection presented with "wave" morphology:

$$w_o(y) = \frac{R}{2}\left(1 + cos\frac{2\pi y}{\lambda}\right) \quad |y| \leq \frac{\lambda}{2} \tag{3.4}$$

where $w_o(y)$ is the wave profile as a function of linear distance, R is the amplitude (the max deformation height of the imperfection), λ is the total wavelength of the imperfection and t, seen in Figure 3.5, is the oxide thickness.

Figure 3.6 illustrates the periodic wave profile that was generated for the current model using

Equation 3.4, where $R = 2\ \mu$m and $\lambda/2 = 10\ \mu$m. This profile was then used to determine the residual stress and critical stress states of the interface.

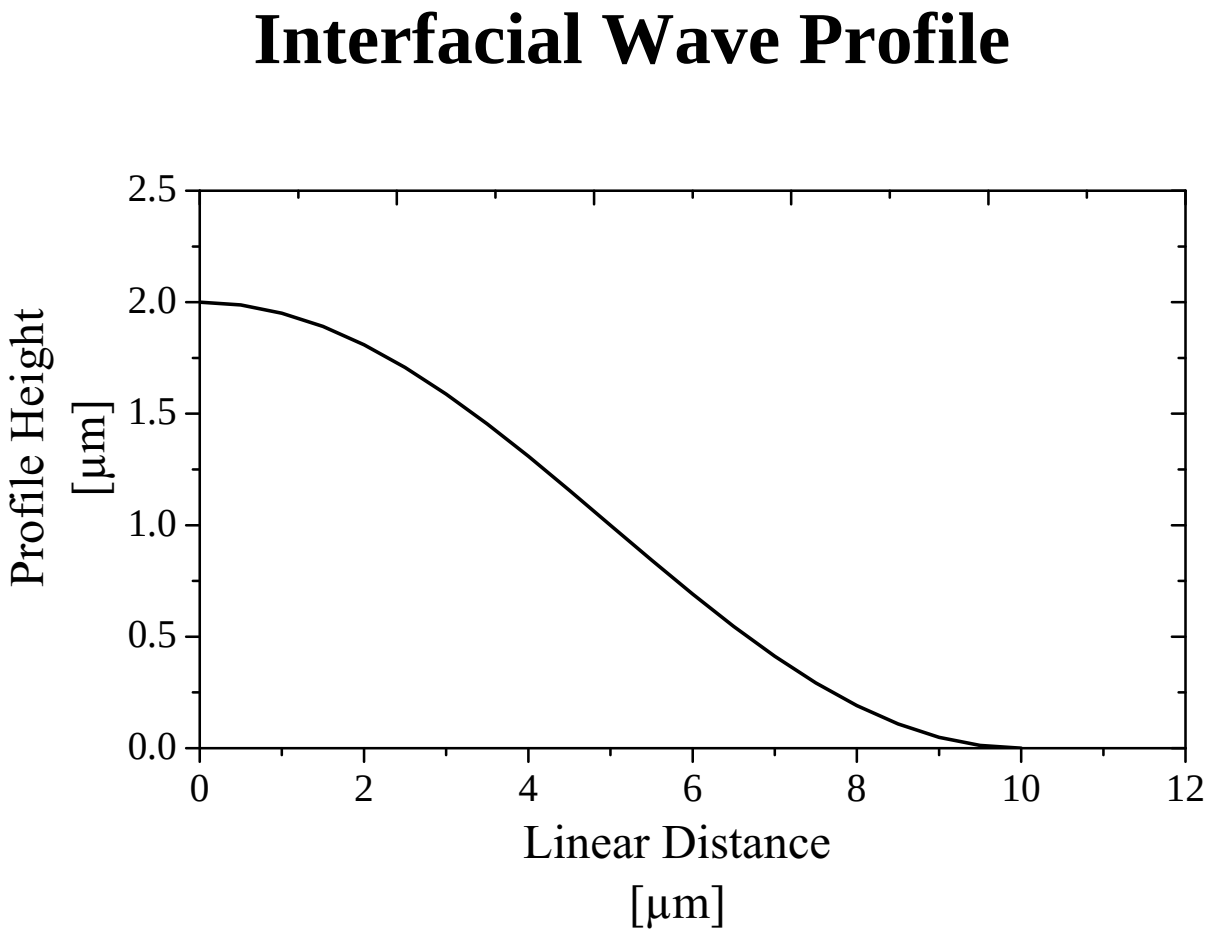

Figure 3.6: Wave profile generated for determining interfacial stress states.

3.3.1 Residual Stress Determination

Consideration of residual stresses is particularly important when dealing with TBC systems. As these coatings are thermally cycled, the increase and decrease in temperature can impose stresses, such as those due to inelastic deformations, for example. The residual stress is the stress state that remains once the cause of the stress is removed. Based on experimental observations [2, 16, 34]

and theoretical approaches [9, 16, 23, 34] it was determined that simulating the buckled interface profile, previously noted, would reflect buckle driven delamination, one of the more commonly attributed spallation mechanisms. The development of the residual stress model was thus built from a previously published approximation [41] based on the solution for the residual stress on an isolated cylinder, shown in the schematic illustrated in Figure 3.7.

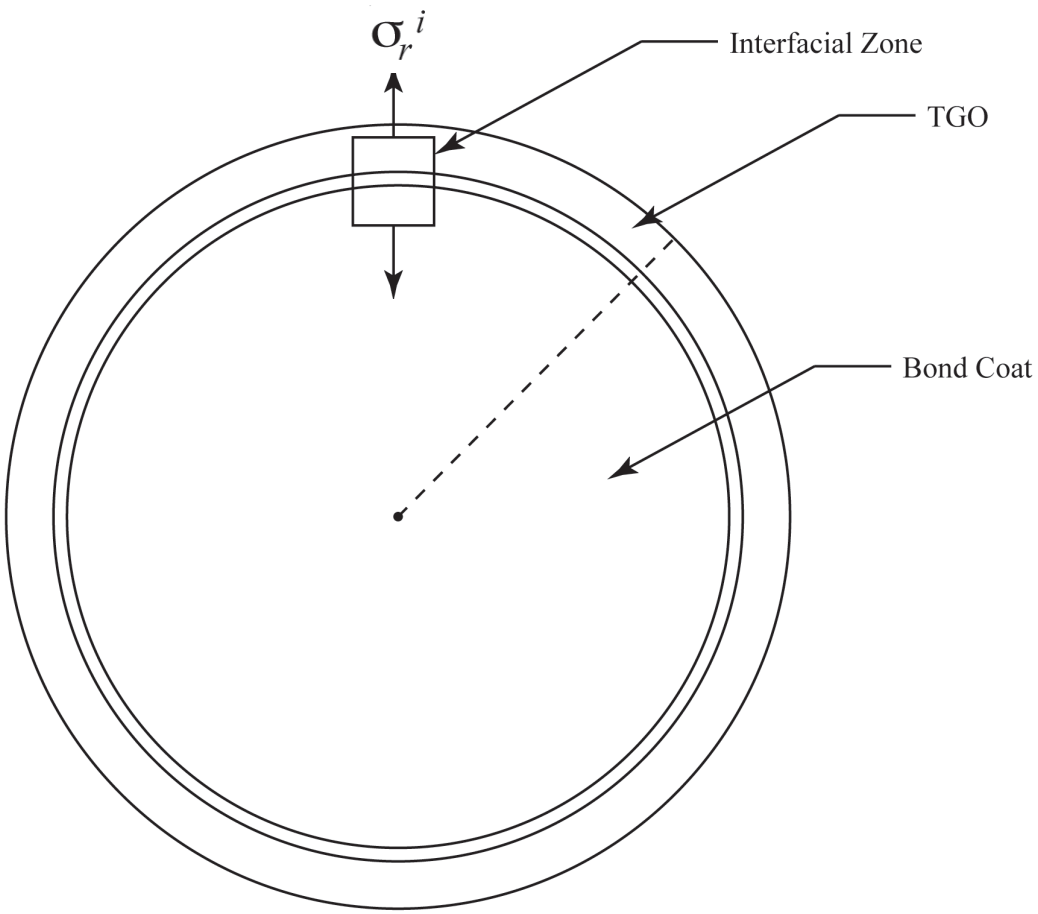

Figure 3.7: Location of residual stress, determined from the previously noted approximation.

Due to the buckled nature of the interface, the residual stresses will resolve to an in-plane residual stress as well as residual stress perpendicular to the in-plane stress. Since the mechanism

of concern is the spallation of the TGO layer due to failure at the interface, the residual stress acting normal to the interface is of utmost concern. The state of residual stress normal to the interface can then be considered to result in a tensile stress acting to delaminate the TGO from the BC at the interface, and is represented by:

$$\sigma_n^i \approx \Delta\varepsilon \frac{[1/\kappa + E_c(1+\nu_s)(R/a)]sin(2\pi y/\lambda)}{1+R/t} = \sigma_r^i \tag{3.5}$$

where:

$$\Delta\varepsilon = \Delta\alpha\Delta T \tag{3.6}$$

$\Delta\varepsilon$ is the mismatch strain that results from a difference in thermal expansion between the substrate and the oxide layers for a given change in temperature, which in this case is between 1000 K and 200 K. E_c is the coating's elastic modulus, previously determined from regression analysis, where the coating in this case is the thermally grown oxide. Conversely, ν_s is poisson's ratio for the substrate, which is the bond coat. R and λ represent the amplitude and wavelength of the undulated interface, schematically described in Figure 3.8. y is the location along the interface, while t is the nominal thickness of the TGO in its corresponding unbuckled state. In this study, location y corresponds to the location of the maximum amplitude, the "crest" of the undulation. Finally, the κ term is used to simplify the equation and is:

$$\kappa = \frac{(1+\nu_c)}{[2E_c + (1-2\nu_s)]/E_s} \tag{3.7}$$

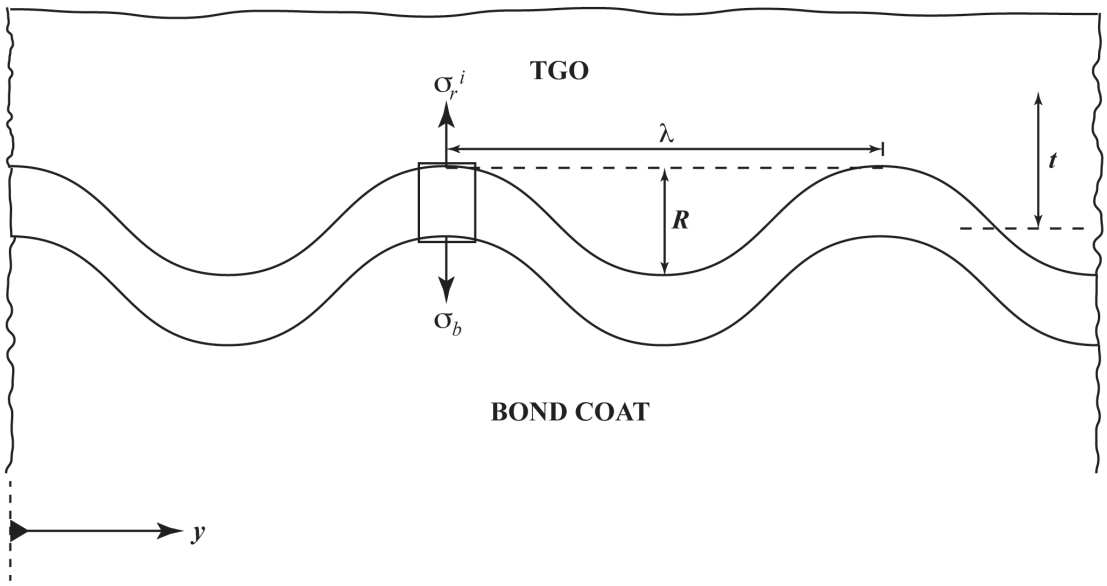

Figure 3.8: Undulating profile of simulated coating interface.

The schematic above is an expanded view of the idealized undulating profile that results from thermal cycling [13,41], where the space between the TGO and the bond coat is the interfacial zone, noted in Figure 3.7. The cylindrical approximation is geometrically congruent with the largest equivalent radius at the peak of the undulation. Since the profile is composed of compound radii, the peak radius was found to confirm the scale of the buckled profile. This radius was determined using the formula for the radius of curvature, which is a relationship based on the first and second derivative of a function. The equation for radius of curvature, a, is as follows:

$$a = \frac{\left[1 + \left(\frac{dy}{dx}\right)^2\right]^{3/2}}{\left[\frac{d^2y}{dx^2}\right]} \tag{3.8}$$

The first and second derivatives of Equation 3.4 were then determined:

- First Derivative:

$$f'(y) = \frac{-\pi\delta sin\left(\frac{2\pi y}{L_o}\right)}{L_o} \tag{3.9}$$

- Second Derivative

$$f''(y) = \frac{-2\pi^2\delta cos\left(\frac{2\pi y}{L_o}\right)}{L_o^2} \tag{3.10}$$

The first and second derivatives were then calculated and the results substituted into Equation 3.8 in order to calculate the equivalent radius of the buckled profile. Based on the crest of the buckled profile, occurring at +/- π/2, the total radius of curvature was found to be 79.3 μm.

3.3.2 Adhesion Strength Determination

Since the residual stress at the maximum amplitude of the buckle resolves to a tensile stress acting to separate the TGO and BC at the interface, the adhesion characteristics of the interface must play a role in opposing this stress. This is the case since, failing the presence of such a stress, the interface would fail immediately and the TGO would separate indiscriminately from the BC. Therefore, a formulation to adequately describe the adhesion characteristics of the interface was required. It should also be noted that while doping elements would understandably contribute to variations in yield strength in bulk materials, even in low concentrations, the dopants in this investigation segregate specifically to the interface. Therefore, it is assumed that this localization minimizes the dopant effect on bulk material properties, such as elastic modulus and yield strength.

Based on previous investigations from Mao and Evans [42] as well as Tymiak *et al.* [43], Ger-

berich and Cordill [44] identified the bond strength of metal/ceramic interfaces as:

$$\sigma_{bond} = \left[\frac{8E_c\,\mu W_{ad}}{3\pi\sigma_{ys}\,h}\right]^{1/2} = \sigma_b \tag{3.11}$$

This equation considers the elastic modulus of the oxide, E_c, the yield strength of the substrate, σ_{ys}, along with the thickness of the oxide layer, h, as well as μ which is the shear modulus of the substrate (in this case, the bond coat), while W_{ad} is work of adhesion.

The shear modulus of the substrate is a value that is required to partially describe the effect of crack tip plasticity at the interface. This parameter is related to the elastic modulus and poisson's ratio of the BC as follows, provided by Hutchinson and Suo [36]:

$$\mu = \frac{E_s(1-\nu)}{2} \tag{3.12}$$

The work of adhesion, W_{ad}, can also be considered as the work of separation. This term describes the amount of energy that is required, per unit area, to separate the two interfacial species from each other without plastic deformation. The work of adhesion is also the term that encompasses the elemental effects of the segregated atomic species. In order to determine the effect these species have on the interfacial work of adhesion, an atomistic modelling investigation was performed [39]. These models relied on simulating the presence of a single atom at the, otherwise clean, interface in a slab model representation, previously seen in Figure 2.8c). Using the quantum mechanical analysis tool, known as Density Functional Theory (DFT), noted earlier, the electronic

activity of the atomic elements present at the interface were analysed. This resulted in data related to the total energy of the slabs. Using the total energies of the slabs, the work of adhesion was then calculated by

$$W_{ad} = \frac{E_{S1} + E_{S2} - E_{S1/S2}}{A} \tag{3.13}$$

where E_{S1}, E_{S2} and $E_{S1/S2}$ represent the total energies of slab$_1$, slab$_2$ and the slab$_1$/slab$_2$ interface, while A is the modelled area. The results from this investigation are tabulated in Table 3.1.

Table 3.1: Interfacial work of adhesion for β-NiAl (110)/Al_2O_3(0001) [39].

Segregants	W_{ad} $[J/m^2]$
None	0.832
Sulphur	0.266
Platinum	0.845
Yttrium	1.049
Hafnium	1.760
Sulphur + Platinum	0.355
Yttrium + Hafnium	3.155
Sulphur + Hafnium	0.749
Platinum + Hafnium	1.764

These results were then included with the thermo-elastic properties development to determine the bond strength of the interface using Equation 3.11.

3.3.3 Critical Stress

Since the residual stress normal to the interface as well as the bond strength of the interface itself had been determined, a criterion was required to describe the balance of these stresses at the

interface.

As previously indicated, since the residual stress state is in tension, this would imply that the TGO would readily spall provided there was no contribution from the adhesion strength of the interface. Therefore, it can be concluded that

$$\sigma_{bond} = \sigma_r \tag{3.14}$$

meaning that the residual stress and the strength of adhesion are in balance immediately prior to failure. Therefore, the critical stress that would represent an intact interface in this case is represented by:

$$\sigma_c = \sigma_{bond} - \sigma_r \tag{3.15}$$

while:

$$\sigma_{bond} \geq \sigma_r \tag{3.16}$$

This equation then represents all the states where the strength of adhesion is of a magnitude sufficient to counteract the magnitude of the tensile stress. Therefore, this criteria can be represented by

$$\sigma_c > 0 \tag{3.17}$$

since the material will remain bonded as long as the condition is maintained.

3.4 Fracture Toughness

Knowing the conditions by which the BC/TGO interface will indicate failure (spallation), the determination of the fracture toughness of the coating can now be pursued.

In order to determine the fracture toughness, the mode by which the interface will fail must be considered. Figure 3.9 depicts the modes by which materials fail due to fracture.

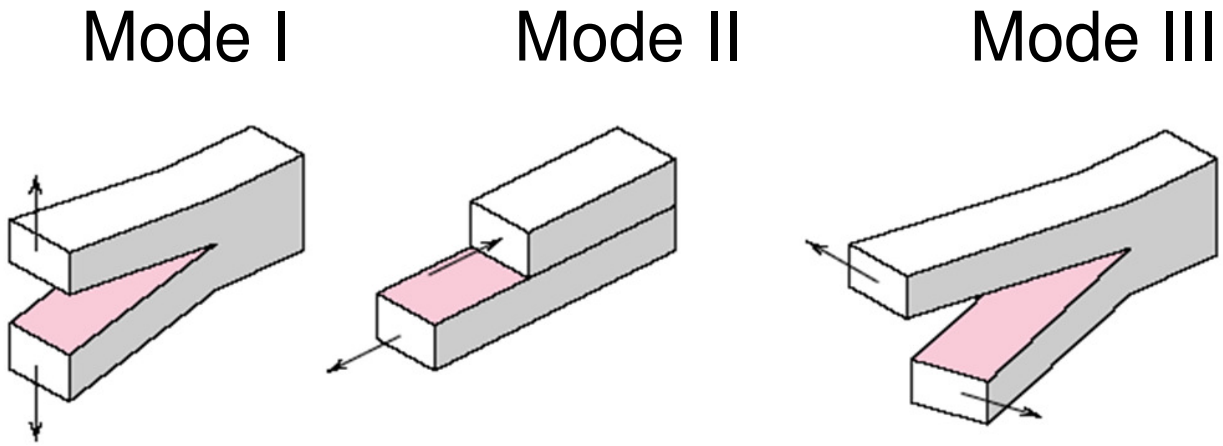

Figure 3.9: General fracture modes, showing Mode I (Opening), Mode II (Sliding), and Mode III (Anti-Plane) [45].

These modes represent the three conventional displacements associated with fracture. The first, mode I, results from tensile loads acting on a body, sometimes called ”opening fracture”. Mode II fracture (“sliding fracture”) is caused by in-plane shear loads, while mode III (“tearing” or “anti-plane”) fracture is caused by out of plane shear. Based on the loading criteria defined in Section 3.2, it can be presumed that the model will fail in mode I. This coincides with experimental and operational observations that indicate that separation due to spallation is often presented as oxide “pop-out”, seen in Figure 3.10. This would indicate that mode I is the most likely fracture mode

for this model.

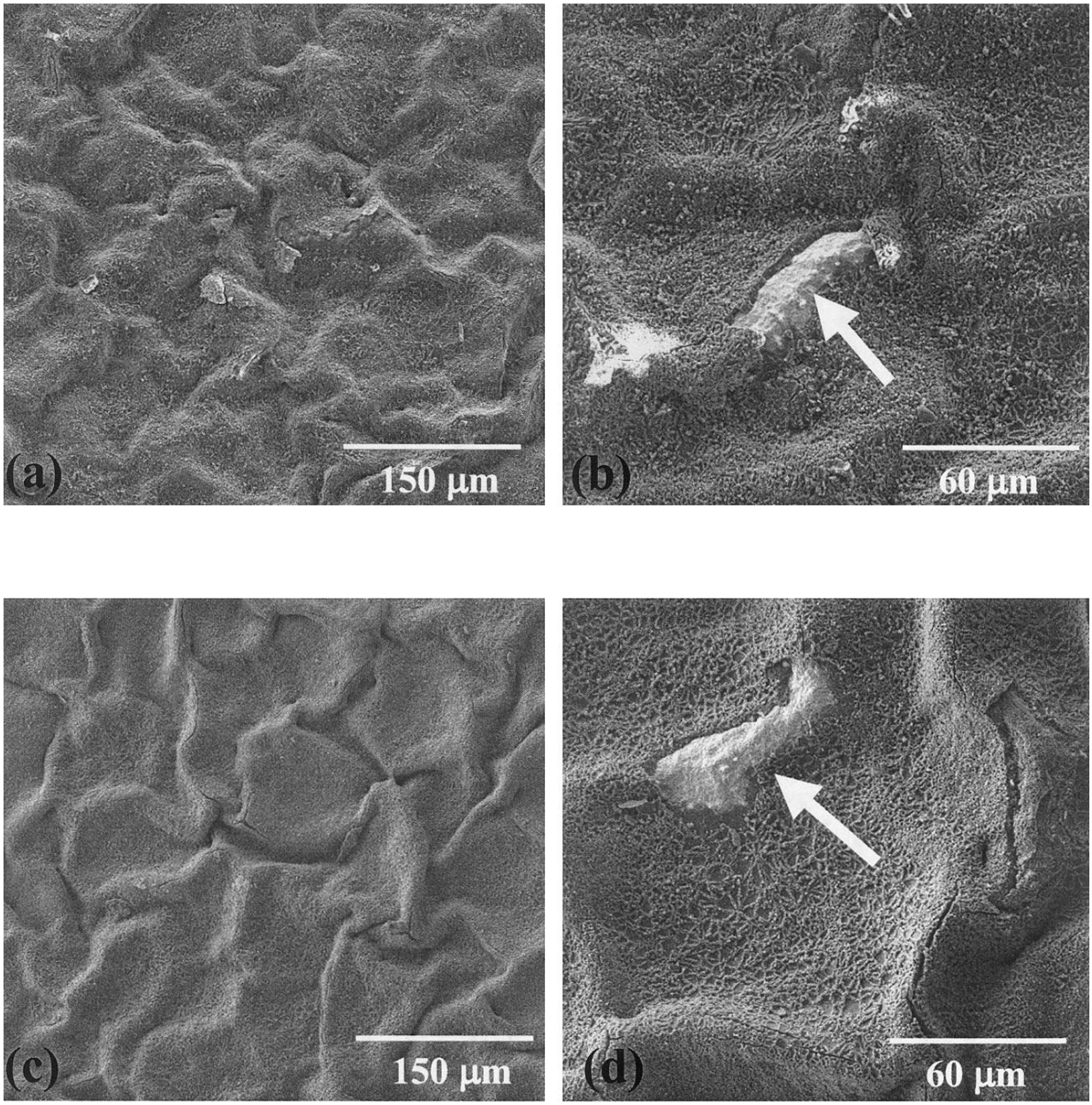

Figure 3.10: CVD NiPtAl bond coats after thermal cycling up to 1150°C. a) and b) are Sample 1 (pre-cycled, then cycled), while c) and d) are Sample 2 [17].

This figure illustrates how the samples failed. Since the spallation occurred in the centre of an arbitrary specimen, it can be concluded that it is unlikely that the spallation underwent sliding or tearing loads. Instead, it appears far more likely that the failure was due to an "opening"-type event

(Mode I).

Materials will exhibit different resistance to the different modes of failure. While a material may provide a notable toughness in mode III, this by no means suggests that it will provide the same resistance in mode I. Therefore, since the model case has been identified as likely failing in mode I, the fracture toughness corresponding to this failure mode must be identified. In this case, the loads are uniaxial, oriented perpendicular to the interface. Thus, based on the uniaxial failure of the interface [46, 47], the fracture toughness, noted as K_{IC}, is[2]:

$$K_{IC} = \sqrt{\left((\sigma_c^2 h \left[\pi F(\alpha_D) + \frac{\sigma_c}{\sqrt{3}\sigma_{ys}} \right] \right)} \tag{3.18}$$

where h is the thermally grown oxide thickness, $F(\alpha_D)$ is a function of the ratio of the elastic moduli (α_D) of the TGO to that of the BC, σ_c is the critical stress of the interface and σ_{ys} is the bond coat yield strength.

Since the model is representative of a thermally cycled component, K_{IC} is temperature dependent. Therefore, the developments for the thermo-elastic properties stipulated from Section 3.1 and calculated in Section 3.2 are substituted into Equation 3.18 to solve for the fracture toughness at temperature increments. Thus, this model provides a parametric evaluation for fracture toughness based on temperature as well as oxide thickness.

[2]In this case, it is assumed that the fracture will be the result of a crack that nucleated from an arbitrary perturbation void (Section 2.4.2) and consequently coalesced, leading to crack formation.

3.5 Simulation and Data Processing

Once equations for the temperature dependent material properties and equations for stress and fracture toughness were determined, the simulation was implemented. The model was built such that the only user modified variable was the work of adhesion value. This ensured that the simulation was identical for each simulation cycle and guaranteed that any observed differences in the results would only be a function of the work of adhesion. Therefore, the simulation provides results for fracture toughness that are determined based solely upon the contribution of the selected atomic species used in each simulation cycle.

The model was coded using Apple Xcode as a command line executable program written in C (programming language). C was the chosen language as it would be cross compatible to other computing platforms. Debugging was performed within the Xcode development environment as well as through the DART supercomputing Linux shell at the National Research Council of Canada (NRC). This was performed in order to guarantee the anticipated cross-platform compatibility of the model. Figure 3.11 is a logic diagram of the simulated cycle within the model.

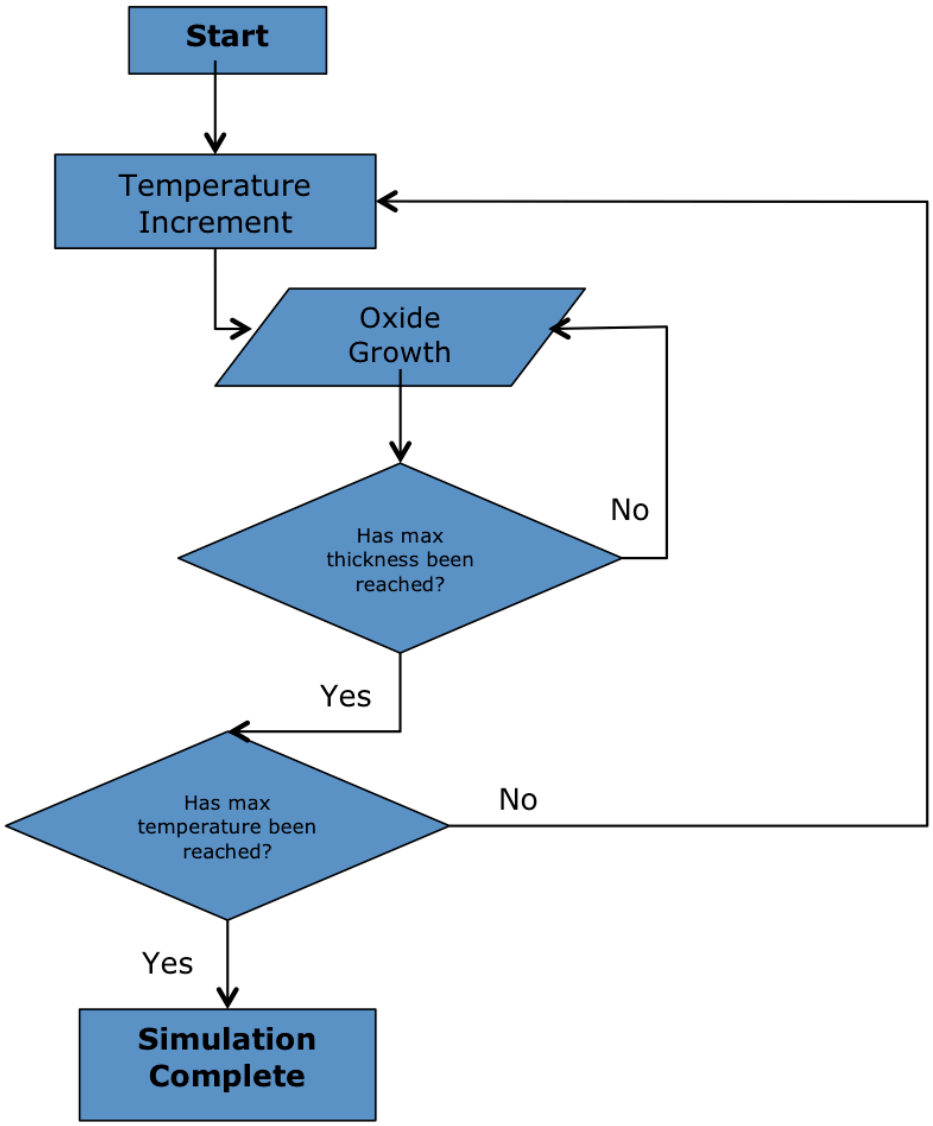

Figure 3.11: Flow diagram of the model simulation logic.

The simulation itself consists of an oxide thickness growth loop nested within an increasing temperature loop. This means that the temperature cycling loop is the "driving" loop. As the value for temperature increases the values for the thermo-elastic properties are calculated. These values are then used within the nested loop. The nested loop increments the oxide thickness and calls two subroutines for calculating the residual stress and bond strength. The results from these subroutines

are returned, with which the critical stress and fracture toughness are ultimately calculated for the current oxide thickness and current temperature. Once the nested loop has cycled through its range of oxide thicknesses, 2 μm to 27 μm, the simulation then increments to the next temperature value and the nested oxide loop cycles with the newly calculated parameters. This pattern continues until the temperature cycle has exhausted its range. The temperature range used in the temperature loop is 300 K to 980 K, separated into discrete 40 K increments.

The simulation proceeded as follows:

1. All variables and values initialized as the simulation begins;
2. Temperature is initialized at 300 K;
3. Thermo-elastic properties are calculated;
4. The simulation falls into the nested oxide loop, and the oxide thickness is initialized at 2 μm;
5. The thermo-elastic properties from Step 3 are fed into two subroutines to calculate the residual stress and the bond strength;
6. The results from Step 5 are returned to calculate the critical stress and the fracture toughness;
7. The nested loop returns to Step 4 and increments the oxide thickness by $\sim$1.4 μm;
8. Steps 4 through 7 are looped until the oxide thickness reaches its maximum, at which point the simulation returns to Step 2;
9. The temperature in Step 2 is incremented by 40 K;

10. This then causes a new cycle of Steps 3 through 9 to begin;

11. The temperature is cycled until it reaches its maximum, at which point the simulation terminates;

These steps were conducted separately for a clean interface as well as for each elemental addition noted in Table 3.1.

Throughout these simulation steps, the program also writes the calculated data to two separate text files. One text file receives the output for all the thermo-elastic properties, while the other receives all the parametric data (temperature and oxide thickness) as well as the stress results and the fracture toughness.

The data was first imported into Excel® for analysis and scaling. Initially the values are calculated in [m], [Pa] and [Pa $m^{1/2}$] SI units. Excel® was used to convert length scale values to [μm], stress values to [MPa] and fracture toughness values to [MPa $m^{1/2}$] to meet standard conventions. These scaled values were then exported to Origin® for detailed analysis. The parameters that were identified as being most critical were the oxide thickness, the exposure temperature and the fracture toughness. The data was then converted to a 3D matrix and plotted in a 3D surface contour.

A collection of the material characteristics that were modelled throughout the simulation can be found in Table 3.2, below.

Table 3.2: Summary of model material properties.

Temperature, T [K]	300-980
*Bond coat elastic modulus, E_s [GPa]	$\sim$ 100-115
*Bond coat yield strength, σ_{ys} [MPa]	$\sim$ 100-750
*TGO elastic modulus, E_c [GPa]	$\sim$ 350-400
TGO thickness, h [μm]	2-27
Shear modulus, μ [GPa]	$\sim$ 70-84
Elastic mismatch function, F(α_D)	0.7

(*-denotes properties whose values were calculated as a function of temperature)

Chapter 4

Simulation Results

The parametric data was first analysed and then plotted using a three dimensional matrix for each dopant acting individually in order to visualise the impact single elemental additions had on the fracture toughness as a function of temperature and oxide thickness. Firstly, as a baseline, the first simulation consisted of determining the fracture toughness of an un-doped “clean” interface, seen in Figure 4.1.

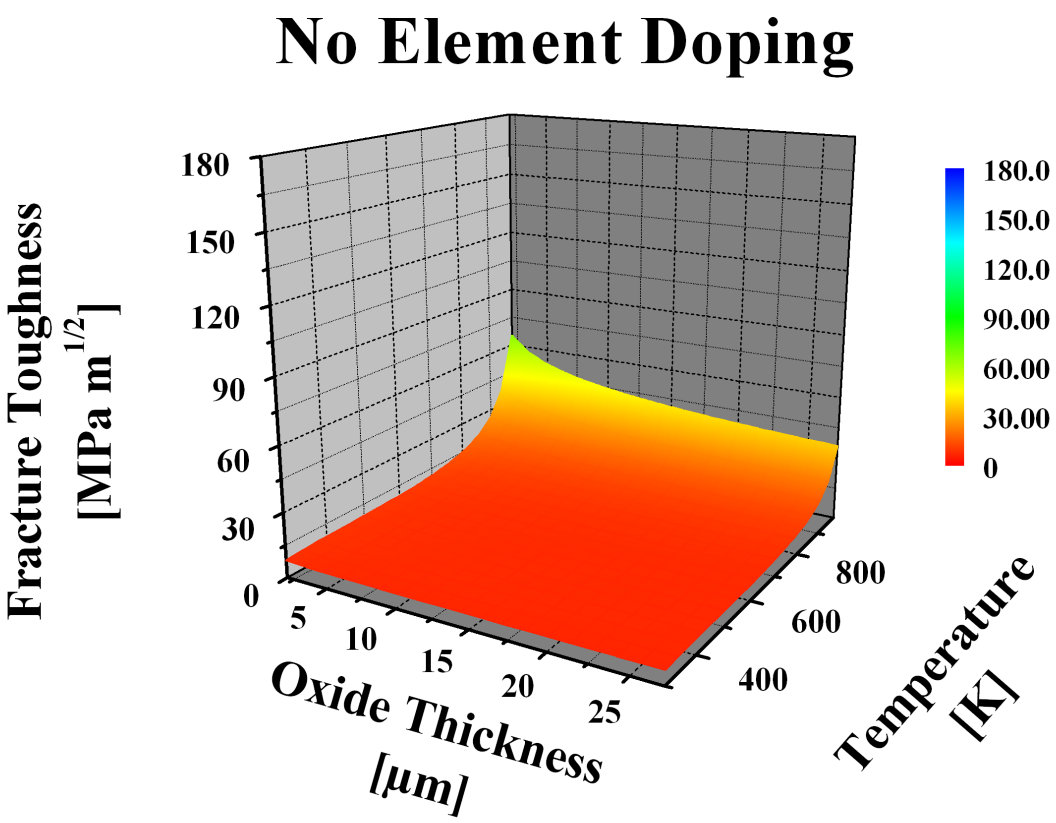

Figure 4.1: Clean β-NiAl / α-Al_2O_3 interface results for fracture toughness as a function of oxide thickness and exposure temperature.

These results serve as the "benchmark" results for the interface. This interface was simulated as a pure β-NiAl / α-Al_2O_3 without any additional interfacial elements. Several trends can be identified from this figure. Firstly, the interfacial fracture toughness is reduced as the oxide thickness increases, as seen in experimental observations [48]. Secondly, the toughness increases as the temperature is increased. These two observations correlate very well with general experimental results for coating thickness and fracture toughness. Typically, as coating thicknesses increase, the toughness of the material will decrease, as the residual stress increases and there is also a higher likelihood of convalescence of perturbations that can lead to fracture. Furthermore, as the material

is exposed to higher temperatures, it will become increasingly compliant as it becomes more ductile and thus more resistant to brittle fracture.

Having established the baseline values of a clean interface, the results of single element doping can now be considered. In order to identify points of interest against which other results can be compared, the following results will be considered:

- Maximum fracture toughness = 64.98 [MPa $m^{1/2}$]
- Fracture toughness at minimum oxide thickness = 8.19 [MPa $m^{1/2}$]
- Fracture toughness at maximum oxide thickness = 6.55 [MPa $m^{1/2}$]

It should be noted that the maximum fracture toughness occurs at 980 K, while the minimum and maximum oxide thickness value for fracture toughness both occur at 300 K.

4.1 Platinum Doping

The first elemental addition simulation that was analysed was the contribution of platinum to the fracture toughness. The plotted results can be seen in Figure 4.2. These results, when compared to the established baseline of the clean interface, are substantially the same. Based on the previously identified values for comparison, Pt provided the following results:

- Maximum fracture toughness = 65.72 [MPa $m^{1/2}$]
- Fracture toughness at minimum oxide thickness = 8.27 [MPa $m^{1/2}$]

- Fracture toughness at maximum oxide thickness = 6.61 [MPa $m^{1/2}$]

These results indicate roughly a 1% increase in fracture toughness at the minimum and maximum oxide thickness, and a 2% increase in overall maximum fracture toughness.

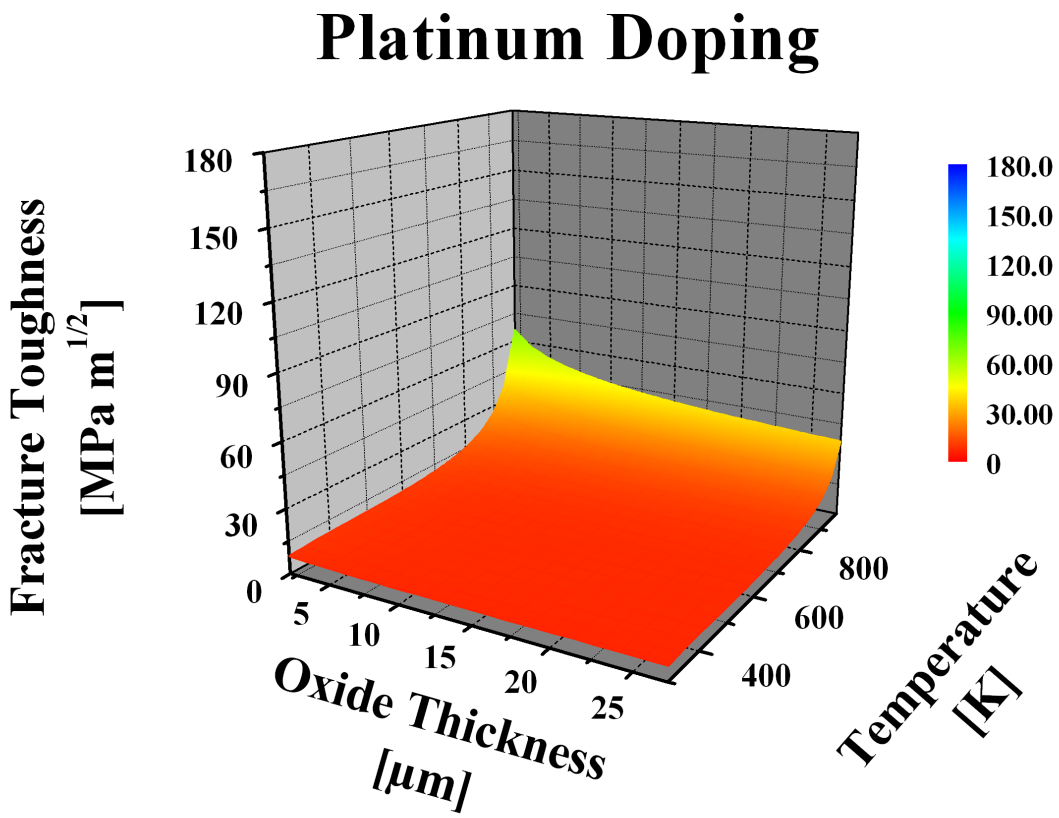

Figure 4.2: Fracture toughness results of a Pt-doped interface.

This would appear to suggest that platinum plays a negligible role in the fracture toughness of the interface.

4.2 Sulphur Doping

Experimental results [11, 13–15, 18, 24] have shown that sulphur plays a deleterious role in the performance of TBC systems. The mechanisms by which it affects the coatings are not clear, but it had been suggested that its presence may reduce the interface's resilience. Based on the results plotted in Figure 4.3, the effect of S-doping becomes less obscure.

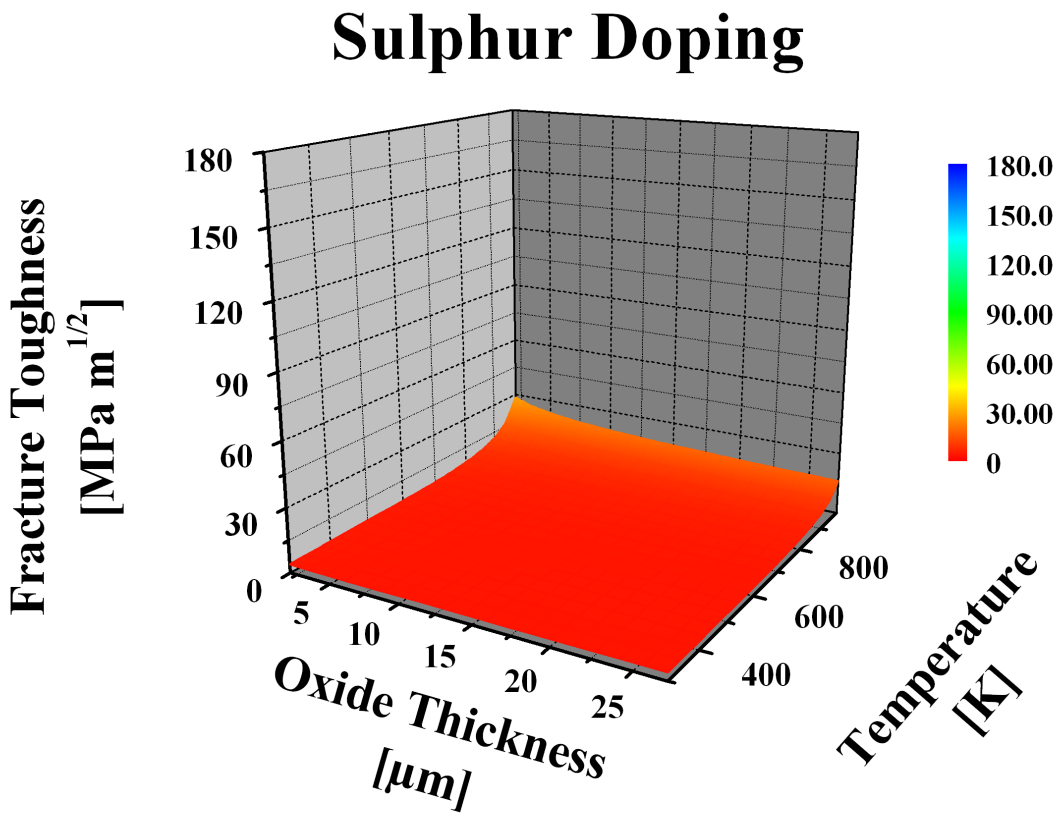

Figure 4.3: Deleterious effect of sulphur on the fracture toughness results of a β-NiAl / α-Al_2O_3 interface.

Again, referring to the baseline results as the benchmark, S-doping results in the following:

- Maximum fracture toughness = 28.15 [MPa $m^{1/2}$]

- Fracture toughness at minimum oxide thickness = 4.10 [MPa $m^{1/2}$]
- Fracture toughness at maximum oxide thickness = 3.53 [MPa $m^{1/2}$]

These results show a staggering overall reduction of ∼50% in each of the benchmark values.

4.3 Hafnium Doping

Contrary to the results from sulphur doping, hafnium doping indicated a substantial increase in toughness throughout the simulated cycle, the results of which are illustrated in Figure 4.4, below.

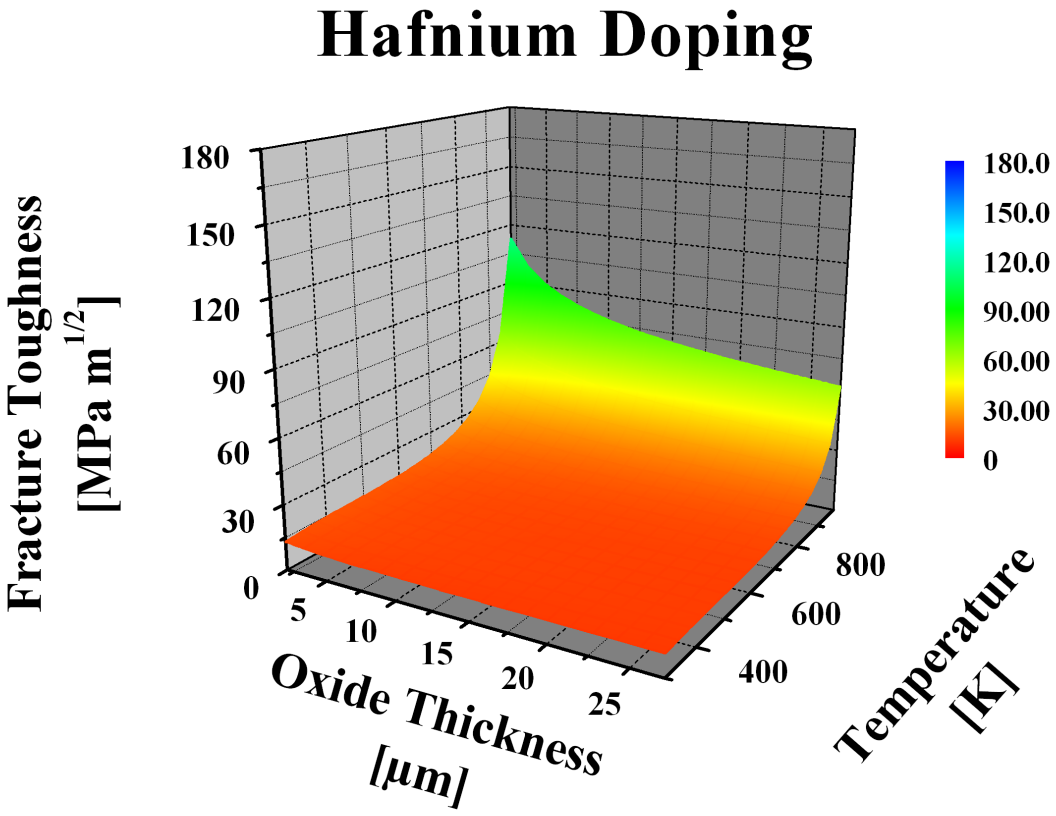

Figure 4.4: Hafnium doping results from the interfacial fracture toughness simulation.

Hafnium provided the following improvements:

- Maximum fracture toughness = 113.08 [MPa $m^{1/2}$]
- Fracture toughness at minimum oxide thickness = 13.18 [MPa $m^{1/2}$]
- Fracture toughness at maximum oxide thickness = 9.97 [MPa $m^{1/2}$]

These results provide clear indication that Hf-doping delivers a marked increase in overall fracture toughness at the interface.

4.4 Yttrium Doping

Similar to hafnium, yttrium also provided notable increases in overall interfacial fracture toughness, seen in Figure 4.5.

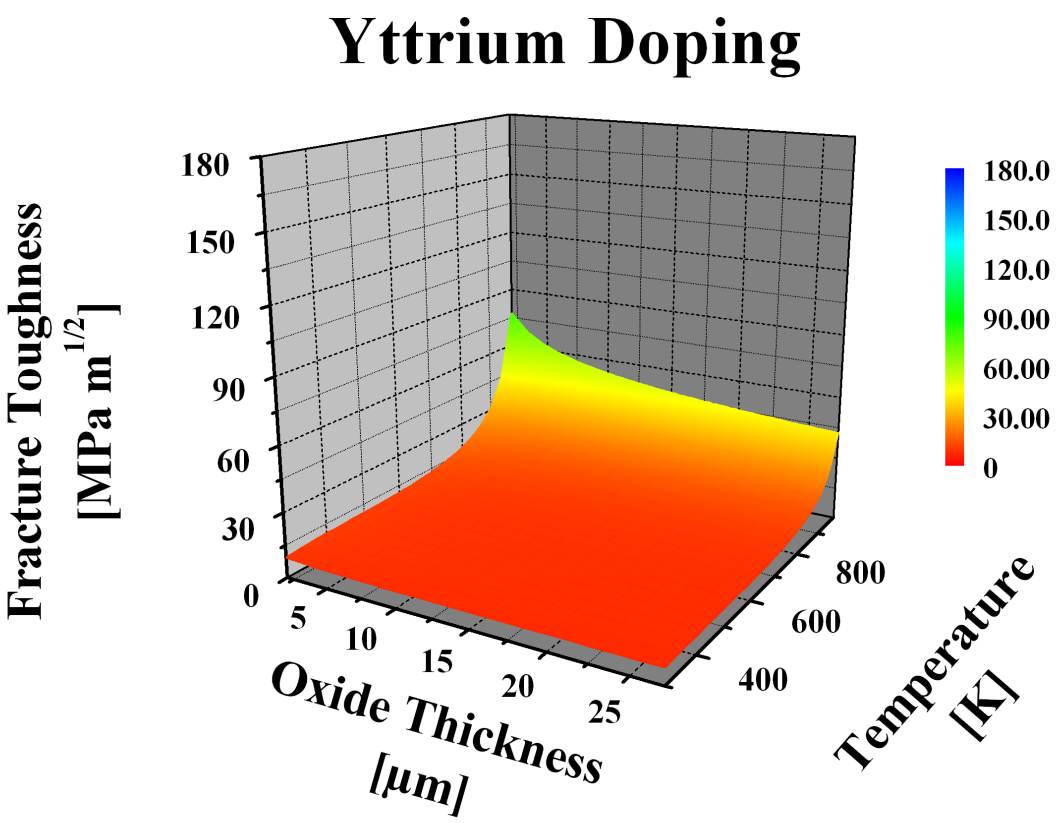

Figure 4.5: Yt-doping results for interfacial fracture toughness.

Considering the same benchmark values from the clean interface, Y provided:

- Maximum fracture toughness = 77.10 [MPa $m^{1/2}$]
- Fracture toughness at minimum oxide thickness = 9.47 [MPa $m^{1/2}$]
- Fracture toughness at maximum oxide thickness = 7.45 [MPa $m^{1/2}$]

These results show that the individual elemental additions alone, with the exception of platinum, provide a notable impact on the fracture toughness of the coating.

4.5 Co-Doping Results

The previous results were based on the insertion of a single dopant species atom into the β-NiAl / α-Al_2O_3 interface. These elements alone provided evidence for substantial influences on the interfacial fracture toughness ranging from staggering reduction to noteworthy increases overall. Some research [11, 15, 31] has indicated the possibility of synergistic effects between elemental additions. In order to explore the possibility of this effect, the model was imparted with a co-doping simulation. The results of which can be seen in Figure 4.7a) through d), and the overall results for single element doping and co-doping can be seen in Table 4.1.

Table 4.1: Summary of model fracture toughness results.

Atomic Species	Maximum Fracture Toughness [MPa $m^{1/2}$]	Fracture Toughness at Min. Oxide Thickness [MPa $m^{1/2}$]	Fracture Toughness at Max. Oxide Thickness [MPa $m^{1/2}$]
Clean Interface	64.98	8.19	6.55
Single Element Results			
Platinum	65.72	8.27	6.61
Sulphur	28.15	4.10	3.53
Hafnium	113.08	13.18	9.97
Yttrium	77.10	9.47	7.45
Co-Doping Results			
Platinum + Sulphur	34.75	4.87	4.12
Hafnium + Sulphur	60.13	7.67	6.18
Hafnium + Platinum	113.27	13.20	9.99
Yttrium + Hafnium	174.42	19.32	13.97

These values are also plotted together in Figure 4.6 to compare these values graphically, to more readily compare these benchmark values across the elemental doping simulations.

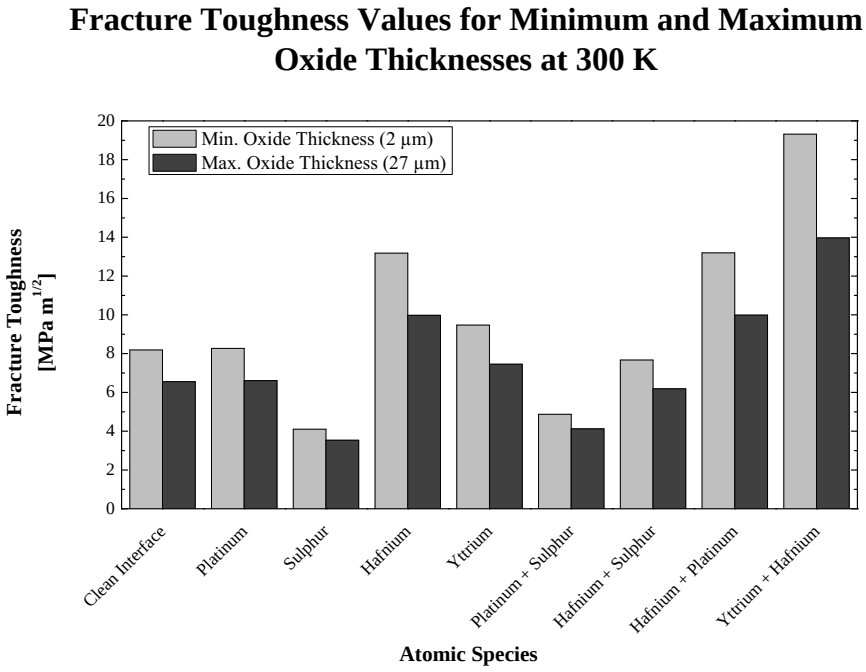

Figure 4.6: Fracture toughness results for minimum and maximum oxide thicknesses at 300 K.

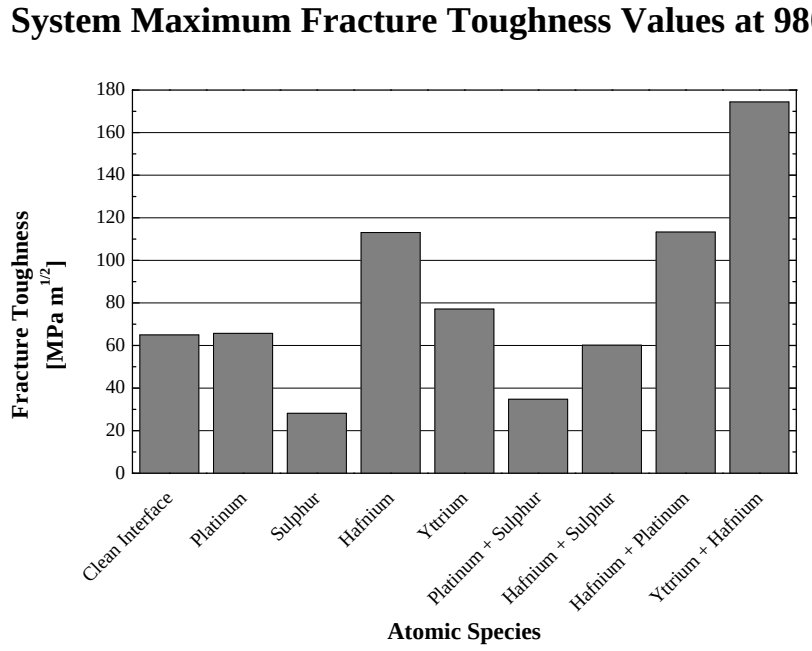

Figure 4.7: Fracture toughness results for maximum system value at 980 K at minimum oxide thickness.

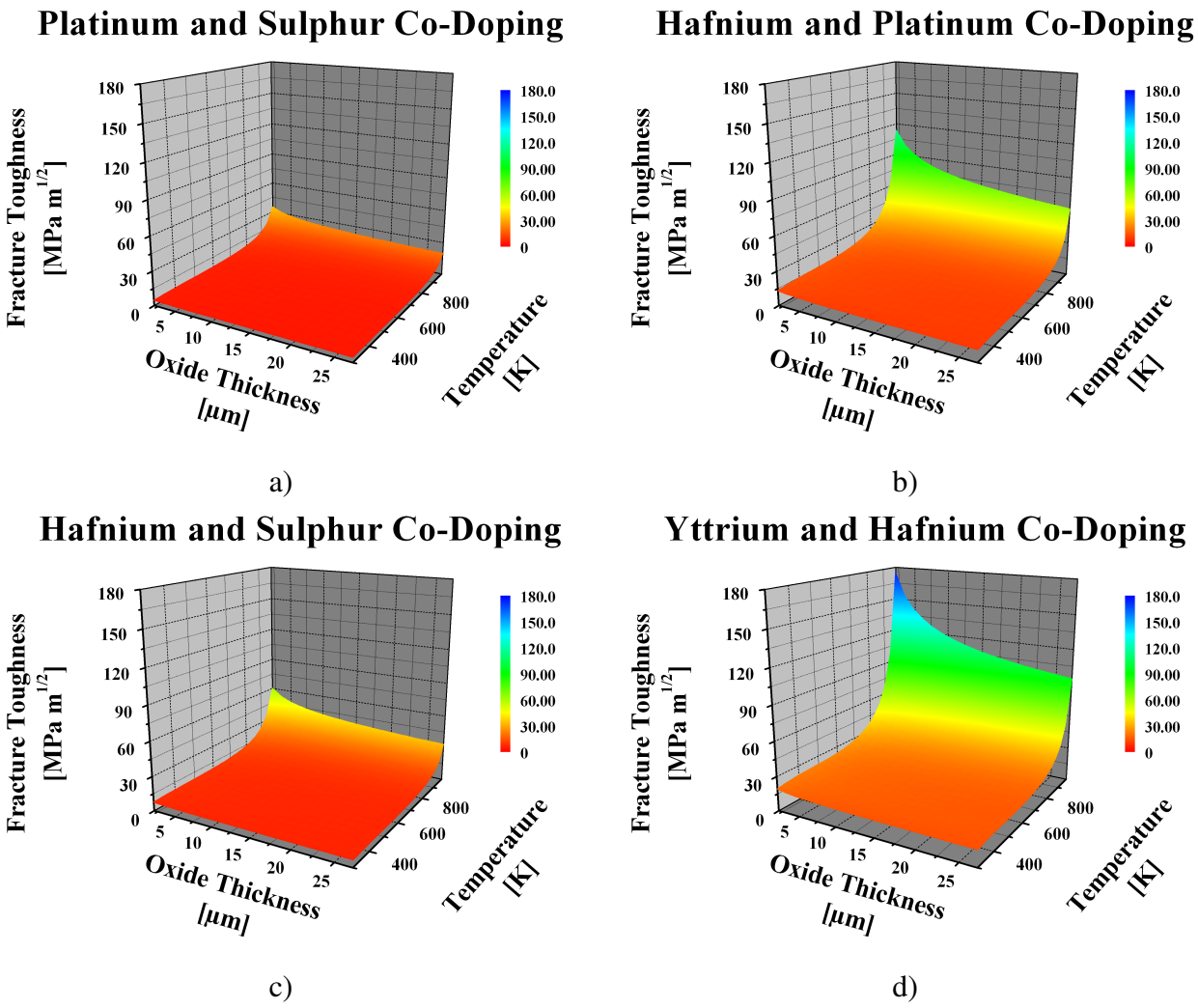

Figure 4.8: Co-doping simulation for interfacial fracture toughness of a) Pt+S, b) Hf+Pt, c) Hf+S and d) Y+Hf.

These results reflect the trends of the single doping results, as well as provide insight into synergistic effects. The benchmark values for these co-doping simulation results are included above in Table 4.1.

Chapter 5

Discussion

The results of these simulations agree with experimental results that indicate that minimal amounts of reactive element additions, S, Hf and Y in this case, can have a dramatic impact on the performance of TBC systems. Specifically, these results indicate that these elements can have particularly unambiguous effects on the fracture toughness of the BC/TGO interface. While Hf and Y displayed improvements to the interface, S led to dramatic reductions in performance, which is reflected in oxidation testing performed in other investigations, particularly in research conducted by Haynes *et al.* [8, 12, 13, 17, 24] and Evans *et al.* [2, 20, 26, 30]. Pt-doped interfaces however provided nominal improvements to the toughness.

5.1 Single Element Effects

As noted from the results of the single atomic species dopants, solo atoms can have a dramatic impact on the fracture toughness of the BC/TGO interface. Most notable are the contributions from sulphur and hafnium. Sulphur resulted in a dramatic reduction in the overall resistance to fracture of the interface. This is likely a result of the atomic interactions that occur at the interface. As described by Ozfidan *et al.* [39], the inclusion of sulphur in the interface results in repulsion between the sulphur atom and its nearest neighbour oxygen atoms from the Al_2O_3 component. This results in a weakening of the interface as these two atomic species seek to repel one another. Therefore, this ultimately reduces the work of adhesion and corresponds to a reduction in the interfacial fracture toughness.

The effect hafnium has on the interface is also a direct result of the atomic activity at the interface. Based on observations [39], it was noted that the Hf distributes in close proximity to O atoms. Due to its reactivity, this leads to the formation of ionic bonds, as well as intermetallic bonding with Ni atoms. It was also observed that the number of bonds between Al_{NiAl}, which represents the aluminum within the NiAl structure, and O was increased. These same bonds also exhibit a shortened bond length. The shortened bond length increases the attraction between the atoms, resulting in a more resilient coupling. The combination of these two phenomena provide a synergistic effect that increases the overall atomic adherence at the interface. This effect would seem to be responsible for the increased fracture toughness of the interface. It was noted that Y seemed to display similar characteristics as it would also form mixed bonds (intermetallic and ionic), but the number of bonds were reduced and the length of the bonds were increased. Therefore, similar to Hf, the

addition of Y increases the toughness through this mixed bonding, though the increase is mitigated by the reduction in adhesion caused by the smaller number of bonds as well as the increased bond length. Conversely to a shortened bond length, the increased bond length reduces the strength of the atomic coupling by increasing the interatomic distance.

Platinum, however, did not provide any notable change in the fracture toughness of the interface. Although the benefit of platinum has been observed, and is generally accepted in commercial practice, its beneficial mechanism would not seem to stem from improving the fracture behaviour of the interface. As seen in Section 4.1, platinum had negligible effect on the fracture toughness. Although platinum has been identified as providing beneficial effects to TBC systems [8, 10, 17] , the mechanism by which it provided this benefit remained elusive. However, the co-doping simulations must be considered before reaching a conclusion.

5.2 Co-Doping Effects

Figure 4.7 provides insight into the effects of co-segregated elements at the interface, especially when compared to the single element results from Figure 4.2 to Figure 4.5. The results from co-doping are varied, but share many similarities with the single element simulations.

Figure 4.7a), the result of co-doping Pt and S, is noted by its similarity to Figure 4.3, which is the result for doping only with S. Comparing Figure 4.7a) with Figure 4.7b), the common element is S. In the first figure, Pt + S, the effect on interfacial fracture toughness seems to be driven by the presence of sulphur. However, if Hf + S is considered [Figure 4.7b], it would seem that the deleterious effect of sulphur is counteracted by the beneficial effect of hafnium. This is likely due

to the force of repulsion, caused by the presence of S, being counteracted by the improved bonding performance imparted by the presence of Hf. Similarly, by comparing the results of Hf + S co-doping with the results from Y + Hf co-doping, a superposition relationship becomes apparent.

When considering Y + Hf co-doping, keeping in mind the individual results from their single element doping simulations, the results would suggest that elements that are beneficial may act synergistically to further enhance the fracture toughness. In the case of Y + Hf, the effect is not purely additive as 174.42 $m^{1/2}$ is less than would be anticipated if the two effects were simply superimposed, which would result in 190.18 MPa $m^{1/2}$. However, it remains clear that the two act in concert to improve the overall interfacial fracture properties, showing drastic improvements during both oxide growth and temperature increase.

Using the apparent effect of superposition related to these element additions, it is observed that Pt, similar to the single element results, tends to play a minor role in the fracture toughness of the interface. These results indicate the value that is imparted by the addition of beneficial reactive elements while also underlining the need to reduce the effect of detrimental atoms, such as S. These findings also indicate that Pt provided relatively little impact on the interfacial fracture toughness. Although determining the exact effect Pt has on these coatings lies outside the scope of this investigation, it is evident that its effect is not acting to directly increase the strength of the interface. Therefore, it is likely that Pt's function lies more in another phenomenon.

5.3 Isothermal Analysis

Since the cycle was simulated as discrete increments in temperature, it is valuable to also consider the behaviour of each addition at an isotherm to gain insight into how each element compares to the others throughout the simulated cycle. In order to conduct this analysis, two isotherms were chosen, one at 620 K and the other at 900 K. The first figure, Figure 5.1, is the behaviour of single element doping at 620 K while Figure 5.2 presents the same isotherm results for co-doped elements.

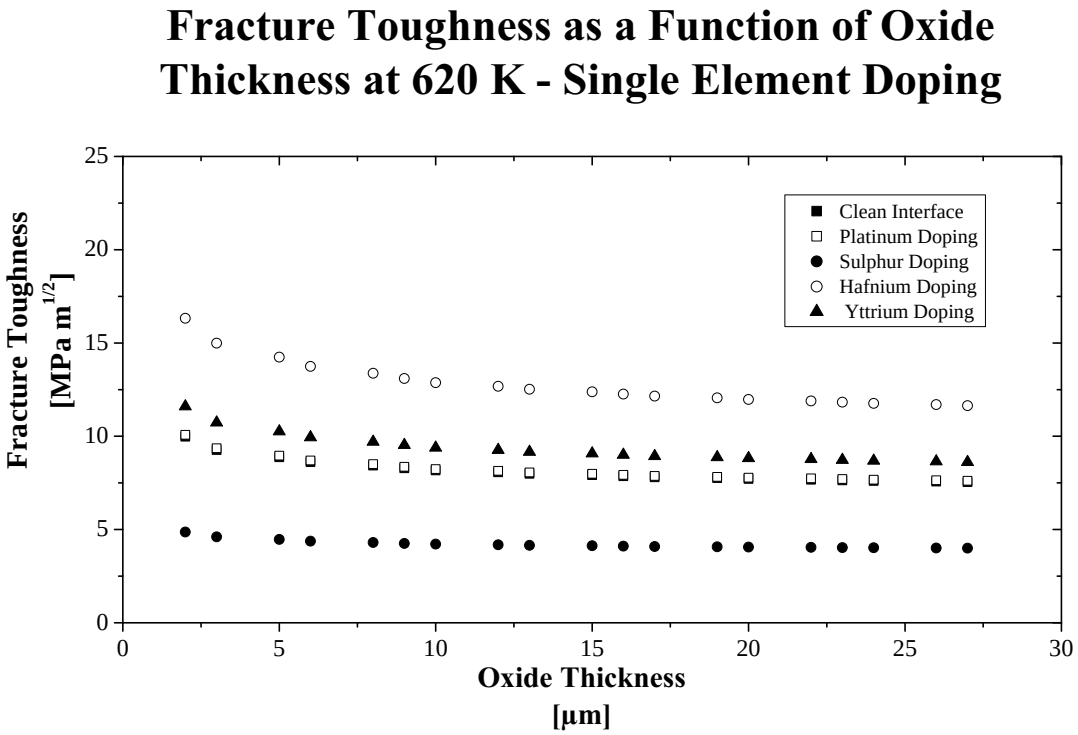

Figure 5.1: Fracture toughness as a function of oxide thickness at 620 K for a clean interface, compared to single element doping contributions.

The first characteristic to note in Figure 5.1 is that for all elements, the fracture toughness decreases with increasing oxide thickness. Secondly, it is relevant to observe, as noted earlier, the

effect of platinum. The profile for platinum is nearly congruent with the clean interface behaviour, effectively obscuring the latter. This figure also shows the increase in toughness that hafnium and yttrium provide, while drawing attention to the negative impact imparted due to the presence of sulphur.

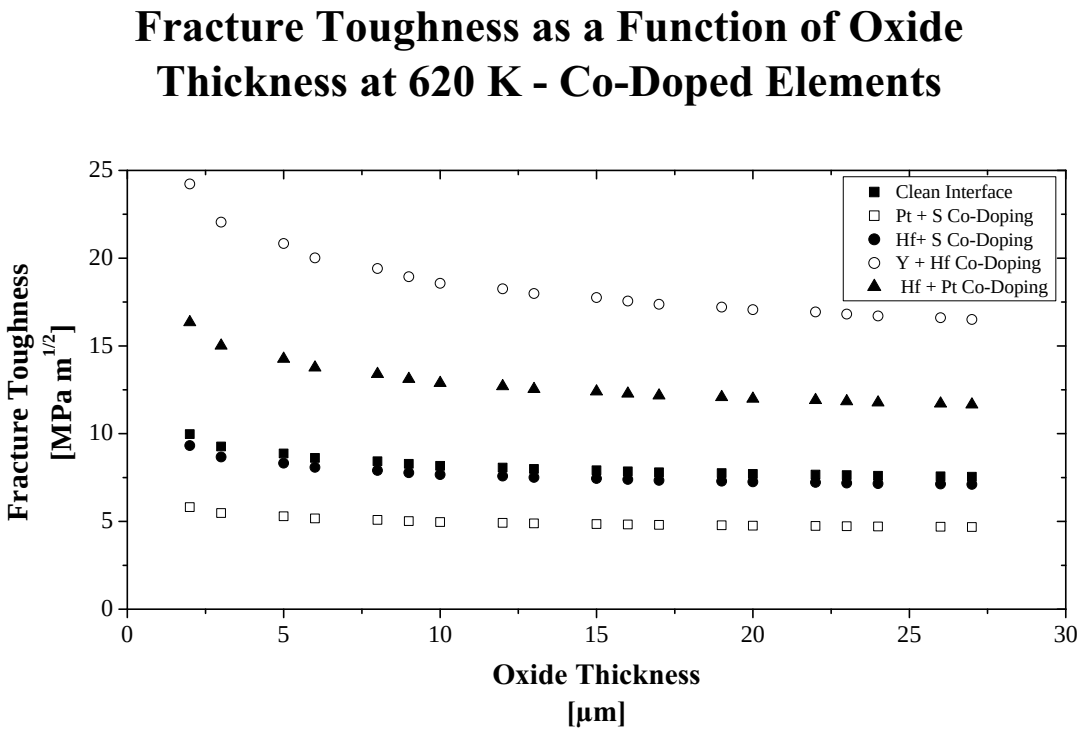

Figure 5.2: Co-doped element fracture toughness results as a function of oxide thickness at 620 K compared to a clean interface.

Similarly to the previously noted results, Figure 5.2 provides clearer examples of behaviour noted above in Section 5.2. For example, the contributions of each element can be seen more clearly when compared in these combined scenarios. Considering the curve for co-doped sulphur with platinum provides further evidence that suggests that while sulphur plays a notable deleterious role in interface toughness, platinum's contribution is negligible. This is determined by comparing

these curves with the results from Figure 5.1. This is more notable when considering hafnium and sulphur co-doping. When considering these elements alone to the clean interface, sulphur reduces the toughness by $\sim 50\%$ while hafnium increases the toughness by nearly the same margin. However, when combined together, their individual effects seem to counteract one another. Since the overall result is a reduction in interfacial toughness, this would imply that sulphur's action of causing a repulsion in the interface is of slightly larger magnitude than hafnium's ability to increase bonding. Conversely, the ability of sulphur to generate repulsions at the interface may simply compromise hafnium's ability to create bonds.

The isotherm analysis for 900K is presented below in Figure 5.3 and Figure 5.4.

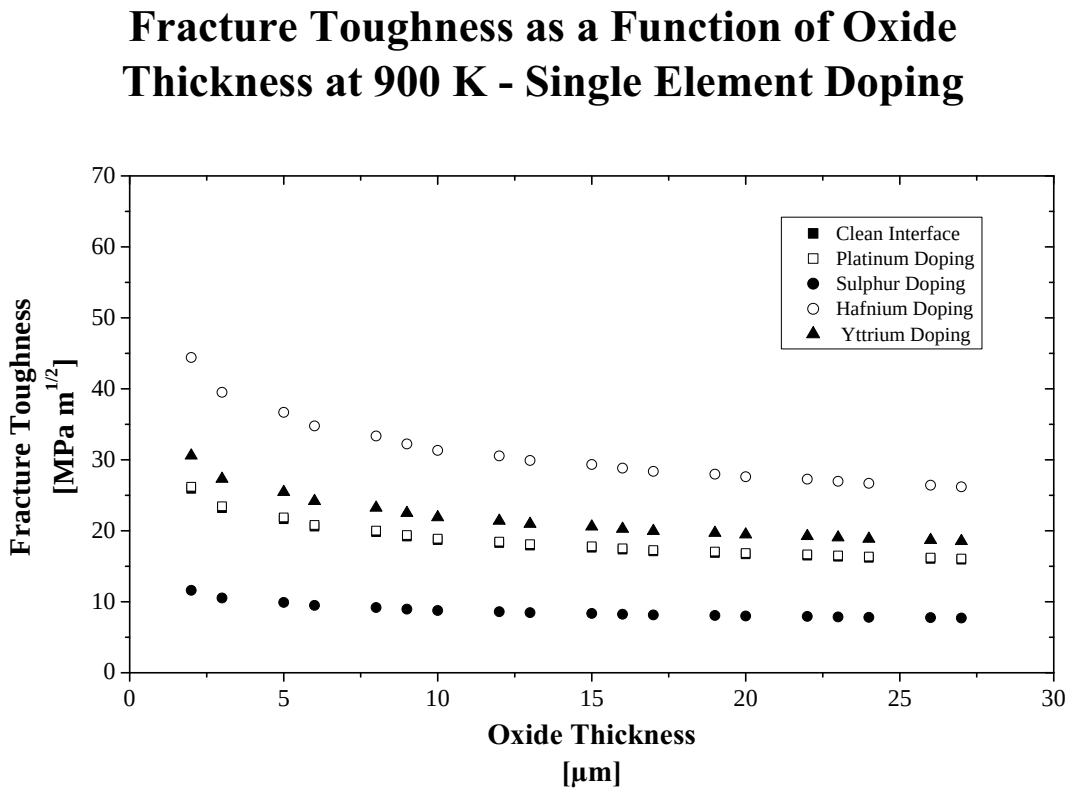

Figure 5.3: Singularly-doped element fracture toughness results as a function of oxide thickness at 900 K compared to a clean interface.

Similar to the isotherm results in Figure 5.1, the 900 K isotherm in Figure 5.3 shows similar trends. The primary difference is that the overall toughness is increased for each sample, accented by the increase in vertical axis scale, at the higher exposure temperature because, as noted earlier, compliance increases with temperature. It is noted that platinum, sulphur, hafnium and yttrium all play the same role at the higher temperatures as they did at 620 K. This is evident throughout the entire temperature cycle, which is why the contours in section 4 have unwrinkled profiles.

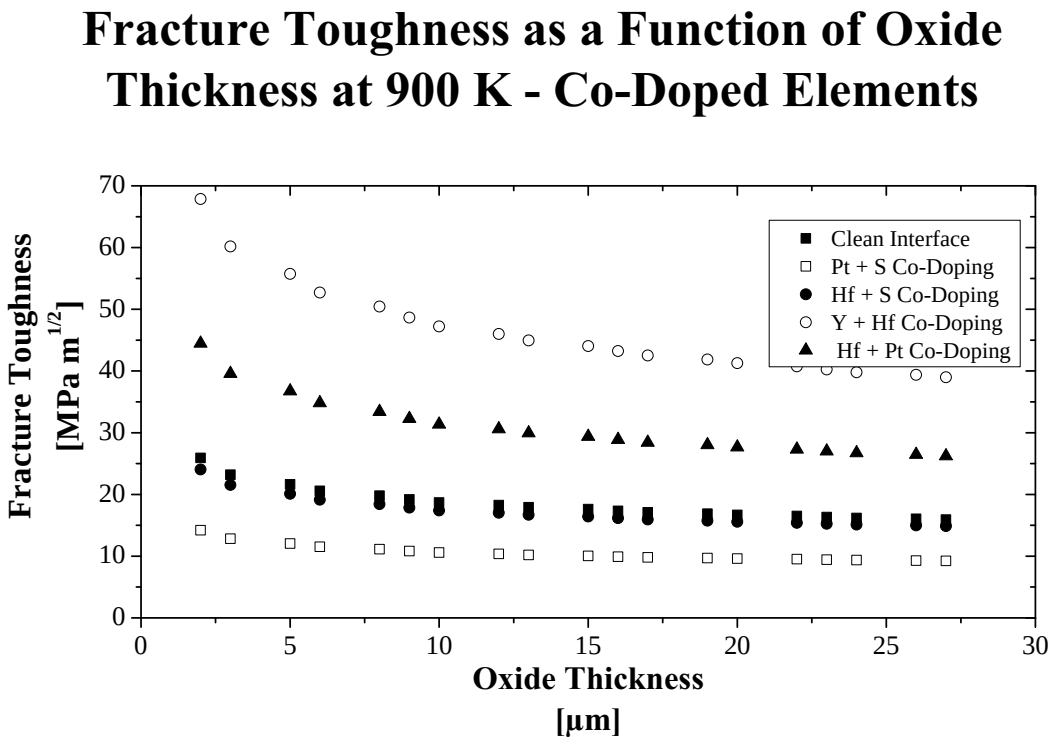

Figure 5.4: Fracture toughness as a function of oxide thickness at 900 K for a clean interface, compared to single element doping contributions.

Further to the previous discussion, hafnium and platinum can also be compared to see how the elements behave. In this case, it has been noted that platinum's contribution is minimal, and this is made more evident when hafnium is co-doped with platinum since the magnitude of the hafnium

addition is the same, regardless of whether it was doped with platinum or by itself.

5.4 Correlation with Experimental Observations

The trends in these results are similar to the trend seen in another modelling investigation. Vasinonta and Beuth [48], in their study using indentation, noted that the fracture toughness at the interface decreases steadily when the ratio of the debonded area to the indenter radius increases. A FE model was developed to determine the normalized displacement of the film layers during indentation, which were indented using a brale C indenter in a Rockwell hardness tester. The fracture toughness at the interface was then calculated based on the displacements determined from the FE model and the radius of delamination observed in the indent test, shown in equations 5.1 and 5.2. The results from these calculations were then validated by previous indenter tests for samples coated with a TBC system.

$$K_c = \sqrt{\frac{G\bar{E}_{TGO}(1-\alpha)}{1-\beta^2}} \tag{5.1}$$

where:

$$G = \frac{3(1-\nu^2)\left(\sigma_o^{TGO} - \sigma_o^{TBC}\right)^2 t_{TGO}^2}{2(t_{TGO}+t_{TBC})E_{TBC}} \tag{5.2}$$

and $\bar{E}_{TGO}$ is the plane strain elastic modulus of the TGO, E_{TBC} the modulus of the top coat, ν is the poisson's ratio of the coating, σ_o^{TGO} and σ_o^{TBC} are the residual stresses of the TGO and TBC top coat respectively, t_{TGO} and t_{TBC} are the thicknesses of the TGO and top coat, while α and β are modified Dundurs parameters.

The results of this study, shown in Figure 5.5 indicate a similar decreasing toughness trend to the trends noted above in Figures 5.1 to 5.4.

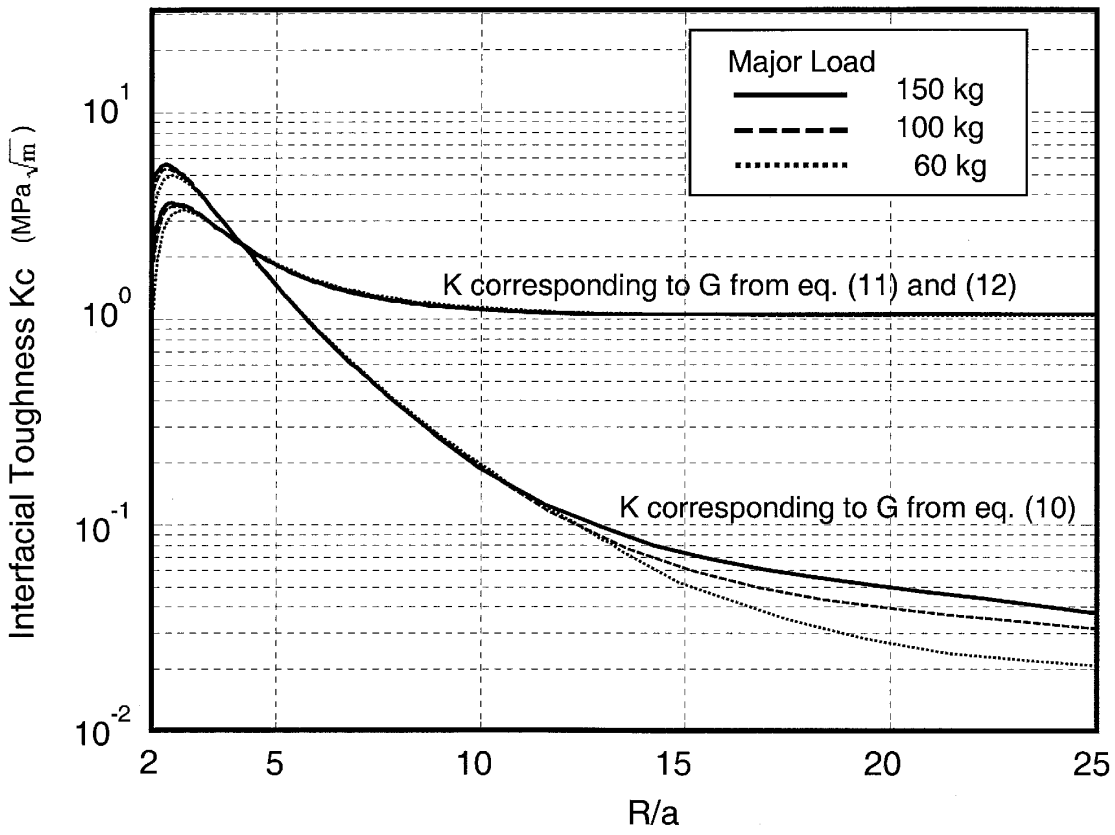

Figure 5.5: Interfacial fracture toughness calculated from indentation tests performed on samples coated in a full depth TBC [48].

This figure indicates that, as the ratio of the radial distance, R, of the observed delamination due to the indentation to the contact radius of the indenter, a, increases, the fracture toughness at the interface declines rapidly following a brief initial increase. Although these results are similar to those previously reported in this document, it is important to note some differences. Firstly, the loading applied is external, however its configuration does provide an analogue for residual stresses caused by mismatches in the coefficients of thermal expansion [48]. Secondly, the testing is carried out on monotonically exposed samples at 1200°C and the loading condition of this scenario

is mixed, leading to a fracture toughness value that is not specific to mode I. However, they do represent experimental measurements of the interfacial fracture toughness with consideration for the TGO and top coat layer thicknesses. This model also correlated well with observed indenter tests [48].

Furthermore, Zhao *et al.* [49] noted that the interfacial fracture toughness decreases in much the same way as noted by Vasinonta and Beuth, when considering longer exposure at temperature.

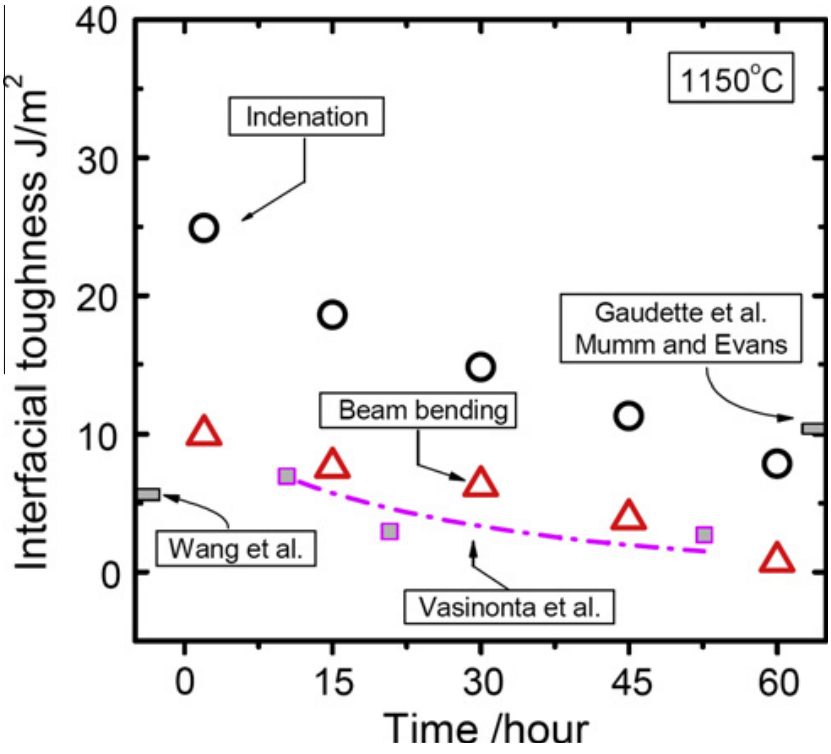

Figure 5.6: Interfacial fracture toughness calculated from beam bending and indentation tests performed on samples with varying exposure times at 1150°C [49].

These results show a similar decreasing trend, with the notable difference that the fracture toughness is decreasing as the exposure time at 1150°C increases. This may be a result of additional oxide growth leading to a weakening of the interface as the oxide layer becomes larger. It is also

compounded by the likely growth of θ-phase Al_2O_3 [49] which, as indicated earlier, is not an ideal oxide as it has lower adhesion characteristics when compared to α-Al_2O_3. Although these studies each consider different phenomena, these results, as well as the results published in this document, show good correlation overall related to the degradation of fracture toughness at BC/TGO interfaces as a function of increased oxide layer thickness and temperature considerations.

Chapter 6

Conclusions

The purpose of this research was to develop a model designed to elicit insight into the effect that Pt, S, Hf and Y elemental additions can have on the fracture toughness of β-NiAl / α-Al_2O_3 interfaces. Previous investigations have considered the oxidation behaviour of these systems as a result of elemental composition [2, 8, 13, 17, 23, 25, 32], while others even dealt with determining the interfacial fracture toughness of these systems [48, 49]. However, to this author's knowledge, only one study has been conducted dealing with chromium addition [30], though it excluded the bond coat. No other studies have been identified that considered the effect that these other doping elements have on the interfacial fracture toughness at the interface when segregant and doping elements are present. Therefore, since it is well known that doping elements, and segregants, have a marked impact on the lifecycle behaviour of TBC systems [1, 8, 12–14, 17, 24, 26, 28–30, 39], an investigation focusing on the contribution of these elements to fracture toughness was conducted. A model was developed that considered previous studies and combined a previous investigation

into the atomic characteristics of this interfacial system [39] with continuum level mechanics to determine the fracture toughness of the interface in the presence of element doping.

In order to develop this model, this research focused on several considerations. First, the model had to simulate exposure of a BC/TGO interface to a temperature cycle. Therefore, since these materials undergo changes in material properties as temperature increases, the thermo-elastic properties of these two materials were required as functions of temperature. It was identified that the BC yield strength would be necessary for the model, as would the elastic moduli of the BC and TGO. Temperature dependent equations were then determined based on published observations [23, 40]. Secondly, as these coatings undergo thermal cycling, they also develop various states of residual stress. In order for these coatings to not immediately fail, this residual stress must also be counteracted by internal adhesion. The mathematical relationship for the residual stress was determined from a published approximation [41]. The bond strength of the coating was then determined [44], and calculated for the various dopant species. Then the critical stress relationship between the two was ascertained. Having determined relationships for the thermo-elastic properties as well as the stresses at the interface, the fracture toughness [46, 47] was then calculated to determine the effect of elemental additions.

It was determined that, for single doping elements, while Hf and Y both provided a marked improvement in interfacial fracture toughness, S reduced the toughness of the interface. It was also determined that, while Pt is noted as a beneficial atomic addition, it's mechanism of action is not related to fracture toughness.

For co-doping elements, it was noted that Hf and Y again provided a noted increase in fracture

toughness and would even offset the deleterious effect of S. This implies that Hf and Y additions at TGO/BC interfaces provide a clear improvement, by superposition, to the fracture toughness of the interface. It was also noted that when Pt and S are doped in tandem at the interface that the effect S has is far more prominent than the minor contribution from Pt. This provided further evidence to conclude that Pt does not provide a marked improvement in fracture toughness. Therefore, after analysing the results from these simulations, it can be argued that Pt's benefit is certainly not derived from an effect related to the fracture toughness of the interface, since the contribution from the reactive elements is far greater. Therefore, Pt's effect is likely the result of another phenomenon, perhaps related to the size of the atom and it's electron activity [39]. It is possible, since Pt is a large atom (139 pm, 1.39 Å) in substitution for nickel, that it may reduce sulphur's ability to diffuse through the bond coat. Since sulphur is also a larger atom (100 pm, 1.0 Å) that tends to segregate through substitution and vacancy occupation rather than interstitial diffusion, Pt can often occupy sites where sulphur would prefer to be located, thus potentially blocking it's path. Obviously, diffusion relies on other considerations aside from atomic size alone, such as energy states and electronic activity, but atomic radii remains a notable contribution.

It should be noted that, while these simulations provided insight that correlate well with observed experimental results [48, 49], the model has some fundamental limitations. For instance, creep is not considered. Creep can serve to relax stresses that develop at the interface, therefore by not including creep in this model it can be argued that the results for residual stress are higher than they would be otherwise. Secondly, the thermo-elastic properties of the bond coat were determined based on direct exposure to high temperatures. This would not be the case in a commercial or experimental TBC system, as the presence of the TGO would limit the BC's direct exposure to

the temperature cycle. This would lead to the model containing a minor overestimate of the effect of temperature on the yield strength and elastic modulus of the bond coat. Thirdly, the data determined from the quantum simulation that was used to calculate the work of adhesion was not varied with temperature as this simulation was carried out in isothermal conditions. Finally, it should also be stated that diffusion effects were also omitted from these simulations. The diffusion of different species into the interface is a phenomenon that occurs during temperature cycling. However, in order to ascertain the specific effects related to the presence of particular atomic species, diffusion effects were omitted in an attempt to limit the possible obfuscation this might have caused.

6.1 Proposed Future Work

Although the results of the simulation provided interesting insight into the fracture toughness behaviour of the BC/TGO interface, the limitations of the model must also be recognized. Therefore, as part of a larger study focused on generating a more detailed understanding of the effects elemental additions have on TBC systems, this investigation has provided the framework upon which subsequent studies can be developed.

6.1.1 Modelling and Simulation Enhancements

Since the goal of modelling is to develop constructs that are representative of real systems in order to experiment and conduct analysis that may otherwise prove difficult or unfeasible, the following enhancements may be investigated to make the presented model more realistic.

1. The inclusion of creep in the model would provide for a stress relaxation throughout the sim-

ulation. This would require a more dynamic simulation, but would provide greater fidelity.

2. Diffusion modelling would greatly enhance the existing model. Inclusion of diffusive elements would allow for a more robust simulation that more closely resembles the effects noted during high temperature cycles in gas turbine engines. Furthermore, this addition would allow the investigator to identify what elements are diffusing to the interface as well as their concentration. This would also ultimately require a greater flexibility in calculations related to the work of adhesion as they could be implemented simultaneously.

3. The current model considers the TGO growth as a discrete event separate from the temperature cycle. Further development can lead to an oxide growth model where the thickness of the oxide can be determined based upon the composition of the BC and the exposure temperature of the cycle. This would create a more dynamic model that can be further enhanced by the previously mentioned diffusion model.

4. It could also be beneficial to model the unit cell fluctuation related to the residual stress variations to determine what, if any, additional or reduced diffusion may take place as a result of an enlargement or reduction in unit cell dimensions.

6.1.2 Further Investigations

Aside from the modelling considerations, this preliminary investigation can also be combined with other areas of interest.

1. Since these coatings are highly susceptible to influence from segregant elements, this simulation could be combined with experimental practices. Provided that most of the substrates and

bond coats used in previous investigation are currently commercially available, these systems could be characterised and then modelled more accurately. This could be used to ultimately develop life cycle predictions.

2. The current model considers dense coatings, however the importance of deposition method had also been identified. Therefore, the model could be further improved by correlating it with experimental investigation using oxidation samples. This could provide correction factors to further improve simulation reliability.

Bibliography

[1] Y. Zhang, D. A. Ballard, J. P. Stacy, B. A. Pint and J. A. Haynes, "Synthesis and oxidation behaviour of platinum-enriched γ+γ' bond coatings on Ni-based superalloys", *Surface & Coatings Technologies*, vol. **201**, pp. 3857-3861, 2006.

[2] A. G. Evans, D. R. Clarke and C. G. Levi, "The influence of oxides on the performance of advanced gas turbines", *Journal of the European Ceramic Society*, vol. **28**, pp. 1405-1419, 2008.

[3] A. G. Evans, M. Y. He and J. W. Hutchinson, "Mechanics-based scaling laws for the durability of thermal barrier coatings", *Progress in Materials Science*, vol. **46**, pp. 249-271, 2001.

[4] J. W. Hutchinson, A. G. Evans, "On the delamination of thermal barrier coatings in a thermal gradient", *Surface & Coatings Technology*, vol. **149**, pp.179-184, 2001

[5] A. Feuerstein, J. Knapp, T. Taylor, A. Ashary, A. Bolcavage and N. Hitchman, "Technical and Economical Aspects of Current Thermal Barrier Coating Systems for Gas Turbine Engines by Thermal Spray and EBPVD: A Review", *Journal of Thermal Spray Technology*, vol. **17**, pp. 199-213, 2008.

[6] R. A. Miller, "History of Thermal Barrier Coatings for Gas Turbine Engines. Emphasizing NASA's Role From 1942 to 1990", *NASA Technical Report*, **NASA/TM-2009-215459**, National Aeronautics and Space Administration, 2009

[7] B. A. Pint, S. A. Speakman, C. J. Rawn, Y. Zhang, "Deformation and Phase Transformations during the Cyclic Oxidation of Ni-Al and Ni-Pt-Al", *The Journal of The Minerals, Metals & Materials Society (TMS)*, vol. **58**, pp.47-52, 2006

[8] J. A. Haynes, B. A. Pint, Y. Zhang and I. G. Wright, "Comparison of the oxidation behavior of β and γ-γ' NiPtAl coatings", *Surface & Coatings Technologies*, vol. **204**, pp. 816-819, 2009.

[9] A. Christensen, E. A. Asche and E. A. Carter, "Atomic Level Properties of Thermal Barrier Coatings: Characterization of Metal-Ceramic Interfaces", *University of California, Los Angeles*, 2001.

[10] X. Zhao and P. Xiao, "Effect of platinum on the durability of thermal barrier systems with a γ+γ' bond coat", *Thin Solid Films*, vol. **517**, pp. 828-834, 2008.

[11] T. Xu, S. Faulhaber, C. Mercer, M. Maloney and A. Evans, "Observations and analyses of failure mechanisms in thermal barrier systems with two phase bond coats based on NiCoCrAlY", *Acta Materialia*, vol. **52**, pp. 1439-1450, 2004.

[12] J. A. Haynes, "Potential Influences of Bond Coat Impurities and Void Growth on Premature Failure of EB-PVD TBCs", *Scripta Materialia*, vol. **44**, pp. 1147-1152, 2001.

[13] J. A. Haynes, B. A. Pint, Y. Zhang and I. G. Wright, "Comparison of the cyclic oxidation behaviour of β-NiAl, β-NiPtAl and γ-γ'. NiPtAl coatings on various superalloys", *Surface & Coatings Technologies*, vol. **202**, pp. 730-734, 2007.

[14] R. Molins, I. Rouzou and P. Hou, "Chemical and morphological evolution of a (NiPt)Al bond-coat", *Oxidation of Metals*, vol. **65**, pp. 263-283, 2006.

[15] J. M. Andersson, "Controlling the formation and stability of alumina phases", *Linköpings universitet*, Linköping, Sweden, 2005.

[16] P. K. Wright and A. G. Evans, "Mechanisms governing the performance of thermal barrier coatings", *Current Opinion in Solid State and Materials Science*, vol. **4**, pp. 255-265, 1999.

[17] J. A. Haynes, B. A. Pint, K. L. More, Y. Zhang and I. G. Wright, "Influence of Sulfur, Platinum and Hafnium on the Oxidation Behavior of CVD NiAl Bond Coatings", *Oxidation of Metals*, vol. **58**, pp. 513-544, 2002.

[18] J. A. Haynes, M. J. Lance, B. A. Pint and I. G. Wright, "Characterization of commercial EB-PVD TBC systems with CVD (Ni,Pt)Al bond coatings", *Surface & Coatings Technologies*, Vols. **146-147**, pp. 140-146, 2001.

[19] N. Curry, N. Markocsan, X. H. Li, A. Tricoire and M. Dorfman, "Next Generation Thermal Barrier Coatings for the Gas Turbine Industry", *Journal of Thermal Spray Technology*, vol. **20**, pp. 108-115, 2010.

[20] A. G. Evans, D. R. Mumm, J. W. Hutchinson, G. H. Meier and G. H. Pettit, "Mechanisms controlling the durability of thermal barrier coatings", *Progress in Materials Science*, vol. **46**, pp. 505-553, 2000.

[21] M. P. Taylor, H. E. Evans, E. P. Busso and Z. Q. Qian, "Creep Properties of a Pt-aluminide coating", *Acta Materialia*, vol. **54**, pp. 3241-3252, 2006.

[22] W. J. Quadakkers, V. Shemet, D. Sebold, R. Anton, E. Wessel and L. Singheiser, "Oxidation characteristics of a platinized MCrAlY bond coat for TBC systems during cyclic oxidation at 1000°C", *Surface & Coatings Technologies*, vol. **199**, pp. 77-82, 2005.

[23] E. P. Busso and Z. Q. Qian, "A Mechanistic Study of Microcracking in Transversely Isotropic Ceramic-Metal Systems", *Acta Materialia*, vol. **54**, pp. 325-338, 2006.

[24] J. A. Haynes, B. A. Pint, Y. Zhang and I. G. Wright, "The effect of Pt content on γ-γ' on NiPtAl coatings", *Surface & Coatings Technologies*, vol. **203**, pp. 413-416, 2008.

[25] G. M. Kim, N. M. Yanar, E. N. Hewitt, F. S. Pettit and G. H. Meier, "The effect of the type of thermal exposure on the durability of thermal barrier coatings", *Scripta Materialia*, vol. **46**, pp. 489-495, 2002.

[26] F. G. Gaudette, S. Suresh and A. G. Evans, "Effects of Sulfur on the Fatigue and Fracture Resistance of Interfaces Between γ-Ni(Cr) and α-Al_2O_3", *Metallurgical and Materials Transactions*, vol. **31**, pp. 1977-1983, 2000.

[27] B. A. Pint, "On the Formation of Interfacial and Internal Voids in α-Al_2O_3 Scales", *Oxidation of Metals*, vol. **48**, pp. 303-328, 1997.

[28] A. G. Evans, J. W. Hutchinson and Y. Wei, "Interface Adhesion: Effects of Plasticity and Segregation", *Acta Materialia*, vol. **47**, pp. 4093-4113, 1999.

[29] D. M. Lipkin, D. R. Clarke and A. G. Evans, "Effects of Interfacial Carbon on Adhesion and Toughness of Gold-Sapphire Interfaces", *Acta Materialia*, vol. **46**, pp. 4835-4850, 1998.

[30] F. Gaudette, S. Suresh, A. G. Evans, G. Dehm and M. Rühle, "The Influence of Chromium Addition on the Toughness of γ-Ni/α-Al_2O_3 Interfaces", *Acta Materialia*, vol. **45**, pp. 3503-3513, 1997.

[31] A. G. Evans, M. Rühle, B. J. Dalgleish and P. G. Charalambides, "The Fracture Energy of Bimaterial Interfaces", *Materials Science and Engineering*, vol. **A126**, pp. 53-64, 1990.

[32] D. Pan, M. W. Chen, P. K. Wright and K. J. Hemker, "Evolution of diffusion aluminide bond coat for thermal barrier coatings during thermal cycling", *Acta Materialia*, vol. **51**, pp. 2205-2217, 2003.

[33] E. P. Busso, J. Lin, S. Sakurai and M. Nakayama, "A Mechanistic Study of Oxidation-Induced Degradation in a Plasma-Sprayed Thermal Barrier Coating System. Part 1: Model Formulation", *Acta Materialia*, vol. **49**, pp. 1515-1528, 2001.

[34] J. W. Hutchinson, M. Y. He and A. G. Evans, "The influence of imperfections on the nucleation and propagation of blucking driven delaminations", *Journal of the Mechanics and Physics of Solids*, vol. **48**, pp. 709-734, 2000.

[35] J. W. Hutchinson, M. D. Thouless and E. G. Liniger, "Growth and Configurational Stability of Circular Buckling-Driven Film Delaminations", *Acta Metallurgica et Materialia*, vol. **40**, pp. 295-308, 1992.

[36] J. W. Hutchinson and Z. Suo, "Mixed Mode Cracking in Layered Materials", *Advances in Applied Mechanics*, vol. 29, pp. 63-262, 1992.

[37] Z. Suo and J. W. Hutchinson, "Sandwich Test Specimens for Measuring Interface Crack Toughness", *Materials Science and Engineering*, vol. **A107**, pp. 135-143, 1989.

[38] T. Suga, G. Elssner and S. Schmauder, "Composite Parameters and Mechanical Compatibility of Material Joints", *Journal of Composite Materials*, vol. **22**, pp. 917-934, 1988.

[39] I. Ozfidan, K. Chen and M. Fu, "Effects of Additives and Impurity on the Adhesive Behaviour of NiAl(110)/α-Al_2O_3(0001) interface: an ab initio study", *Metallurgical and Materials Transactions*, vol. **42A**, pp. 4126-4136, 2011.

[40] R. D. Noebe, R. R. Bowman and M. V. Nathal, "Physical and Mechanical Properties of the B2 Compound NiAl", *International Materials Reviews*, vol. **38-4**, pp. 193-232, 1993.

[41] A. G. Evans, G. B. Crumley and R. E. Demaray, "On the mechanical behaviour of brittle coatings and layers," *Oxidation of Metals*, vol. **20**, pp. 193-216, 1983.

[42] S. X. Mao and A. G. Evans, "The Influence of Blunting on Crack Growth at Oxide/Metal Interfaces", *Acta Materialia*, vol. **45**, pp. 4263-4270, 1997.

[43] N. I. Tymiak, A. A. Volinsky, M. D. Kriese, S. A. Downs and W. W. Gerberich, "The Role of Plasticity in Bimaterial Fracture With Ductile Interlayers", *Metallurgical and Materials Transactions A.*, vol. **31**, pp. 863-872, 2000.

[44] W. W. Gerberich and M. J. Cordill, "Physics of Adhesion", *Reports on Progress in Physics*, vol. **69**, pp. 2157-2203, 2006.

[45] M. Nganbe, Ch. 1.2 - Fracture Mechanics, *University of Ottawa*, Ottawa, Canada, 2011.

[46] M. S. Hu and A. G. Evans, "The Cracking and Decohesion of Thin Films on Ductile Substrates", *Acta Metallurgica*, vol. **37**, pp. 917-925, 1988.

[47] B. A. Latella, B. K. Gan, K. E. Davies, D. R. McKenzie and D. G. McCulloch, "Titanium Nitride/Vanadium Nitride Alloy Coatings: Mechanical Properties and Adhesion Characteristics", *Surface & Coatings Technologies*, vol. **200**, pp. 3605-3611, 2006.

[48] A. Vasinota and J. L. Beuth, "Measurement of interfacial toughness in thermal barrier coating systems by indentation", *Engineering Fracture Mechanics*, vol. **68**, pp. 843-860, 2001.

[49] X. Zhao, J. Liu, D.S. Rickerby, R.J. Jones, P. Xiao, "Evolution of interfacial toughness of a thermal barrier system with a Pt-diffused γ/γ' bond coat", *Acta Materialia*, vol. **59**, pp.6401-6411, 2011

"Learn from yesterday, live for today, hope for tomorrow.

The important thing is not to stop questioning."

-Albert Einstein